Agostinho Luís Pereira Lemos

Design and synthesis of aminoxanthone derivatives as promising disruptors of p53:MDM2 interaction

Dissertação do 2º Ciclo de Estudos Conducente ao Grau de Mestre em Química Farmacêutica, Faculdade de Farmácia, Universidade do Porto

Trabalho realizado sob a orientação de:

Professora Doutora Emília Sousa

Doutora Andreia Palmeira

Professora Doutora Lucília Saraiva

Julho de 2015

Author's declaration:

Under the terms of the Decree-Law nº 216/92, of October 13th, is hereby declared that the author afforded a major contribution to the conceptual design and technical execution of the work and interpretation of the results included in this dissertation. Under the terms of the referred Decree-Law, is hereby declared that the following articles/communications were prepared in the scope of this dissertation.

The results presented in this dissertation are part of the following scientific communications:

- **Synopsis of a review article submitted for publication:**

A. Lemos, M. Leão, J. Soares, A. Palmeira, M. Pinto, L. Saraiva, E. Sousa. "Medicinal Chemistry strategies to disrupt p53:MDM2/MDMX interaction". *Medicinal Research Reviews*. 2015.

- **Invited lectures**

E. Sousa*****, **A. Lemos**, P. Puthongking, A. Kijjoa, M. Pinto. Experiences with amination of xanthones to obtain bioactive compounds. 7th Spanish, Portuguese, Japanese Organic Chemistry Symposium, 23-26 June 2015, Seville, Spain, IL1, pp 68.

- **Selected oral communications**

A. Lemos*, P. Brandão, A. Palmeira, M. Pinto, L. Saraiva, E. Sousa. "A hybridization approach to obtain new xanthone derivatives as potential inhibitors of p53:MDM2 interaction". 3rd National Meeting of Chemistry Students, Aveiro, Portugal, 27-29 March 2015.

A. Lemos*, P. Puthongking, A. Palmeira, A. Kijjoa, L. Saraiva, M. Pinto, E. Sousa. "Xanthone as a promising scaffold to develop new potential inhibitors of p53:MDM2 interaction". 8th Meeting of Young Researchers of University of Porto, Porto, Portugal, 13-15 May 2015.

- **Poster communications**

A. Lemos*, P. Brandão, A. Palmeira, M. Pinto, L. Saraiva, E. Sousa. "Design and synthesis of new xanthone derivatives as potential disruptors of p53:MDM2 interaction". 10th Spanish-Portuguese Meeting of Chemistry, Porto, Portugal, 26-28 November 2014, QS48.

A. Lemos*, P. Brandão, A. Palmeira, M. Pinto, L. Saraiva, E. Sousa. "A hybridization approach to obtain new xanthone derivatives as potential inhibitors of p53:MDM2 interaction". 3rd National Meeting of Chemistry Students, Aveiro, Portugal, 27-29 March 2015, P9.

A. R. Moreira*, G. Moreira, **A. Lemos**, E. Sousa, M. Pinto, P. Costa, D. Ferreira. "Synthesis of a xanthonic compound with antitumor activity and development of proliposomes as its delivery system". 8th Meeting of Young Researchers of University of Porto, Porto, Portugal, 13-15 May 2015, P38, 6038.

A. Lemos*, P. Puthongking, A. Palmeira, A. Kijjoa, L. Saraiva, M. Pinto, E. Sousa. "Development of promising inhibitors of p53:MDM2 interaction using a xanthone scaffold". 2nd Young Researchers Symposium of the Spanish Society of Medicinal Chemistry, Madrid, Spain, 12 June 2015, P51.

A. Lemos*, P. Puthongking, A. S. Gomes, A. Palmeira, A. Kijjoa, L. Saraiva, M. Pinto, E. Sousa. “Development of new promising drug candidates as p53 activators based on xanthone scaffold”. 10th Young European Scientist Meeting, Faculty of Medicine of University of Porto, Portugal, 17-20 September 2015 (ongoing).

* presenting author

ACKNOWLEDGEMENTS

First of all, I would like to acknowledge all of the professors of Organic and Pharmaceutical Chemistry for creating a Master's Degree that allowed us to get a greater knowledge of organic and medicinal chemistry that, in my case, was crucial for construction of this dissertation.

To Prof. Emilia Sousa, my advisor, for allowing me to take part in this research project, which has been a major learning experience, for her support and guidance in the supervision of the work and for believing in my capabilities.

To Prof. Madalena Pinto, coordinator of CEQUIMED-UP and director of Organic and Pharmaceutical Laboratory of Faculty of Pharmacy, University of Porto, for the availability on the transmission of knowledge.

To Dr. Andreia Palmeira, my co-advisor, for supporting me in computational chemistry area.

To Prof. Lucília Saraiva, my co-advisor, for giving me the opportunity to test biologically the LEM2 derivatives and to acquire a better knowledge of this scientific area at experimental and theoretical level.

To Dr. Sara Cravo for the technical assistance in microwave synthesis, HPLC equipment, for performing GC-MS analysis on the compounds.

To Ms. Gisela Adriano for assisting me in many different ways.

To MsC Ana Sara Gomes for supporting and helping me in biological activity part and for contributing to the development of my knowledge in this area.

To Ploenthip Puthongking, a post-doc fellow, for her availability to transmit her knowledge in the organic synthesis area, for her sympathy and friendship.

To MsC Pedro Brandão for helping me in organic synthesis of the carbaldehydic xanthone LEM2.

To colleagues of Master's Degree of Pharmaceutical Chemistry for their friendship and support.

To my parents for supporting me and giving me the opportunity to dedicate exclusively to the Master's Degree.

This work was developed in the Centro de Química Medicinal da Universidade do Porto- CEQUIMED-UP, Laboratório de Química Orgânica e Farmacêutica, Departamento de Ciências Químicas, Faculdade de Farmácia da Universidade do Porto, and Laboratório de Microbiologia, Departamento de Ciências Biológicas, Faculdade de Farmácia da Universidade do Porto. This research was partially supported by the Strategic Funding UID/Multi/04423/2013 through national funds provided by FCT – Foundation for Science and Technology and European Regional Development Fund (ERDF), in the framework of the programme PT2020 and the Project Pest-OE/SAU/UI4040/2014 and REQUIMTE-Pest-C/EQB/LA0006/2013.

INDEX

INDEX OF FIGURES

INDEX OF TABLES

INDEX OF SCHEMES

ABSTRACT

The activation of tumor suppressor proteins, as p53, constitutes one of the several cellular mechanisms to protect human cells. Upon stress signals, p53 acts as a transcription factor, inducing the expression of several downstream targets responsible for the antiproliferative activity of p53. The growth-suppressive activity of p53 is tightly controlled by interaction with two negative modulator proteins, MDM2 and MDMX, which are overexpressed in about half of all human tumors. Inhibition of p53:MDM2/MDMX interaction may reactivate the p53 pathway and represent an alternative therapeutic strategy for cancer therapy. The elucidation of the crystal structures of p53 in complex with MDM2 and MDMX has led to the identification of several classes of small-molecule disruptors with favorable drug-like properties. Xanthone derivatives have been reported as promising anticancer agents with the ability to disrupt p53:MDM2 interaction. In fact, the naturally-occuring xanthones, α-mangostin and gambogic acid, and the synthetic derivatives pyranoxanthone **LEM1** exhibited potent cytotoxic activity against several human tumor cell lines accompanied by an inhibitory effect on p53:MDM2 interaction. Overall, the xanthone scaffold has revealed to be promising for the search of new small-molecule disruptors of p53:MDM2 interaction.

In this dissertation, the recently developed synthetic pathway of the 3,4-dimethoxy-9-oxo-9*H*-xanthene-1-carbaldehyde (**LEM2**) resulted in improved reaction yields when compared to previous synthetic pathway. Based on the pattern of substitution of **LEM2** derivatives, a potent inhibitor of p73:MDM2 interaction, and on the amine moiety of known p53:MDM2 inhibitors, a molecular hybridization strategy was followed to obtain new potential p53:MDM2 disruptors with drug-like properties and antitumor activity. By a reductive amination procedure, a library of aminoxanthone derivatives of **LEM2** was successfully synthesized. The optimization of the reaction conditions was accomplished by using sodium triacetoxyborohydride and tetrahydrofuran as a reducing agent and solvent, respectively. Eleven new aminoxanthone derivatives were obtained and their structures were elucidated by spectroscopic techniques, including NMR (^{1}H and ^{13}C), IR and mass spectrometry. Docking studies were carried out to rank the aminoxanthones according to their binding affinity towards MDM2. These studies have shown a higher binding affinity of these derivatives against MDM2 when compared to the respective precursors and a similar binding affinity with known small-molecule disruptors of p53:MDM2 interaction. Using yeast-screening assays, the inhibitory activity of the aminoxanthones on p53:MDM2 interaction was investigated. No significant effects were observed on the growth of yeast cells co-expressing p53 and MDM2 proteins after the

treatment with compounds. Further studies on p73:MDM2 may disclose potential inhibitors of p73:MDM2 interaction.

These studies will contribute to the knowledge of structural requirements for the construction of novel potent and selective small-molecule p53/p73 activators with antitumor activity.

Keywords: antitumor activity, MDM2, molecular hybridization, p53, p73, reductive amination, xanthone.

RESUMO

A ativação de proteínas supressoras tumorais, como a p53, constitui um dos diversos mecanismos celulares de proteção das células humanas, em resposta a sinais de stress intrínsecos e extrínsecos. A proteína supressora tumoral p53 atua como um fator de transcrição e estimula a expressão de diversas proteínas responsáveis pela atividade antiproliferativa da p53. A atividade supressora do crescimento associada à p53 é controlada pela sua interação com duas proteínas, MDM2 e MDMX, que estão sobreexpressas em cerca de metade dos tumores humanos. O bloqueio da interação p53:MDM2/MDMX permite a reativação da p53 e representa uma estratégia terapêutica promissora para o tratamento de tumores. A elucidação estrutural por cristalografia de raios X da p53 complexada com cada uma das proteínas MDM2 e MDMX tem permitido a identificação de diversas classes de inibidores da interação p53:MDM2/MDMX com propriedades *drug-like* favoráveis. Os derivados xantónicos têm sido documentados como agentes antitumorais promissores e com capacidade de bloquear a interação p53:MDM2. De facto, as xantonas naturais, α-mangostin e ácido gambógico, e o derivado xantónico sintético, piranoxantona **LEM1** exibiram uma atividade citotóxica marcada quando testadas em várias linhas celulares tumorais humanas, um efeito mediado por uma inibição na interação p53:MDM2. De uma forma geral, o núcleo xantónico tem-se revelado promissor na pesquisa de novas pequenas moléculas inibidoras da interação p53:MDM2.

Nesta dissertação, a via de síntese do 3,4-dimethoxi-9-oxo-9*H*-xantene-1-carbaldeído (**LEM2**) recentemente desenvolvida resultou numa melhoria do rendimento da reação de síntese quando comparado com o da via de síntese anteriormente existente. Tendo como base o padrão de substituição dos derivados do **LEM2**, um potente inibidor da interação p73:MDM2, e a porção amina de inibidores conhecidos da interação p53:MDM2, foi seguida uma estratégia de hibridização molecular com o objetivo de obter novas moléculas inibidoras da interação p53:MDM2 com propriedades farmacocinéticas favoráveis. A otimização das condições de reação foi conseguida através da utilização de triacetoxiboroidreto de sódio e tetraidrofurano como agente redutor e solvente, respetivamente. Através de um processo de aminação redutiva, foi sintetizada uma biblioteca de derivados aminoxantónicos do **LEM2**. Onze derivados aminoxantónicos recém-sintetizados foram elucidados estruturalmente por técnicas espectroscópicas, incluindo RMN (^{1}H e ^{13}C), IV e espetrometria de massa. Estudos de *docking* foram realizados de modo a classificar os derivados aminoxantónicos de acordo com a afinidade de ligação à proteína MDM2. Estes estudos demonstraram que os

derivados aminoxantónicos têm uma maior afinidade de ligação a MDM2 do que os respetivos precursores e uma afinidade de ligação semelhante à de pequenas moléculas inibidoras da interação p53:MDM2 já conhecidas. Recorrendo a ensaios de *screening* com levedura, a atividade inibitória dos derivados aminoxantónicos na interação p53:MDM2 foi investigada. Não foram observadas alterações significativas na percentagem de crescimento de leveduras que expressam as proteínas p53 e MDM2 após o tratamento com os compostos. Estudos posteriores envolvendo a interação p73:MDM2 poderão resultar em potenciais inibidores desta interação.

Estes estudos poderão contribuir para o conhecimento dos requisitos estruturais mais favoráveis para a síntese de pequenas moléculas ativadoras da p53/p73 mais potentes e seletivas, com promissora atividade antiumoral.

Palavras-chave: atividade antitumoral, aminação redutiva, hibridização molecular, MDM2, p53, p73, xantona.

ABBREVIATIONS

^{13}C NMR – Carbon nuclear magnetic resonance

^{1}H NMR – Proton nuclear magnetic resonance

Asp – Aspartate

ATP – Adenosine triphosphate

(BMIM)BF_4 - 1-Butyl-3-methylimidazolium tetrafluoroborate

BPO – Benzoyl peroxide

CBP – cAMP-responsive element-binding protein

CEQUIMED – UP – Centro de Química Medicinal da Universidade do Porto

CFU – Colony-forming units

Cys – Cysteine

d – Doublet

DBD – DNA-binding domain

dd – Double doublet

ddd – Double double doublet

DNA – Deoxyribonucleic acid

ELISA – Enzyme-linked immunosorbent assay

FRET – Fluorescence resonance energy transfer

Gly - Glycine

His – Histidine

HMBC – Heteronuclear multiple bond correlation

HMTA – Hexamethylenetetramine

HSQC – Heteronuclear single quantum coherence

HTRF – Homogenous time resolved fluorescence

Ile – Isoleucine

IR – Infrared

J – Coupling constant

LEM1 - 12-Hydroxy-2,2-dimethyl-3,4-dihydro-2*H*,6*H*-pyrano[3,2-b]xanthen-6-one

LEM2 - 3,4-Dimethoxy-9-oxo-9*H*-xanthene-1-carbaldehyde

Leu – Leucine

m – Multiplet

MDM2 – Murine double minute 2

MDMX – Murine double minute X

Met – Methionine

mRNA – Messenger RNA

MS – Mass spectrometry

MSTFA – *N*-Methyl-*N*-(trimethylsilyl)trifluoroacetamide

MW – Microwave

NBS – *N*-Bromosuccinimide

nm – Nanometers

NMR – Nuclear magnetic ressonance

OD – Oligomerization domain

PDB – Protein Data Bank

Phe – Phenylalanine

PK - Pharmacokinetic

(pmIm)BF_4 - 1-Methyl-3-pentylimidazolium tetrafluoroborate

PPI – Protein-protein interaction

Pro - Proline

PRR – Proline-rich region

q – Quintet

qRT-PCR – Quantitative real time – polymerase chain reaction

Rf – Retention factor

RING – Really interesting new gene

r.t. – Room temperature

s – Singlet

SAR – Structure-activity relationship

SPE – Solid phase extraction

STAB – Sodium triacetoxyborohydride

t - Triplet

TAD – Transactivation domain

THF - Tetrahydrofuran

TLC – Thin-layer chromatography

Trp – Tryptophan

UV – Ultraviolet

Val – Valine

OUTLINE OF THE DISSERTATION

The present dissertation consists of six chapters. This dissertation involves three main areas of research: synthesis of formylated xanthone **LEM2** and their aminoxanthone derivatives, docking simulation studies of these derivatives against MDM2 and the evaluation of their inhibitory activity on p53:MDM2 interaction.

CHAPTER 1 – INTRODUCTION

The introductory chapter of the present dissertation is divided in two sections. In the first part, a general review about biological functions of p53 and the influence of two negative protein modulators, MDM2 and MDMX, in p53 activity and function will be discussed as well as the structural requirements for the identification of p53:MDM2 and p53:MDMX disruptors. Also, a brief reference will be given to the isoforms of p53 protein. In the second part, an introduction to xanthone derivatives will be given and their promising inhibitory activity on p53:MDM2 will be highlighted.

CHAPTER 2 – AIMS

Herein, the main objectives of the present dissertation are described.

CHAPTER 3 - RESULTS AND DISCUSSION

Results are subdivided in three sections. In the first part, the different reaction steps for the synthesis of carbaldehydic xanthone **LEM2** will be described as well as its structural elucidation. In the second part, the synthesis and the structure characterization of aminoxanthone derivatives of **LEM2** will be presented. In the third part, the results concerning the docking simulation studies of these derivatives against MDM2 are discussed and preliminary results concerning the inhibition of p53:MDM2 interaction will be presented. The biological assay was performed with the assistance of Master Ana Sara Gomes and with the supervision of Prof. Lucília Saraiva at UCIBIO, Laboratory of Microbiology, FFUP.

CHAPTER 4 – CONCLUSIONS

This chapter includes the general conclusions of the present dissertation.

CHAPTER 5 - MATERIAL AND METHODS

In this chapter, the experimental procedures for the synthesis and structure characterization of the new synthesized derivatives of **LEM2** will be detailed. Also, the conditions applied for the docking studies and biological tests will be described.

CHAPTER 6 – REFERENCES

The references will be presented at the end of this dissertation. The references followed the American Chemical Society style guide. The main bibliographic research motors were ISI Web of Knowledge, from Thomson Reuters, Scopus, and Google.

CHAPTER 1

INTRODUCTION

CHAPTER 1 - INTRODUCTION

1.1. The p53 tumor suppressor protein

The p53 tumor suppressor protein is encoded by the *TP53* gene[1], which is span about 20 kb of DNA[2] and is located on the short arm of chromosome 17[3]. It acts mainly as a transcription factor and is biologically active as a homotetramer containing 393 amino acid residues each monomer[4] (**Figure 1**).

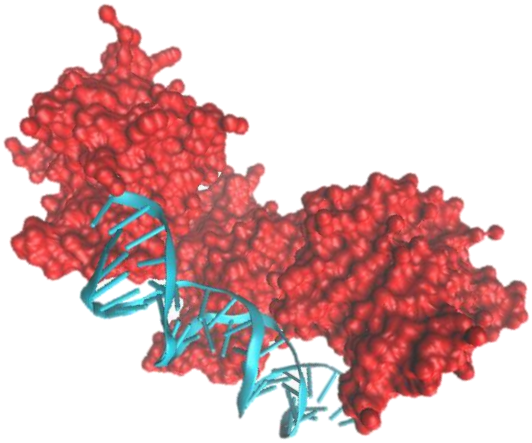

Figure 1 - Crystal structure of self-assembled p53 tetramer bound to DNA (PDB code 3KMD).

Structurally, p53 is characterized by a modular domain which consists of folded DNA-binding and tetramerization domains. The NH_2-terminal region contains a transactivation domain (TAD) followed by a proline-rich region (PRR). A DNA-binding domain (DBD) is in the middle of the protein and connected to oligomerization domains (OD) through a flexible linker region. A regulatory domain is located at the COOH-terminal region[4] (**Figure 2**). This structure allows the tetrameric p53 protein, on binding to DNA, to regulate the expression of several genes responsible for tumor suppressor effect of p53[1,5].

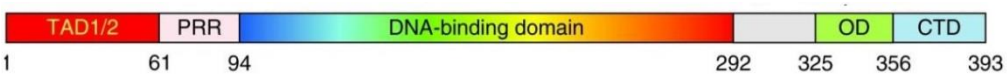

Figure 2 - The p53 protein contains, in the NH_2-terminal region, a transactivation domain (TAD) followed by a proline-rich region (PRR). The DNA-binding domain (DBD), located in the middle of the protein, is linked to the oligomerization domain (OD) (adapted from [4]).

1.1.1. Biological functions of p53

Under physiological (unstressed) conditions, p53 is unstable with a short half-life and is held in an inactive state that undergoes to a significant increase in its activity and

stability in response to various stress signals[6]. Upon DNA-damaging agents, the p53 acts as a transcription factor, inducing the expression of several downstream targets which play an important role in regulation of cell cycle, apoptosis, DNA repair, senescence and angiogenesis[7]. Therefore, upon stress signals, the activation of p53 can suppress the tumor development and growth, preventing damaged cells from multiplying and passing mutated genes with oncogenic potential to the next generation[8]. For that reason, it is not surprising that p53 is considered "the guardian of genome" as it contributes to genome integrity[9].

A defective p53 regulation may hinder p53 activation, resulting in inadequate tumor suppression and in an uncontrollable proliferation of cancer cells[10]. However, the growth-suppressive and proapoptotic activity of p53 is lethal for normal cells if left uncontrolled. Thus, p53 activity must be tightly regulated in order to maintain tissue homeostasis[11].

1.1.2. Regulation of p53

Under normal physiological conditions and during stress, the cellular level and activity of p53 are subjected to tight control by several modulators[10]. The two main negative regulatory proteins, murine double minute 2 (MDM2) and X (MDMX; also known as MDM4), are crucial for the regulation of p53 function[11] (**Figure 3**).

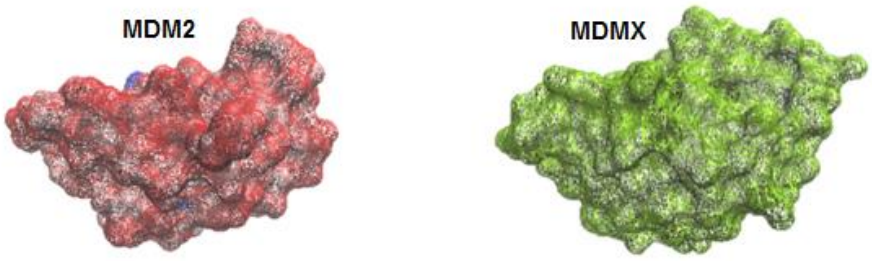

Figure 3 – Crystal structures of oncoproteins MDM2 (PDB code 1YCR) and MDMX (PDB code 3DAC).

Human MDM2 and MDMX are structurally related oncoproteins composed by 491 and 490 amino acids respectively, with three well-conserved domains: an NH_2-terminal domain which is important for binding to the NH_2-terminal region of p53, a zinc finger domain and a COOH-terminal really interesting new gene (RING) domain (**Figure 4**). MDM2 and MDMX also contain a region rich in acidic residues, without any significant sequence conservation[12].

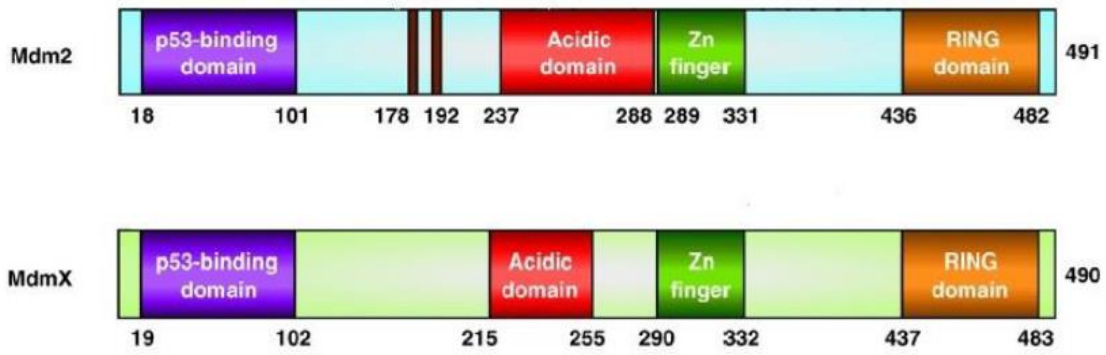

Figure 4 – Similarity of structural domains of MDM2 and MDMX oncoproteins (adapted from [11]).

1.1.2.1. The role of MDM2 in negative regulation of p53

The *MDM2* gene was initially discovered in DNA associated with paired acentric chromatin bodies, termed double minutes, in spontaneously transformed mouse 3T3 fibroblasts[13]. It was found that MDM2 and p53 mutually regulate each other through an autoregulatory feedback loop[7]. The physiological relevance of this autoregulatory loop was shown by genetic evidence that embryonic lethality of *MDM2*-null mice can be rescued only upon deletion of *TP53* gene[14]. In fact, MDM2 is a transcriptional target of p53, which attenuates p53 activity through diverse mechanisms[7] (**Figure 5**).

Under stress conditions, the high p53 levels in nucleus stimulate the MDM2 transcription through binding of p53 at the p53-binding domain of MDM2 gene. This up-regulation results in an increase of the MDM2 levels. Consequently, MDM2 physically interacts with the NH_2-terminal domain of p53[15]. The p53:MDM2 interaction results in a partial overlapping of TAD (located at NH_2-terminal region of p53) and in an inactivation or attenuation of transcriptional function of p53[10].

The growth suppressive activity of p53 can also be controlled by its ubiquitination and proteossomal degradation. Protein ubiquitination involves three ATP-dependent enzymes in a sequential reaction: an ubiquitin activating enzyme (E1), an ubiquitin conjugating enzyme (E2) and an ubiquitin protein ligase (E3). E1 forms a thioester bond between its active site cysteine residue and glycine residue of ubiquitin. E1-ubiquitin complex is transferred to E2 by transthioesterification. Then, E3 catalyzes the final step of the ubiquitination cascade. This enzyme binds to the E2-ubiquitin complex and enables the formation of an isopeptide linkage between the COOH-terminal region of ubiquitin and the lysine residue in the target protein. Once four or more ubiquitin molecules (poly-ubiquination) are attached, the modified protein is recognized and degraded by the 26S proteasomes[16]. MDM2 belongs to the family of E3 ubiquitin ligases that contain a RING

domain. These enzymes are structurally defined by cross-branched active site histidine and cysteine residues bound to two zinc ions. This RING domain is located at the COOH-terminal region of MDM2 and shows to have a crucial role in its E3 ligase activity. This oncoprotein mediates the direct transfer of ubiquitin from an E2 enzyme (ubiquitin conjugating enzyme) onto lysine residues located at the COOH-terminal domain of p53, catalyzing its ubiquitination[10, 16].

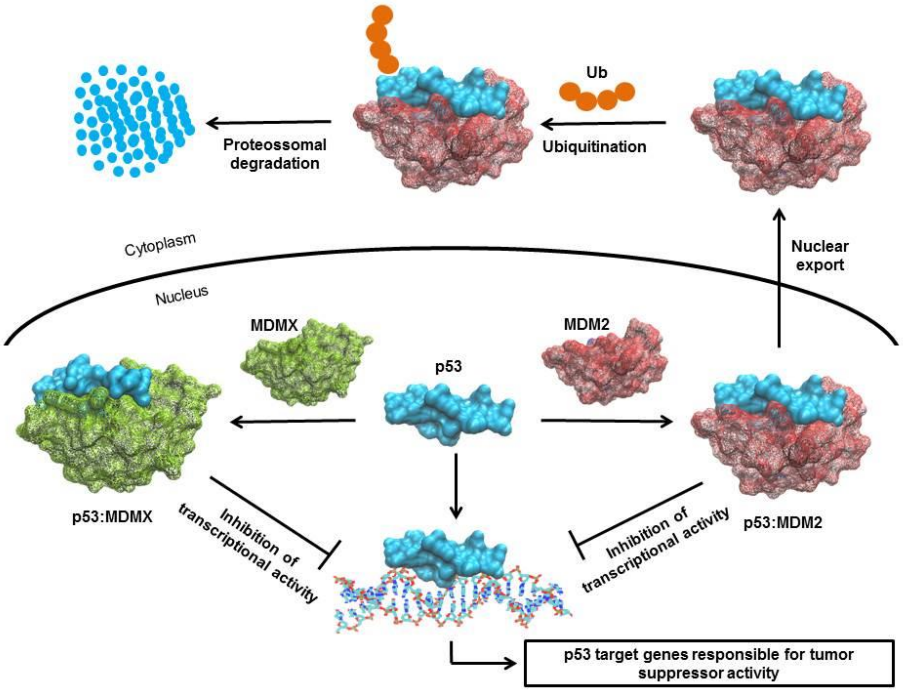

Figure 5 - Regulation of p53 by MDM2 and MDMX through autoregulatory feedback loop. Under both physiological and during stress, the cellular level and activity of p53 are subjected to tight control mainly by MDM2 and MDMX by several mechanisms: MDM2 interacts with NH_2–terminal region of p53 leading to the inactivation of p53 transcriptional activity and also enables nuclear export of p53, keeping it away from nuclear DNA; MDM2 mediates p53 degradation via the ubiquitin-proteasome pathway (adapted from [8]).

Lastly, MDM2 facilitates export of p53 out of the cell nucleus, *via* MDM2 RING finger domain, making p53 inaccessible to targeted DNA for transcription[7, 17].

This autoregulatory negative feedback loop between p53 and MDM2 is essential for restricting p53 activity in unstressed cells and for eliminating accumulated p53 upon stress signals[17].

1.1.2.2. The role of MDMX in negative regulation of p53.

The MDMX protein has emerged only recently as a critical p53 negative regulator and is a close homolog of MDM2[18]. Like MDM2, the embryonic lethal phenotypes of MDMX-null mice can be rescued by simultaneous knockout of *TP53* gene[19] As referred above, MDM2 and MDMX share a high sequence homology mainly in their p53-binding

domains and RING finger domains[7]. MDMX acts cooperatively with MDM2, potentiating its ubiquitin ligase activity and enhancing p53 degradation. Both MDM2 and MDMX regulate p53 transcriptional activity through interactions mediated by their NH_2-terminal domains and the NH_2-terminal TAD of p53[20]. Despite sharing high sequence and structural homology, MDM2 and MDMX regulate p53 by distinct manners. While MDM2 promotes the down-regulation of p53 activity by promoting its ubiquitination and subsequent degradation, MDMX abolishes the p53 function by sequestering it into an inactive p53:MDMX complex[21]. Although MDMX is not active as an E3 ligase, it can form heteroligomers with MDM2, acting as a negative regulator of p53[19].

1.1.3. The isoforms of the p53 protein: p63 and p73

Two p53-related genes, p63 and p73, were first identified in 1997 and exhibit, like p53, the aminoterminal transactivation domain (TAD) followed by a proline rich region (PRR), the central DNA-binding domain (DBD), and the carboxy-terminal oligomerization domain (OD)[22] (**Figure 6**). In p63 and p73, there is an additional COOH-terminal sterile-α motif. The high structural and functional homology between p53, p63 and p73 proteins, particularly in the DNA binding domain, allows the transactivation of p53-responsive genes by p63 and p73, inducing apoptosis and cell-cycle arrest[23]. These three proteins form a family of transcription factors which are not functionally entirely redundant and so that each p53 famile member has its own unique biological functions[24]. The p53 gene family members express multiple mRNA variants due to multiple splicing and alternative promoters. Therefore, p53 gene family members express different forms of p53 protein containing different domain of the protein (isoforms)[23].

The human p63 gene express at least three alternatively spliced COOH-terminal isoforms (α, β, γ), while the p73 gene express at least seven alternatively spliced COOH-terminal isoforms (α, β, γ, δ, ε, ζ, η) and four alternatively spliced NH_2 terminal isoforms[25]. Both p63 and p73 genes can be transcribed from one promoter upstream of exon 1, which leads to the expression of TAp63 and TAp73 (transcriptionally proficient), and one promoter located on intron 3, that leads to the expression of ΔNp63 and ΔNp73 isoforms lacking transactivation domain (transcriptionally inactive)[26].

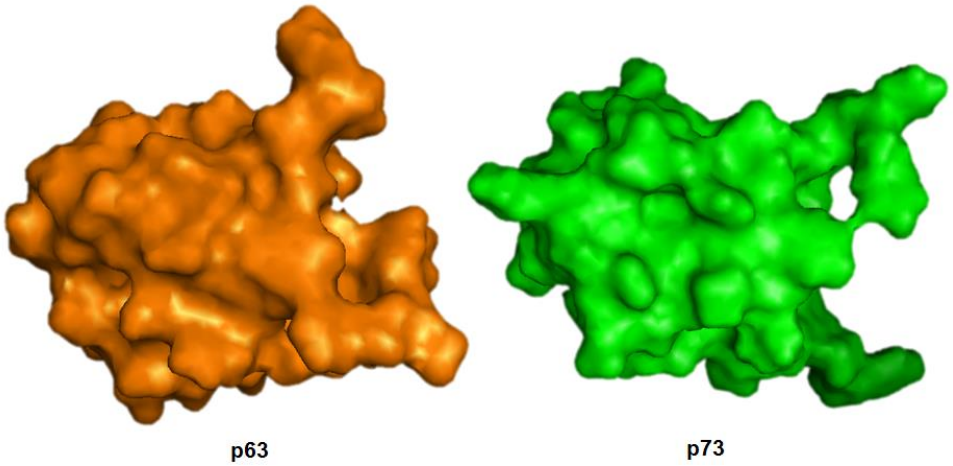

Figure 6 – Crystal structures of p63 (PDB code 1RG6) and p73 (PDB code 1COK).

In a similar manner of p53, p73 is also regulated by its interaction with MDM2 and MDMX. However, unlike p53, MDM2 does not promote p73 ubiquination and degradation[27]. It was found that MDM2 inhibits p73 transcriptional activity by preventing its interaction with the coactivators p300/CBP and RNA-polymerase associated factors[28].

Relatively to p63, it was found that this protein weakly interacts to both MDM2 and MDMX[29,29b].

The p53 family proteins have a central role in the control of cell proliferation and death, constituting a valuable therapeutic targets for cancer therapy.

1.1.4. p53, a valuable target for cancer treatment

As p53 has the ability of suppressing the development and propagation of damaged cells to protect the normal tissues, it's not surprising that the inactivation of p53 function may represent almost an universal feature of human cancer cells. In fact, approximately 50% of all human tumors are caused by mutations in the *TP53* gene. It has been reported that the majority of these mutations occurs in the DBD region which is responsible to the specific DNA-binding function of p53. The main functional deficiency of p53 mutation is the specific DNA-binding ability and its transcriptional activity, which directly causes the attenuation of antiproliferative activity of p53[10]. In the remaining 50%, human cancer cells exhibit a p53 wild-type phenotype. However, an aberrant p53 regulation and signaling of p53 pathway, which is caused by an overexpression of oncoproteins MDM2 and MDMX, stimulates the cell growth and tumorigenesis, compromising the tumor suppressor effect of p53[30]. Therefore, the p53 protein has become one of the most important therapeutic targets in cancer treatment[9].

1.1.5. Therapeutic strategies for cancer treatment: activation of p53-dependent pathway

Several therapeutic targets have been developed for treatment of wild-type p53 and mutant p53 tumors to restore p53 activity and function. For cancer cells which express mutant p53, restoration of p53 wild-type function may result in considerable therapeutic responses. In this case, the following strategies can be applied: (1) gene therapy with wild-type p53 and (2) reactivation of mutant p53 with peptides and small-molecules. On the other hand, when tumors express wild-type p53, efforts should be aimed on the stabilization of p53 protein and activation of p53-dependent pathway. The following therapeutic strategies can be used: (1) blockade of MDM2 expression, (2) inhibition of MDM2 ubiquitin ligase activity and (3) disruption of p53:MDM2/MDMX interaction[10]

1.1.6. Targetting p53:MDM2/MDMX interaction as a promising approach for cancer therapy

The p53:MDM2/MDMX interface is defined as a protein-protein interaction (PPI). PPIs have proved to be challenging for drug discovery since the interface between two proteins is generally large, flat and involve interactions with a high number of amino acid residues from each protein[30]. These characteristics appear to be unfavorable on identification of compounds with drug-like properties[10]. In fact, small-molecules are preferred in drug discovery, comparing with peptide, peptidomimetics and macromolecular inhibitors, because of several advantages, such as better stability and bioavailability (especially oral bioavailability) and enhancement of absorption, distribuition, metabolism and excretion (ADME) characteristics[10, 30]. However, it has been shown that though these two proteins make many contacts with each other, there is generally a small pocket of a few amino acid residues that make up for the majority of the binding energy. In the context of p53:MDM2 and p53:MDMX interaction, just three amino acid residues of p53, Phe19, Trp23 and Leu26 contributed to a large extent for the physical interaction and binding energy of the p53:MDM2/MDMX complex[5].

1.1.7. The p53:MDM2/MDMX interaction: structural requirements

In 1996, it was published a high resolution crystal structure of MDM2 in complex with a short p53-peptide (NH_2-terminal residues 15-29)[31] and in 2008, the crystal structure

of human MDMX bound a peptide derived from human p53 NH_2-terminal domain was elucidated[32] (**Figure 7**). The crystal structures of both p53:MDM2 and p53:MDMX complexes revealed these interactions are mediated by the three key hydrophobic residues in p53 (Phe19, Trp23 and Leu26) and a hydrophobic surface groove in MDM2 and MDMX proteins. Therefore, the p53:MDM2 and p53:MDMX interaction result in formation of complexes which display similar binding features[9]. In spite of the similarity of most residues in the MDM2 and MDMX binding pockets, some amino acid residues located around the Leu26 binding pocket are different, leading to distinct shape and size of MDMX groove comparing to the MDM2 groove. In fact, the presence of MDMX amino acid residues Met53 (Leu54 in MDM2), Leu98 (Ile99 in MDM2), Leu102 (Ile103 in MDM2) and Pro95 (His96 in MDM2) resulted in smaller binding groove in MDMX compared to MDM2[33].

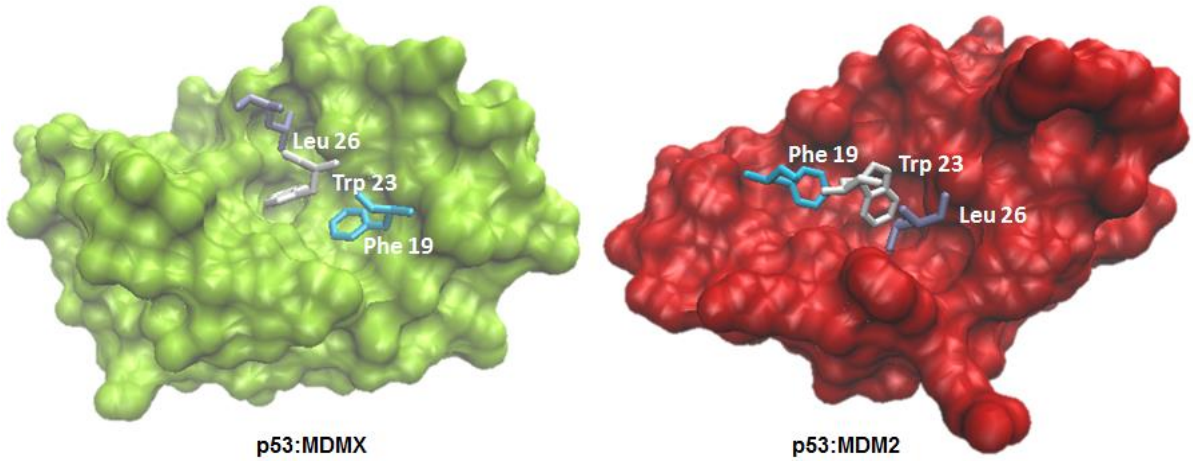

Figure 7 – Hydrophobic amino acid residues of p53 that contribute to large extent for the binding energy of p53:MDMX (PDB code 3DAC) and p53:MDM2 interaction (PDB code 1YCR).

The knowledge of crystallographic structures of p53 in complex with MDM2 and MDMX has led to the identification of several classes of promising small-molecule inhibitors with antitumor effectiveness.

1.1.8. Small-molecule inhibitors of p53:MDM2 and p53:MDMX interaction

Low-molecular weight inhibitors are preferred as drug candidates due to their favorable pharmacokinetic (PK) properties in alternative to peptides or macromolecular inhibitors. Upon the realization that impairing the interaction between p53 and MDM2/MDMX are dependent on interactions of “three finger pharmacophore” with hydrophobic clefts of MDM2 and MDMX, efforts have been made in order to find out and develop potent small molecule antagonists of p53:MDM2 and p53:MDMX interaction with

potential antitumor activity. In this section, the most relevant classes of small molecule inhibitors of p53:MDM2 (**Table 1**) and p53:MDMX (**Table 2**) interactions will be presented as well as some information about strategies used in their discovery and their PK profile and progress in the pipeline. Comparing the two tables which represent the different classes of small molecule inhibitors of p53:MDM2 and p53:MDMX interaction, it can be observed that only a few number of MDMX inhibitors exists when compared to the high number of p53:MDM2 interaction disruptors. In fact, there are several classes of MDM2 antagonists which have shown not only to be potent in inhibiting the mentioned interaction but also exhibited a selective antitumor activity in some cancer cell lines with a wild-type p53.

Table 1 – Classes of small-molecule inhibitors of p53:MDM2 interaction.

<table>
<tr><td colspan="2">Chemical Family: Benzodiapedinedione</td></tr>
<tr><td>Structure of lead compound</td><td>Relevant Members</td></tr>
<tr><td> 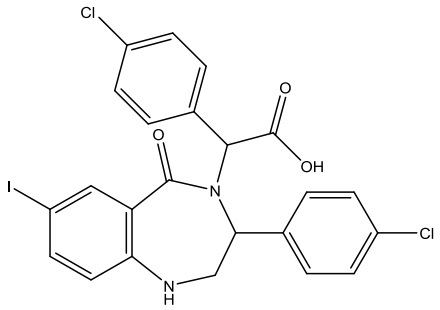

TDP222669</td><td>TDP222669
TDP521252
TDP665759</td></tr>
<tr><td>Drug discovery: strategy</td><td>Drug discovery: assay</td></tr>
<tr><td>Structure-based design</td><td>Temperature-dependent protein unfolding assay (ThermoFluor microcalorimetry)

Fluorescence polarization assay</td></tr>
<tr><td>Pharmacokinetic profile</td><td>In the pipeline</td></tr>
<tr><td>TDP222669 showed poor cell membrane permeability, a rapid clearance and almost no bioavailability.

TDP521252 and TDP665759 resulted from optimization of PK properties of TDP222669, showing an enhanced bioavailability and cell permeability in a CACO-2 assay.</td><td>TDP521252 and TDP665759 are under preclinical trials.</td></tr>
<tr><td colspan="2">References</td></tr>
<tr><td colspan="2">9, 10, 17, 34, 35, 36</td></tr>
</table>

(continuing)

<table>
<tr><td colspan="2">Chemical Family: Chromenotriazolopyrimidine</td></tr>
<tr><td>Structure of lead compound</td><td>Relevant Members</td></tr>
<tr><td> 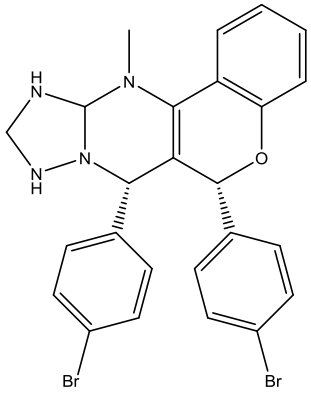
Chromenotriazolopyrimidine 1</td><td>Chromenotriazolopyrimidine 1 [(6R,7S)-6,7-bis(4-bromophenyl)-12-methyl-7,9,10,11,11a,12-hexahydro-6H-chromeno[4,3-d][1,2,4]triazolo[1,5-a]pyrimidine]

Chromenotriazolopyrimidine 2 [2-((6R,7S)-6,7-bis(4-bromophenyl)-6H-chromeno[4,3d][1,2,4]triazolo[1,5-a]pyrimidin-12(7H)-yl)acetic acid]

Chromenotriazolopyrimidine 3 [5-((6R,7S)-6,7-bis(4-bromophenyl)-6H-chromeno[4,3-d][1,2,4]triazolo[1,5-a]pyrimidin-12(7H)-yl)pentanoic acid]</td></tr>
<tr><td>Drug discovery: strategy</td><td>Drug discovery: assay</td></tr>
<tr><td>Structure-based design</td><td>Homogenous time resolved fluorescence (HTRF) assay</td></tr>
<tr><td>Pharmacokinetic profile</td><td>In the pipeline</td></tr>
<tr><td>Chromenotriazolopyrimidine 1 displayed poor pharmacokinetic properties. In rat, this compound exhibited a low solubility in PBS and moderate-to-high clearance and a low oral bioavailability (23%). An improvement on PK profile has led to the identification of the derivatives 2 and 3, which are more potent and metabolically stable. In rat, derivative 2 exhibited a high clearance and derivative 3 had shown a low clearance and an improved oral bioavailability.</td><td>-</td></tr>
<tr><td colspan="2">References</td></tr>
<tr><td colspan="2">37</td></tr>
</table>

(continuing)

<table>
<tr><td colspan="2">Chemical Family: Cis-imidazoline</td></tr>
<tr><td>Structure of lead compound</td><td>Relevant Members</td></tr>
<tr><td> 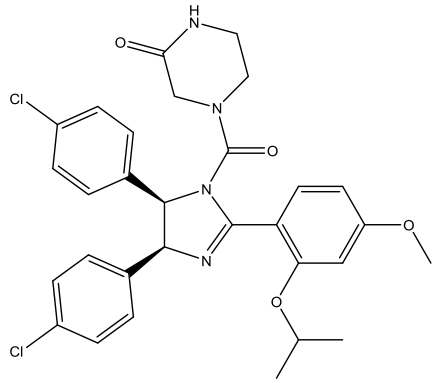
Nutlin-3</td><td>Nutlin-1
Nutlin-2
Nutlin-3
RG7112</td></tr>
<tr><td>Drug discovery: strategy</td><td>Drug discovery: assay</td></tr>
<tr><td>Structure-based design</td><td>Biacore surface plasmon resonance assay</td></tr>
<tr><td>Pharmacokinetic profile</td><td>In the pipeline</td></tr>
<tr><td>Pharmacological properties of nutlins were inadequate for clinical development. The imidazoline core of nutlins can be converted to the inactive imidazole form.

RG7112 resulted from optimization of nutlins structure for clinical use. This compound has good oral bioavailability. Introduction of methyl groups contributes to a greater structural rigidity in imidazoline scaffold and blocks metabolic conversion to the inactive imidazole form.</td><td>Nutlin-3a is in phase I clinical trial for the treatment of retinoblastoma.

RG7112 completed phase I clinical studies in advanced solid tumors and hematological neoplasms.</td></tr>
<tr><td colspan="2">References</td></tr>
<tr><td colspan="2">9, 10, 35, 38, 39, 40, 41</td></tr>
</table>

(continuing)

Chemical Family: Diphenylbutylpiperidine	
Structure of lead compound	**Relevant Members**
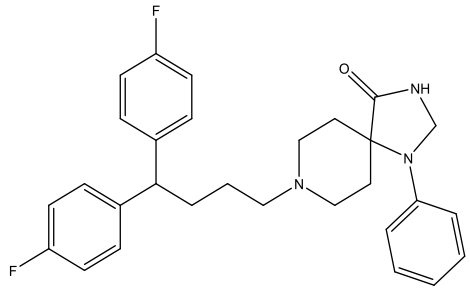 Fluspirilene	Fluspirilene
Drug discovery: strategy	**Drug discovery: assay**
Structure-based design	Virtual screening
Pharmacokinetic profile	**In the pipeline**
-	Fluspirilene is a long-acting injectable antipsychotic drug which showed an inhibitory activity on p53:MDM2 interaction in human tumor cell lines.
References	
42	

(continuing)

Chemical Family: Isoindolinone	
Structure of lead compound	**Relevant Members**
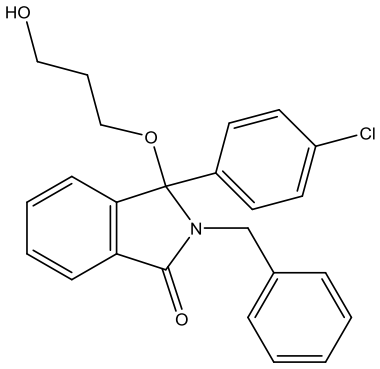 NU8165	NU8165 NU8231
Drug discovery: strategy	**Drug discovery: assay**
Structure-based design	NMR binding assay Enzyme-linked immunosorbent assay (ELISA)
Pharmacokinetic profile	**In the pipeline**
-	Further studies to address potency, selectivity and drug-like properties for this class of inhibitors are ongoing. -
References	
43, 44	

(continuing)

<table>
<tr><td colspan="2">Chemical Family: Isoquinolinone</td></tr>
<tr><td>Structure of lead compound</td><td>Relevant Members</td></tr>
<tr><td> 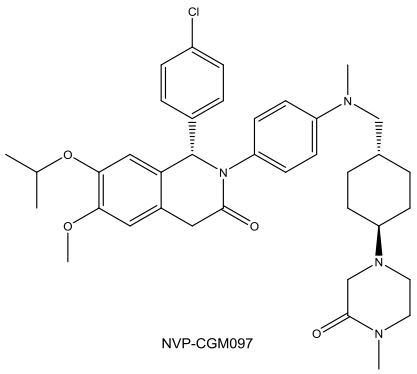

NVP-CGM097</td><td>NXN-7
NXN-561
NVP-CGM097</td></tr>
<tr><td>Drug discovery: strategy</td><td>Drug discovery: assay</td></tr>
<tr><td>Structure-based design</td><td>NMR binding assay</td></tr>
<tr><td>Pharmacokinetic profile</td><td>In the pipeline</td></tr>
<tr><td>NXN-7 was found to have poor in vivo solubility.

NXN-561 displayed increased solubility and improved cellular activity.

NVP-CGM097 is soluble in DMSO and not in water.</td><td>NVP-CGM097 is undergoing a phase I dose scalation study in adult patients with advanced solid tumors.</td></tr>
<tr><td colspan="2">References</td></tr>
<tr><td colspan="2">10, 35, 45</td></tr>
</table>

(continuing)

Chemical Family: Morpholinone	
Structure of lead compound	**Relevant Members**
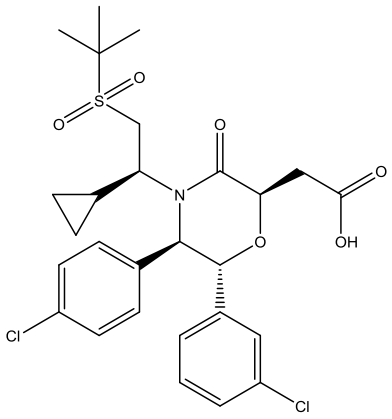 AM-8735	AM-8735
Drug discovery: strategy	**Drug discovery: assay**
Structure-based design Design based on piperidinone scaffold	HTRF assay
Pharmacokinetic profile	**In the pipeline**
AM-8735 exhibited metabolic stability in human hepatocytes and exhibited low clearance in rats. AM-8735 is preferentially metabolized by oxidation pathways	-
References	
46	

(continuing)

<table>
<tr><td colspan="2">Chemical Family: Piperidinone</td></tr>
<tr><td>Structure of lead compound</td><td>Relevant Members</td></tr>
<tr><td> 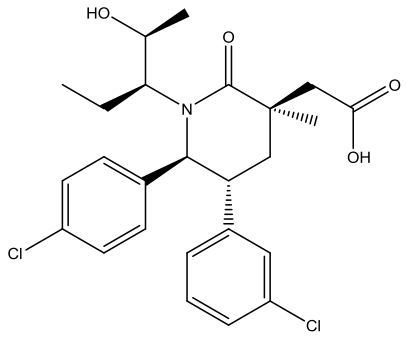

AM-8553</td><td>AM-8553
AMG-232
AM-6761
AM.7209</td></tr>
<tr><td>Drug discovery: strategy</td><td>Drug discovery: assay</td></tr>
<tr><td>Structure-based design</td><td>EdU cell proliferation assay
HTRF assay</td></tr>
<tr><td>Pharmacokinetic profile</td><td>In the pipeline</td></tr>
<tr><td>AM-8553 had an oral bioavailability of 100% in rats and 12% in mice. It had a reduced liability in human pregnane X receptor (hPXR), CYP3A4 and time-dependent inhibition (TDI) assays. This compound presented a low human hepatocyte intrinsic clearance with a high volume of distribution and a long human half-life (>12h).

AMG-232 displayed low intrinsic clearance in human hepatocytes and in vivo clearance in rats. This compound was found to have minimal liabilities in the CYP inhibition, TDI of CYP3A4, and PXR induction assays. AMG-232 is preferentially metabolized to an acylglucuronide derivative when incubated in rat, dog, cyno and human hepatocytes.

AM-6761 exhibited low intrinsic clearance in human hepatocytes and low CYP3A4 TDI activity. This compound exhibited improved metabolic stability in mouse and rats and increased oral bioavailability. It is cleared primarily by oxidation pathways.

AM-7209 displayed a low intrinsic clearance in human hepatocytes and a reduced liability hPXR, CYP3A4 and TDI assays. An oxidation pathway is the preferred metabolic route of AM.7209 in dog, cyno, rat and human hepatocytes.</td><td>AM-8553: No information on the advancement of this series to clinical settings is available yet.

AMG-232 is undergoing phase I clinical studies in acute myeloid leukemia and in advanced solid tumors. It is also undergoing phase Ib/IIa in metastatic melanoma. AMG-232 is undergoing phase I alone and in combination with Trametinib in acute myeloid leukemia.</td></tr>
<tr><td colspan="2">References</td></tr>
<tr><td colspan="2">44, 46, 47, 48, 49, 50, 51</td></tr>
</table>

(continuing)

Chemical Family: Pyrrolidine	
Structure of lead compound	**Relevant Members**
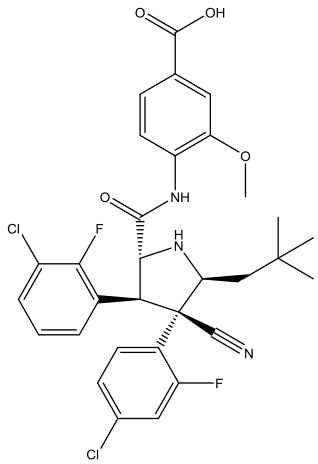 RG7388	RG7388
Drug discovery: strategy	**Drug discovery: assay**
Structure-based design	HTRF assay
Pharmacokinetic profile	**In the pipeline**
RG7388 presented oral bioavailability (80%), metabolic stability and low clearance.	RG7388 is undergoing clinical investigation in solid and hematological tumors (phase I). It is also undergoing in patients with polycythemia vera and essential thrombocythemia.
References	
52	

(continuing)

Chemical Family: Pyrrolidinone	
Structure of lead compound	**Relevant Members**
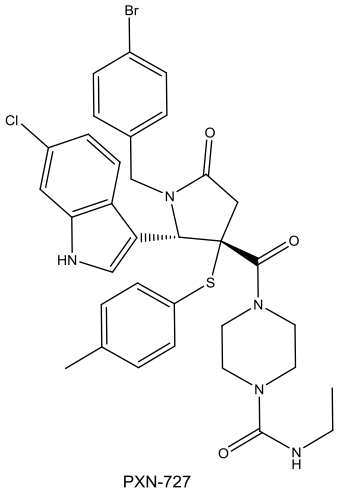 PXN-727	PXN-727 PXN-822
Drug discovery: strategy	**Drug discovery: assay**
Structure-based design	Fluorescence polarization assay
Pharmacokinetic profile	**In the pipeline**
PXN-727 has low toxicity and presents a better bioavailability when compared to nutlin-3.	PXN-727 and PXN-822 are undergoing preclinical studies.
References	
35, 36, 53, 54, 55	

(continuing)

Chemical Family: Quinolinol	
Structure of lead compound	**Relevant Members**
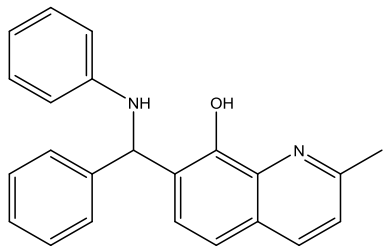 NSC 66811	NSC 66811
Drug discovery: strategy	**Drug discovery: assay**
Structure-based design	Fluorescence polarization assay
Pharmacokinetic profile	**In the pipeline**
NSC 66811 is cell-permeable.	Further investigation of quinolinol derivatives in mouse model is still undergoing.
References	
10, 49, 56	

(continuing)

Chemical Family: Spiro-(oxindole-3,3'-pyrrolidine)	
Structure of lead compound	**Relevant Members**
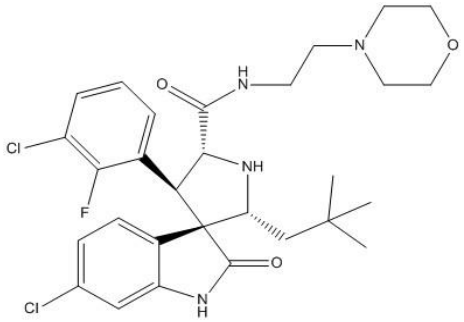 MI-63	MI-63 MI-147 MI-219 MI-319 MI-888 SAR405838 MI-1061
Drug discovery: strategy	**Drug discovery: assay**
Structure-based design *De novo* design	Fluorescence polarization assay
Pharmacokinetic profile	
Presence of fluorine group on the phenyl ring of MI-63 increased its metabolic stability. However, it was found to be unsuitable due to its poor PK properties and oral bioavailability MI-219 displays highly desirable PK properties and an improved oral bioavailability in mice. This compound also revealed minimal toxicity. MI-147 revealed to be more potent than MI-219 in cell growth inhibition and in induction of p53 activation with an improved oral bioavailability and low toxicity. Using wild type p53 xenograft of Capan-2, MI-319 revealed to be orally bioavailable, resulting in significant tumor growth inhibition without any observed toxicity in animals. No tumor inhibition was found in mutant p53 BxPC3 xenografts. MI-888 was found to be highly potent with an excellent oral PK profile and in vivo activity. This compound was capable of achieving complete and long-lasting tumor regression in animal models of human cancer upon oral administration without signs of toxicity. MI-888 revealed metabolic stability, which was confirmed in rat, mouse and human microssomes and an excellent oral bioavailability in rats. MI-1061 was orally bioavailable and showed excellent chemical stability in mice.	
In the pipeline	
MI-147 is currently undergoing preclinical studies. MI-219 and MI-319 are undergoing preclinical studies. MI-888 is undergoing phase I clinical trials. SAR405838 is undergoing phase I study to assess safety on neoplasma malignancies and a phase I study in patients with advanced cancer when combined with Pimasertib.	
References	
10, 44, 45, 57, 58, 59, 60, 61, 62, 63, 64, 65, 66, 67	

(continuing)

<table>
<tr><td colspan="2">Chemical Family: Spiro-(oxindole-3,3′-thiazolidine)</td></tr>
<tr><td>Structure of lead compound</td><td>Relevant Members</td></tr>
<tr><td> 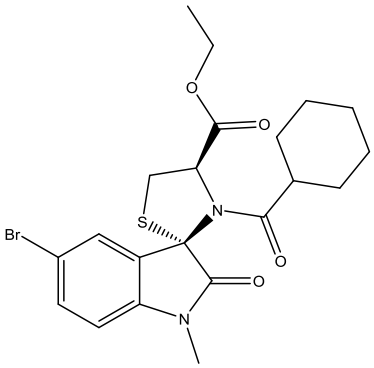

SM13</td><td>SM13
ISA27</td></tr>
<tr><td>Drug discovery: strategy</td><td>Drug discovery: assay</td></tr>
<tr><td>Structure-based design (design based on spiro-oxindole derivatives)</td><td>Antagonist induced dissociation assay (AIDA)
ImmunoSet p53:MDM2 complex ELISA</td></tr>
<tr><td>Pharmacokinetic profile</td><td>In the pipeline</td></tr>
<tr><td>-</td><td>SM13 could be a good anticancer to be used in combination with common anticancer agents and can be used as a prototype molecule for the design of more potent spirothiazolidin-based derivatives.</td></tr>
<tr><td colspan="2">References</td></tr>
<tr><td colspan="2">68, 69, 70</td></tr>
</table>

(continuing)

<table>
<tr><td colspan="2">Chemical Family: Sulfonamide</td></tr>
<tr><td>Structure of lead compound</td><td>Relevant Members</td></tr>
<tr><td> 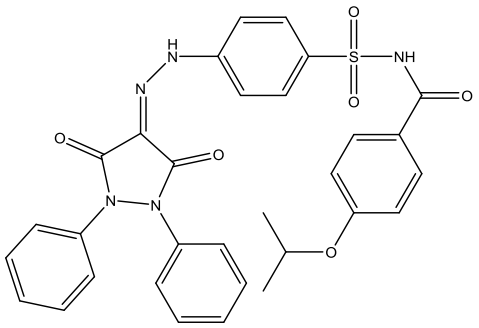
NSC 279287</td><td>NSC 279287</td></tr>
<tr><td>Drug discovery: strategy</td><td>Drug discovery: assay</td></tr>
<tr><td>Structure-based design

Pharmacophore-based virtual screening</td><td>p53 luciferase reporter assay</td></tr>
<tr><td>Pharmacokinetic profile</td><td>In the pipeline</td></tr>
<tr><td>-</td><td>NSC 279287 exhibited low binding affinity to MDM2 and its potential as anticancer drugs has not been established yet.</td></tr>
<tr><td colspan="2">References</td></tr>
<tr><td colspan="2">71</td></tr>
</table>

(continuing)

Chemical Family: Terphenyl	
Structure of lead compound	**Relevant Members**
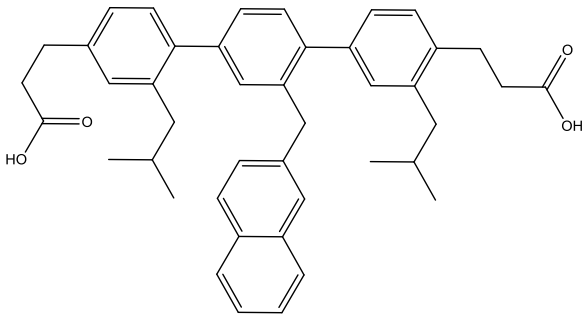 Terphenyl 1	Terphenyl 1
Drug discovery: strategy	**Drug discovery: assay**
Structure-based design	Fluorescence polarization assay
Pharmacokinetic profile	**In the pipeline**
The presence of acid group contributed to its solubility in aqueous solution.	The potential of terphenyl derivatives as anticancer drugs has not been established yet.
References	
10, 72, 73	

(continuing)

Chemical Family: Xanthone	
Structure of lead compound	**Relevant Members**
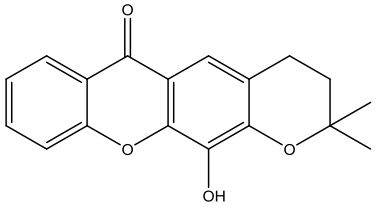 LEM1	α-Mangostin Gambogic acid Pyranoxanthone LEM1
Drug discovery: strategy	**Drug discovery: assay**
Structure-based design	Virtual screening High-throughput screening by a yeast phenotypic assay
Pharmacokinetic profile	**In the pipeline**
-	Preclinical studies, pyranoxanthone LEM1 represents a useful lead compound for the structure-based design of more potent drug-like analogs.
References	
74, 75, 76	

Table 2 – Classes of small-molecule inhibitors of p53:MDMX interaction.

Chemical Family: Benzofuroxan	
Structure of lead compound	**Relevant Members**
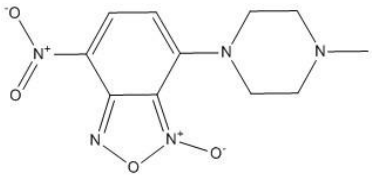 XI-006	XI-006
Drug discovery: strategy	**Drug discovery: assay**
Structure-based design	FRT-based recombinant technology Quantitative real time-PCR (qRT-PCR) assays
Pharmacokinetic profile	**In the pipeline**
XI-006 exhibited low toxicity.	Preclinical studies, XI-006 can be used as a lead compound for further development of a new class of therapeutic agents targeting MDMX.
References	
36, 77	

(continuing)

Chemical Family: Pseudourea	
Structure of lead compound	**Relevant Members**
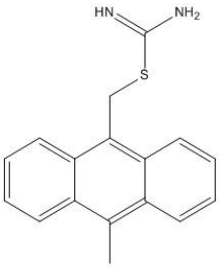 XI-011	XI-011
Drug discovery: strategy	**Drug discovery: assay**
Structure-based design	qRT-PCR assays
Pharmacokinetic profile	**In the pipeline**
XI-011 showed selectivity in decreasing viability of cancer cells without genotoxicity.	XI-011 can serve as a lead compound for further development into a therapeutic agent for breast cancer treatments.
References	
78	

(continuing)

<table>
<tr><td colspan="2">Chemical Family: Pyrazolylidene</td></tr>
<tr><td>Structure of lead compound</td><td>Relevant Members</td></tr>
<tr><td> 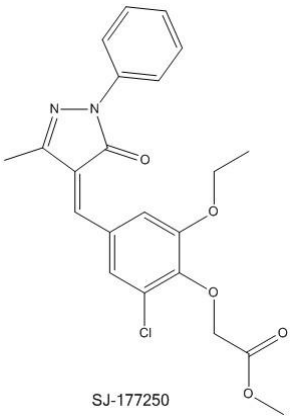

SJ-177250</td><td>SJ-177250</td></tr>
<tr><td>Drug discovery: strategy</td><td>Drug discovery: assay</td></tr>
<tr><td>Structure-based design</td><td>MDMX high throughput fluorescence polarization assay</td></tr>
<tr><td>Pharmacokinetic profile</td><td>In the pipeline</td></tr>
<tr><td>SJ-172250 exhibited chemical stability, thermal stability, undetectable redox activity and solubility, and low cell permeability.</td><td>Preclinical studies: SJ-172250 represents a lead compound with a useful chemical scaffold for further optimization of MDMX inhibitors for treatment of human tumors which overexpress MDMX.</td></tr>
<tr><td colspan="2">References</td></tr>
<tr><td colspan="2">36, 79, 80</td></tr>
</table>

1.2. Xanthones: a promising scaffold for inhibition of p53:MDM2 interaction

Xanthone derivatives comprise a class of natural products orignally isolated from plants and microrganisms[81]. From the chemical point of view, xanthones are hetero-tricyclic planar compounds which contain a dibenzo-ɣ-pyrone scaffold and they are structurally related with other compounds that contain ɣ-pyrone scaffold: flavonoids and chromones (**Figure 8**).

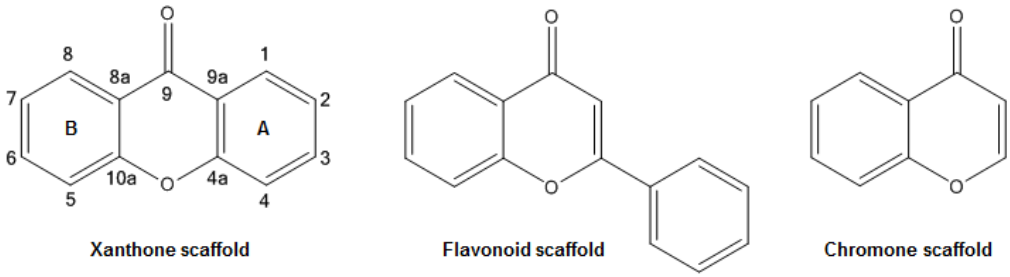

Figure 8 - Scaffolds of different classes of secondary metabolites with a dibenzo-ɣ-pyrone.

Biossynthetically, xanthones are formed through conjugation of molecular percursors of acetate pathway (ring A) and shikimate pathway (ring B). According to nature of the substituents in the dibenzo-ɣ-pyrone scaffold, xanthone can be classified into five major groups: simple oxygenated xanthones, glycosylated xanthones, prenylated xanthones and their derivatives, xanthonolignoids, and miscellaneous xanthones. Simple oxygenated xanthones can be subdivided according to their degree of oxygenation into non-, mono-, di-, tri-, tetra-, penta- and hexaoxygenated derivatives[82]. A great interest has been given to the naturally-occuring xanthones because they have been a source of bioactive compounds with different types of substituents in different positions and with a large diversity of pharmacological activities[83]. Although natural products may represent an important source of new interesting scaffolds in Medicinal Chemistry, the biossynthetic pathway of xanthones only allows the presence of certain groups in specific positions of the xanthone scaffold[81a]. Since their biosynthetic pathways are a limiting factor for the structural diversity of naturally-occuring xanthones, the use of chemical synthesis increased the possibilities of obtaining new derivatives having different nature and position of the substituents on the xanthone scaffold[84]. Furthermore, the synthesis of more diverse and complex xanthonic compounds for biological activity allows more detailed structure-activity relationship (SAR) studies.

Among the diversity of biological activities described for naturally-occuring and synthetic xanthones, their antitumor activity accompanied by an inhibitory activity on p53:MDM2 interaction has been widely reported. Among the naturally-occuring

xanthones, some compounds are remarkable anticancer agents via disruption of p53:MDM2 interaction: α-mangostin and gambogic acid (**Figure 9**). The prenylated xanthones α-mangostin and gambogic acid are obtained from the mangosteen fruit of *Garcinia mangostana* L. (Clusiaciae) and from a resin extracted from the *Garcinia hanburyi* tree (Clusiaceae), respectively[85]. Initially, the inhibitory activity of these natural products as potential inhibitors of the p53:MDM2 interaction was hypothesized based on previous studies that have shown a correlation between the cytotoxic activity of these xanthones and the activation of p53 pathway[86]. Based on a yeast-based approach, a effective procedure to search for p53:MDM2 inhibitors, α-mangostin and gambogic acid were found to revert the inhibitory effect of MDM2 on p53-induced growth inhibition and on p53-dependent transcriptional activity. The increase of p53-dependent transcriptional activity was confirmed in a MDM2-overexpressing human adenocarcinoma-derived MCF-7 tumor cell line with wild-type p53. In contrast to wild-type p53, these xanthones had no impact on growth of yeast expressing mutant p53, suggesting that, as inhibitors of p53:MDM2 interaction, α-mangostin and gambogic acid may act on MDM2. Furthermore computational docking studies performed against MDM2 indicated that the binding affinity values for these two xanthones were similar to nutlin-3a, a known inhibitor of p53:MDM2 interaction. Also the predicted binding model of these compounds indicate that these compounds adopted a pose that filled the binding site critical for interaction between the NH_2 terminal domain of p53 with the respective binding site[74].

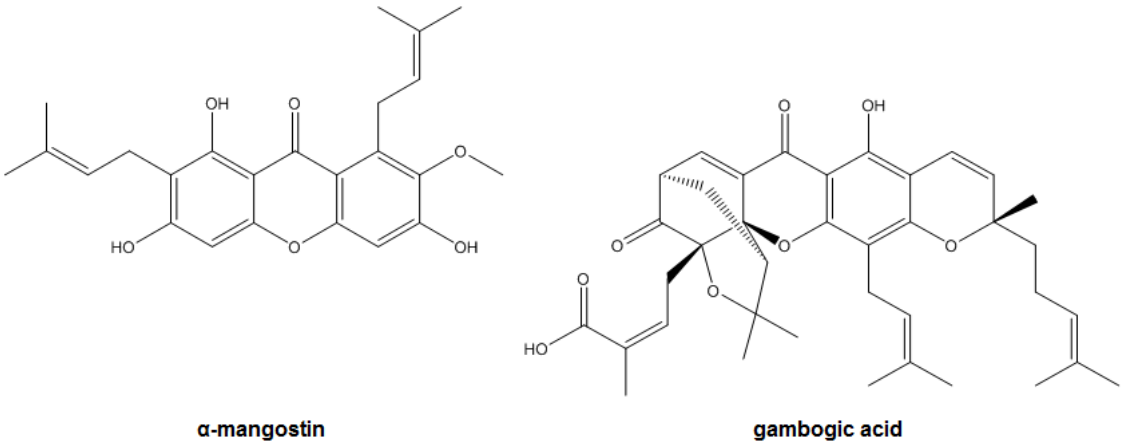

Figure 9 – Chemical structures of naturally-occuring prenylated xanthones α-mangostin and gambogic acid.

Pyranoxanthone **LEM1** was initially identified as a potential inhibitor of p53:MDM2 interaction, employing a virtual screening strategy (**Figure 10**). With the virtual screening, the most promising MDM2 ligands were identified and their inhibitory activities as inhibitors of p53:MDM2 interaction were evaluated using yeast screening assays. Among

the tested xanthones, only **LEM1** significantly reduced the MDM2 inhibitory effect on p53 activity in yeast cells co-expressing p53 and MDM2 interaction without inducing cytotoxic effects on control yeast. Also, **LEM1** reverted the MDM2 inhibitory effect on p53 transcriptional activity. The molecular mechanism of action of **LEM1** was corroborated in MDM2-overexpressing human tumor cell lines with a wild-type phenotype. In fact, **LEM1** selectively increased the p53-dependent transcriptional activity and induced the activation of p53-dependent pathway in HCT116 p53 $^{+/+}$ cell line. Therefore, **LEM1** represents a useful lead compound for the structure-based design of more potent drug-like derivatives[75].

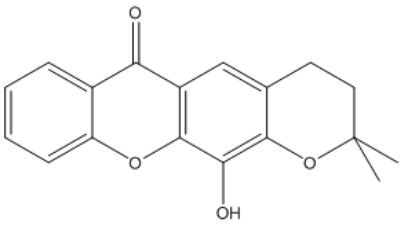

LEM1

Figure 10 – Chemical structure of pyraoxanthone **LEM1**.

CHAPTHER 2

AIMS

CHAPTER 2 - AIMS

Xanthone derivatives have been reported as promising antitumor agents and, in the last years, molecular modifications on xanthone scaffold were performed in order to obtain new and potent small-molecules with antitumor activity. In fact, some of the xanthones with antitumor activity have also shown to be potent inhibitors of p53:MDM2 interaction: the naturally-occurring xanthones, α-mangostin and gambogic acid, and the synthetic xanthone **LEM1**.

α-Mangostin and gambogic acid are naturally occurring prenylated xanthones which are isolated from the mangosteen fruit of *Garcinia mangostana* L. (Clusiaceae) and from the resin of *Garcinia hanburyi* Hook.f. (Clusiaceae), respectively. **LEM1** is a prenylated xanthone synthetized by our research group (CEQUIMED-UP). The effectiveness of these molecules as promising antitumor agents with the ability to disrupt p53:MDM2 interaction was shown in yeast-screening assays and also in several human tumor cell lines[74-75]. Recently, 3,4-dimethoxy-9-oxo-9*H*-xanthene-1-carbaldehyde (**LEM2**) has displayed an inhibitory activity on p73:MDM2 interaction in a p53-null human colon carcinoma tumor cell line expressing p73 (not p53 and p63)*. The carbaldehydic xanthone **LEM2** may represent a promising anticancer agent to be explored in cancer therapy.

Based on these considerations, the main aim of the present dissertation consisted in the synthesis of a library of aminoxanthone derivatives of **LEM2** by a process of reductive amination (**Figure 11**).

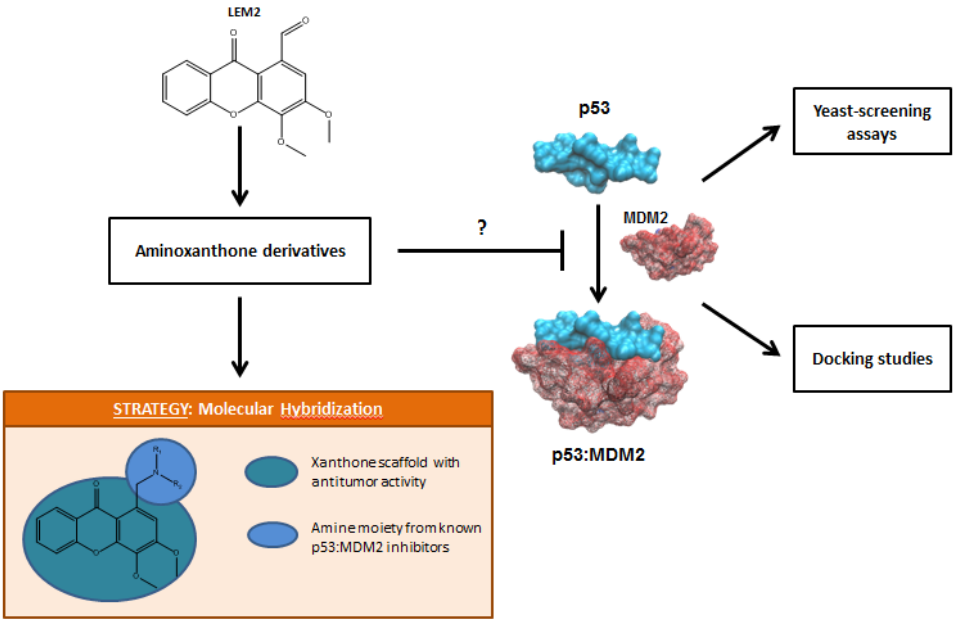

Figure 11 - Schematic representation of the main aims of the present dissertation.

* Ramos, H., Leão, M., Soares, J., Raimundo L., Queiroz, G., Brandão, P., Pinto, M., Sousa, E., Saraiva, L."LEM2: a new small-molecule inhibitor of the p73:MDM2 interaction". Book of Abstracts-8th Meeting of Young Researchers of University of Porto, 13-15 May 2015, p.165.

To synthesize the diverse derivatives, a scale-up of the synthesis of carbaldehydic xanthone **LEM2** was followed. The planning strategy consisted in applying a molecular hybridization approach. Based on known small-molecule inhibitors of p53:MDM2 interaction, amine moieties of these inhibitors were selected for conjugation with the carbaldehydic xanthone **LEM2**. The introduction of these amines in the aminoxanthone derivatives simultaneously will present the combination of a priviliged moiety of antitumor activity (xanthone scaffold) and a pharmacophoric moiety of inhibitory activity on p53:MDM2 interaction (amine moiety).

The amines used for reductive amination resulted from a selection of the amine moieties contained in the structure of known inhibitors of p53:MDM2 interaction (**Figure 12**). The replacement of the carbonyl group of **LEM2** by an amine moiety of the aminoxanthone derivatives may contribute to the establishment of additional interactions to the active site of MDM2, improving their binding affinity and their pharmacodynamic profile. Besides that, the introduction of an amine moiety may result in a potential enhancement of drug-like properties, as water solubility, a crucial requirement for the identification of promising drug candidates.

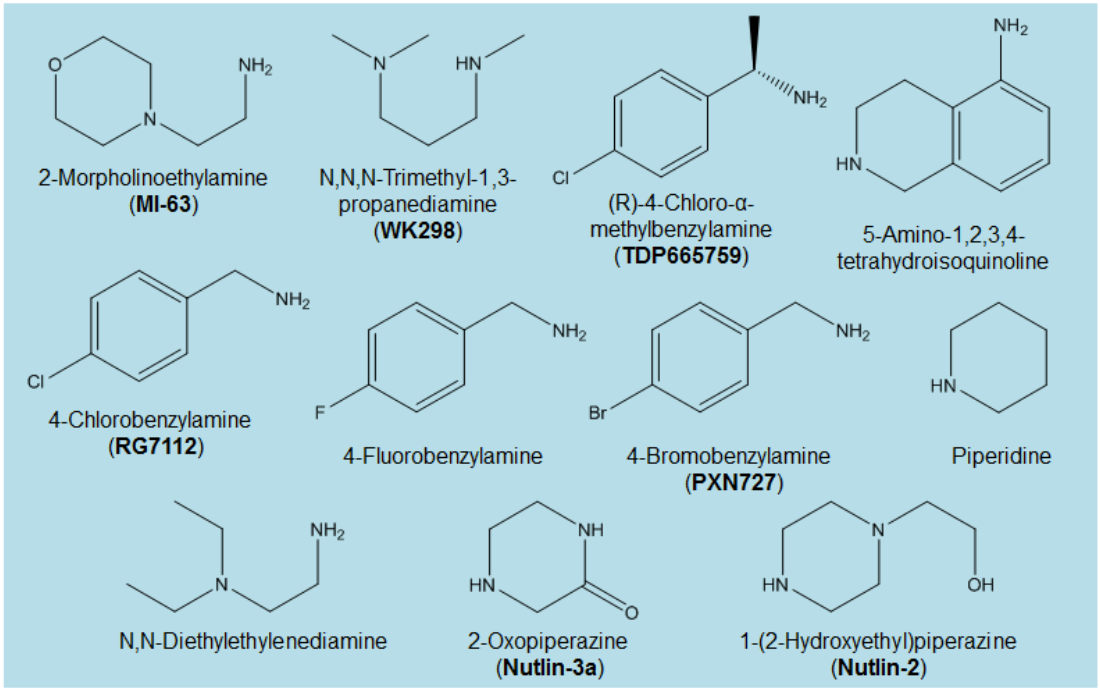

Figure 12 – Selected amines from known p53:MDM2 inhibitors for reductive amination and respective p53:MDM2 inhibitors

In silico studies were also performed with the objective of predicting and ranking the binding affinity of the aminoxanthone derivatives against MDM2. To confirm the docking results, the investigation of the potential of these derivatives to disrupt p53:MDM2 interaction was assessed using yeast-screening assays.

CHAPTER 3

RESULTS AND DISCUSSION

CHAPTER 3 – RESULTS AND DISCUSSION

3.1. Synthesis of the carbaldehydic xanthone LEM2

LEM2 is synthetic carbaldehydic xanthone which has displayed an inhibitory activity of p73:MDM2 interaction in a p53-null human colon carcinoma tumor cell line expressing p73 (not p53 and p63)*.

The previous synthetic pathway in obtaining the carbaldehydic xanthone **LEM2**, described on **Scheme 1**, consisted of five reaction steps: (1) a Friedel-Crafts acylation using aluminum chloride as an acid catalyst; (2) a nucleophilic addition followed by an elimination of methanol under basic conditions and microwave heating; (3) a selective demethylation of the methoxyl group at position 4 using as a dealkylating agent aluminium chloride; (4) a Duff formylation at position 1 using hexamethylenetetramine as a formyl group source; (5) a methylation of the phenolic hydroxyl group at position 4 with methyl sulfate (unpublished results).

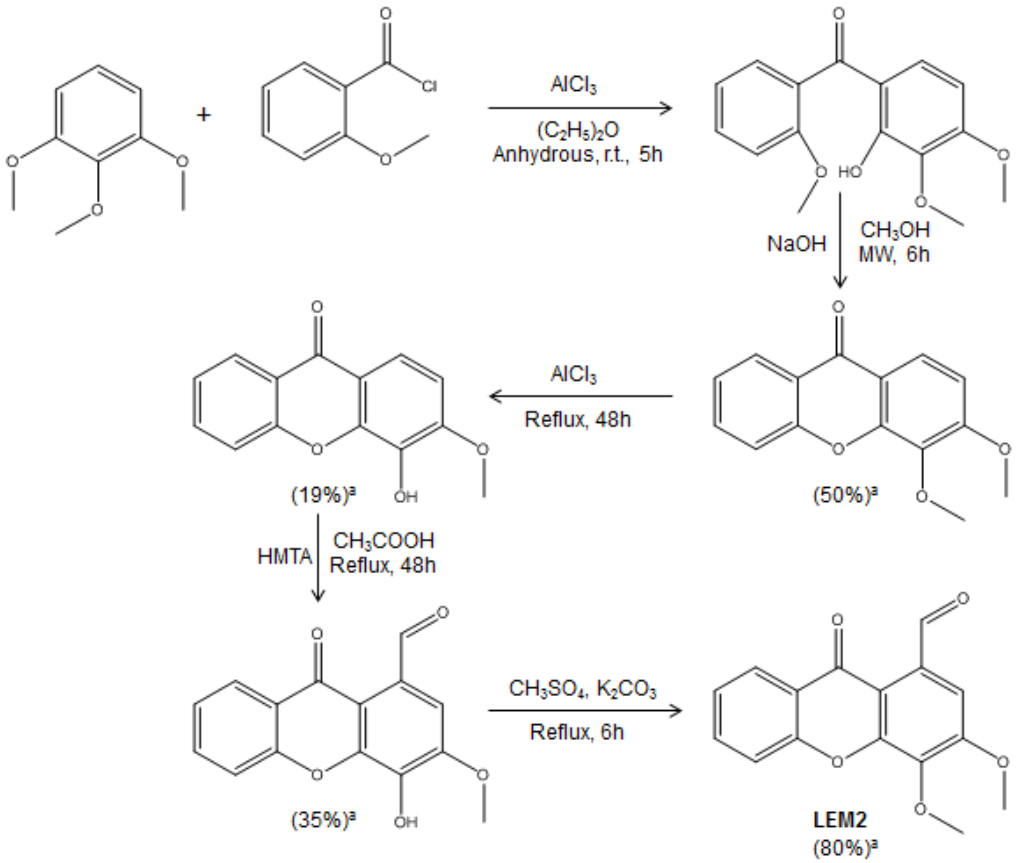

Scheme 1 – Different reaction steps of the previous synthesis of carbaldehydic xanthone **LEM2**. HMTA = hexamethylenetetramine; r.t. = room temperature; MW = microwave. [a] isolated yields.

* Ramos, H., Leão, M., Soares, J., Raimundo L., Queiroz, G., Brandão, P., Pinto, M., Sousa, E., Saraiva, L."LEM2: a new small-molecule inhibitor of the p73:MDM2 interaction". Book of Abstracts-8th Meeting of Young Researchers of University of Porto, 13-15 May 2015, p.165.

The high number of reaction steps needed to synthesize the carbaldehydic xanthone **LEM2** as well as the low overall yield of the process demanded a synthetic pathway more appropriate for scale-up with a lower number of reaction steps. The alternative synthetic pathway of **LEM2** consisted in obtaining the carbaldehyde from an appropriate methyl derivative and four reaction steps were needed as will be described below.

3.1.1. Synthesis of the benzophenone intermediate 3, (2-hydroxy-3,4-dimethoxy-6-methylphenyl) methoxyphenyl) methanone

The synthesis of benzophenone intermediates suitable as precursors for cyclisation of xanthones is achieved at room temperature by the Friedel-Crafts acylation of methoxybenzene derivatives with the properly substituted benzoyl chloride in the presence of a Lewis acid, as aluminium chloride (**Scheme 2**). To obtain benzophenone intermediate **3**, aluminium chloride anhydrous was added to a dry diethyl ether solution of 2-methoxybenzoyl chloride (**2**) and trimethoxytoluene (**3**). After completing the reaction, the suspension was acidified with HCl (5M) to convert the phenolate group of the benzophenone derivative to a non-ionized form. Then, the non-ionized form of the benzophenone derivative was extracted with chloroform. A brown oil which contains the final product was obtained and used without further purification processes to the next reaction step.

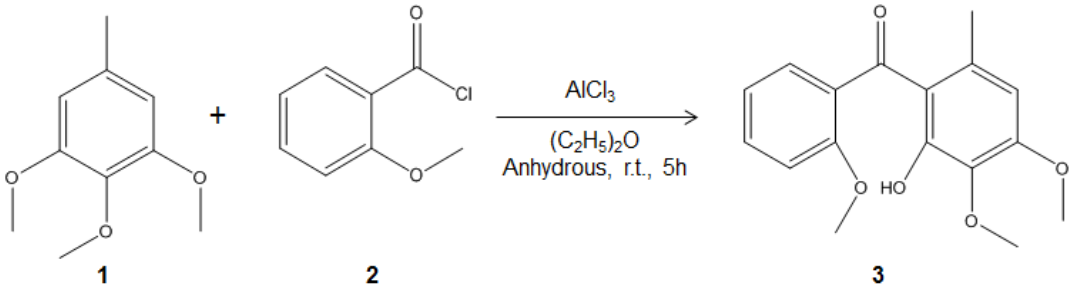

1 2 3

Scheme 2 - Friedel-crafts acylation of trimethoxytoluene (**1**) with 2-methoxybenzoyl chloride (**2**) to obtain benzophenone intermediate **3**. r.t. = room temperature.

3.1.2. Synthesis of 3,4-diethyl-1-methyl-9*H*-xanthen-9-one (4): cyclization of benzophenone intermediate 3

The benzophenone intermediate **3** contained in the crude product formed in the previous reaction was then cyclized to a xanthone intermediate through a reaction that involves a nucleophilic addition followed by an elimination of methanol (**Scheme 3**).

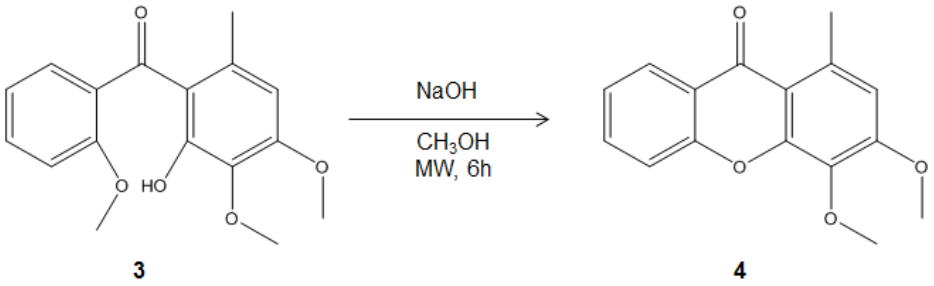

Scheme 3 – Cyclization of the benzophenone intermediate **3** to xanthone intermediate **4**. MW = microwave.

The cyclization of benzophenone intermediates is time-consuming when performed under conventional heating. In this context, the use of microwave heating constituted an alternative approach of obtaining the xanthone intermediate **4**, demanding lower reaction times when compared to conventional heating[87]. The reaction of cyclization was undergone in basic solution, contributing to the deprotonation of acidic phenolic hydroxyl group and the subsequent nucleophilic addition. A white solid insoluble in basic solution was formed and contained the xanthone intermediate **4.** After completing the reaction, the solid was trapped by a vacuum filtration. The intermediate **4** contained in solid was identified by comparing with a standard sample after crystallization. Since a great amount of xanthone intermediate **4** can be lost by crystallization, the impure white solid containing the intermediate **4** was used for next reaction step.

3.1.3. Synthesis of 1-(dibromomethyl)-3,4-dimethoxy-9*H*-xanthen-9-one (5)

The synthesis of the dibrominated xanthone intermediate **5** can be accomplished by a benzylic bromination (Vohl-Ziegler reaction) of xanthone intermediate **4** catalyzed by free radicals (**Scheme 4**). The oxygen-oxygen bond of benzoyl peroxide is weak, and so benzoyl peroxide (BPO) can readily undergo homolytic cleavage, forming reactive free radicals which act as initiators of the reaction of benzylic bromination. *N*-bromosuccinimide (NBS) is a reactant extensively used in these radical reactions as a source of bromine radicals[88]. The reaction was performed under reflux (85°C) using carbon tetrachloride as solvent. In the course of reaction, by analysis of TLC plate, an intense spot corresponding to the dibrominated xanthone intermediate **5** was forming. At the same time, the intensity of the spot corresponding to xanthone intermediate **4** was diminishing, which indicated that the starting material in this reaction was being consumed. After completing, a vacuum filtration was carried out to trap some non-soluble impurities. The dibrominated xanthone intermediate **5** was exclusively found in the mother liquor. Based on TLC analysis, it was observed the presence of several spots in mother

liquor and so an additional step of purification was required. In this context, a flash column chromatography was performed as a strategy of purification of intermediate **5**.

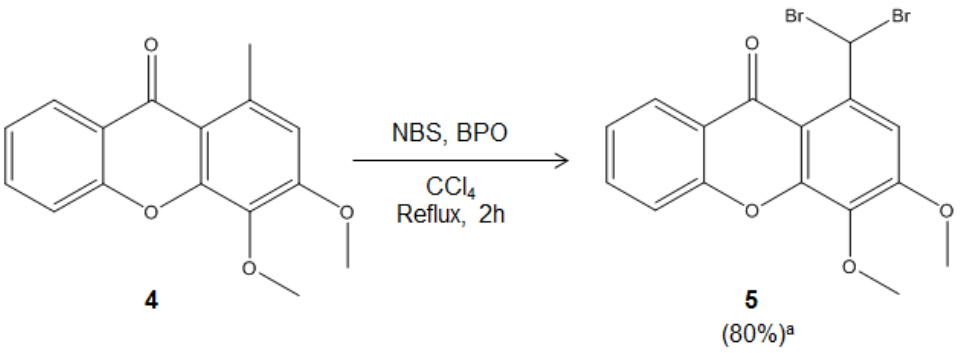

Scheme 4 – Vohl-Ziegler reaction: synthesis of dibrominated xanthone intermediate **5** from xanthone intermediate **4** by a benzylic bromination catalyzed by free radicals. NBS = *N*-bromosuccinimide; BPO = benzoyl peroxide. [a] isolated yield.

The reaction conditions described in this section were planned for the synthesis of the monobrominated derivative instead of dibrominated xanthone intermediate **5**, according to a previously described procedure[89]. The high yield of the referred reaction (80%) indicated that a dibromination of xanthone intermediate **4** was the preferential pathway based on the reaction conditions employed. The identity of products **3-5** were confirmed by TLC comparing with standards previously obtained (unpublished results).

3.1.4. Synthesis of 3,4-dimethoxy-9-oxo-9*H*-xanthene-1-carbaldehyde (LEM2)

As in the previous reaction step, a dibrominated intermediate was preferentially synthesized, a debromination reaction step was needed to convert the intermediate **5** into a monobrominated xanthone derivative to proceed with an oxidation to the carbaldehydic xanthone **LEM2**. On literature, it was found a promising strategy of selective debromination promoted by an ionic liquid[90]. The ionic liquids have been extensively used in organic synthesis for last few years. They are classified as green solvents since they are non-flammable, non-volatile and recyclable[91]. However, according to the procedure described on literature, there are some considerations that should be taken into account: (1) the experimental procedure for selective debromination was employed for α-dibromoketones and the intermediate **5** is a ɣ-dibromoketone; (2) the reaction was performed under conventional heating (100°C) and not under microwave heating; (3) the ionic liquid used in this reaction was 1-butyl-3-methylimidazolium tetrafluoroborate [(BMIm)BF_4], instead of 1-methyl-3-pentylimidazolium tetrafluoroborate [(pmIm)BF_4] described in literature. In the course of the reaction, an intense spot with a different Rf of

the xanthone intermediate **5** was forming, while the spot corresponding to intermediate **5** was progressively disappearing. After finishing the reaction, the crude material was submitted to a liquid-liquid extraction with ethyl acetate in order to remove the ionic liquid and the water used in this reaction. A flash column chromatography was performed to remove the impurities contained on the crude material. It was hypothesized that the intense spot found on TLC plate corresponded to the monobrominated intermediate. Surprisingly, structural elucidation techniques have shown that the product formed was the carbaldehydic xanthone **LEM2**. According to these unexpected results, it is hypothesized that a solvolytic displacement of the intermediate **5** using water and [(BMIm)BF_4] was the preferential pathway instead of a debromination pathway[92] (**Scheme 5**).

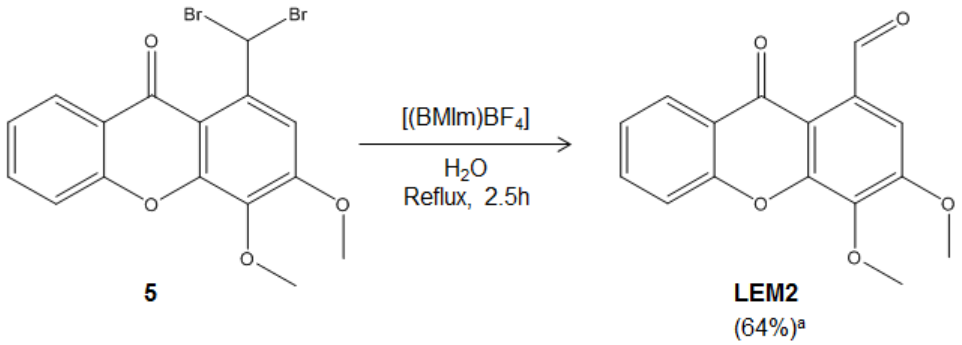

Scheme 5 - Synthesis of carbaldehydic xanthone **LEM2** by a solvolytic displacement of dibrominated xanthone intermediate **5** using water and ionic liquid as solvents. [(BMIm)BF_4] = 1-butyl-3-methylimidazolium tetrafluoroborate. [a] isolated yield.

3.2. Synthesis of aminoxanthone derivatives

Several strategies to synthesize a library of aminoxanthone derivatives were employed using different reaction conditions. Regardless of the different reaction conditions used, the aminoxanthone derivatives were obtained by reductive amination of the carbaldehydic xanthone **LEM2**. The general reaction is represented in **Scheme 6**.

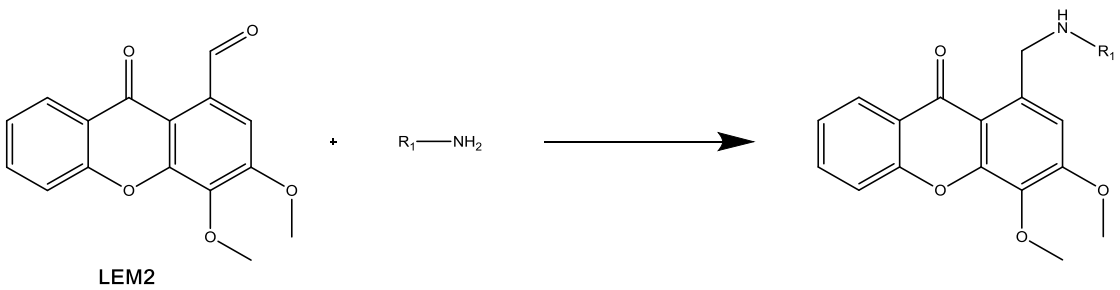

Scheme 6 – General reaction of reductive amination of **LEM2** with a primary amine.

The reductive aminations or reductive alkylations are among the most useful and important strategies in the synthesis of different kinds of amines. In fact, reductive amination is in the top 10 reactions most used to obtain drug candidates[93]. The aminoxanthone derivatives were synthesized in a one pot conversion resulting from the reaction of the carbonyl group of the carbaldehydic xanthone **LEM2** with the amines, in the presence of a reducing agent. In the mechanistic point of view (**Scheme 7**), the condensation reaction of **LEM2** (**6**) with the amine (**7**) initiates by a nucleophilic addition of the amine group to the electrophilic carbon of the carbonyl group of **LEM2**, leading to the formation of the intermediate hemiaminal, also called carbinolamine (**8**), which is generally unstable and cannot be isolated. The carbinolamine intermediate **8** is then dehydrated by protonation of its hydroxyl group to form the intermediate **9**, a Schiff base (an imine or an enamine, if the reactant is a primary or secondary amine, respectively). Subsequently, the intermediate Schiff base is reduced to furnish the alkylated amine product (**10**). In fact, in the presence of a suitable reducing agent, the reaction of **LEM2** with a primary amine yields a secondary amine, via an imine intermediate and the reaction with a secondary amine yields a tertiary amine, via an enamine intermediate[94]. The reductive amination with tertiary amines is not mechanistically possible.

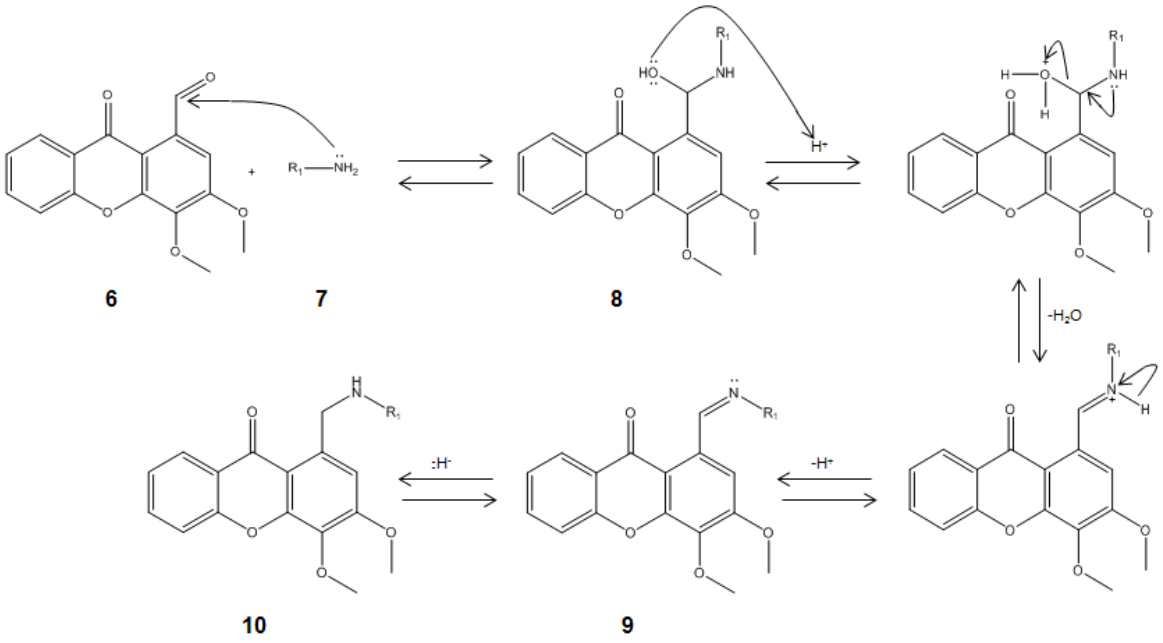

Scheme 7– Mechanism of the reaction of the carbaldehydic xanthone **LEM2** (**6**) with a primary amine (**7**), via an imine intermediate (**9**), to yield a secondary amine (**10**), in presence of suitable reducing agents.

The reductive amination reactions can be described as direct reactions, when a carbonylated compound and the amine are mixed with a suitable reducing agent without prior formation of the intermediate Schiff base, and indirect reactions, when the reductive

amination occurs in two separated steps: the formation of intermediate Schiff base followed by reduction to obtain the final product[94].

In case of direct reductive aminations, the choice of a reducing agent is crucial for the success of these reactions, because a suitable reducing must reduce the intermediate Schiff base selectively over carbonylated compounds. A better understanding of the characteristics of the each reducing agent is essential to select the most favorable reaction conditions for the synthesis of a library of aminoxanthone derivatives of carbaldehydic xanthone **LEM2**.

Initially, a solid-supported reactant containing borohydride (MP-BH_4) was used since previously it was successfully used in our research group to synthesize an aminoxanthone derivative (unpublished results). Nevertheless, under the conditions described in **Scheme 8**, the carbaldehydic xanthone **LEM2** was not completely consumed and the reduction of the carbonyl group to the alcohol derivative of **LEM2** (**11**) was the preferential synthetic pathway. In fact, the major product formed in the course of reaction was isolated by a column chromatography and spectroscopic techniques have shown that the product formed was 1-(hydroxymethyl)-3,4-dimethoxy-9*H*-xanthen-9-one (**11**). The reaction yield of formation of the alcohol derivative was not determined.

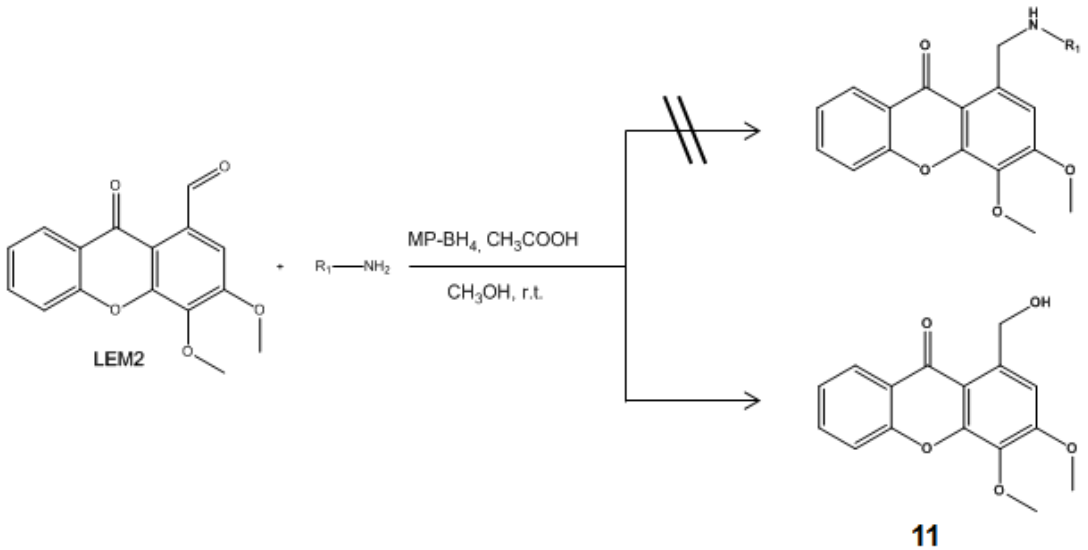

Scheme 8 – Reaction conditions employed for reductive amination of the carbaldehydic xanthone **LEM2**, using MP-BH_4 as a reducing agent and methanol as solvent. r.t. = room temperature.

In fact, according to the literature, sodium borohydride ($NaBH_4$) is not suitable for direct reductive aminations, since $NaBH_4$ reduces the Schiff base intermediates in the same manner that it reduces the carbonyl group of the carbonylated compounds[95]. For that reason, alternative reducing agents need to be used in order to overcome the lack of selectivity of $NaBH_4$. The application of the selective sodium cyanoborohydride

($NaBH_3CN$) has emerged as a successful approach, however the toxicity associated to the reducing agent limits its use in reductive aminations[96]. Another selective reducing agent, sodium triacetoxyborohydride [$NaBH(OAc)_3$], is selective in direct reductive aminations and constitutes an appealing alternative to surmount the toxicity issues of $NaBH_3CN$. The replacement of cyano group of $NaBH_3CN$ with acetoxy groups of $NaBH(OAc)_3$ lead to an increased safety. Structurally, the steric and the electron-withdrawing effects of the three acetoxy groups stabilize the B-H bond and are responsible for its mild reducing properties[94].

In this context, a different procedure for synthesis of aminoxanthone derivatives was employed in order to promote a full consumption of **LEM2** and avoid the undesirable reduction of the carbonyl group. The reaction conditions described in **Scheme 9**, using the sodium triacetoxyborohydride/tetrahydrofuran system, allowed a total consumption of the carbalhdehydic xanthone **LEM2**, favoring the amination synthetic pathway.

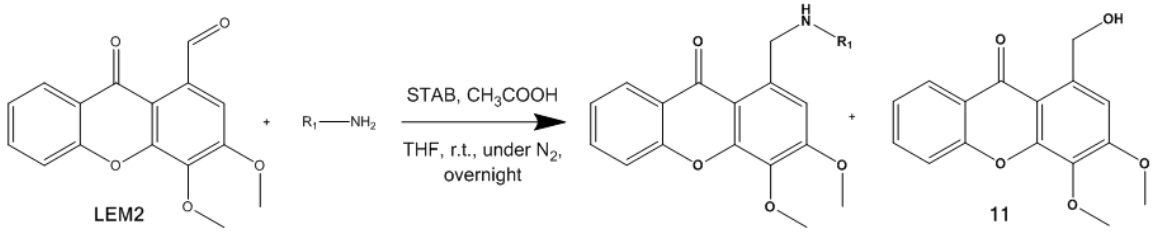

Scheme 9 – General reaction of reductive amination of the carbaldehydic xanthone **LEM2**, using STAB as a reducing agent and THF as solvent. THF = tetrahydrofuran, r.t. = room temperature, STAB = sodium triacetoxyborohydride.

For monitoring the synthesis of aminoxanthone derivatives by TLC, two different chromatographic systems were used, one to observe the disappearance of the carbaldehydic xanthone **LEM2** (*n*-hexane/ethyl acetate, 7:3) and another to visualize both amine precursor and the appearance of the desired product (methanol/TEA, 100:0.1 for amines **12-18**, chloroform/acetone/TEA, 5:5:0.1 for amines **19-22**). The syntheses of each derivative were grouped according to the structural similarity of the aminoxanthone derivatives: (1) alkylated linear, (2) heterocyclic and (3) halogenated aromatic aminoxanthone derivatives. The general work-up of these derivatives is outlined on **Scheme 10**.

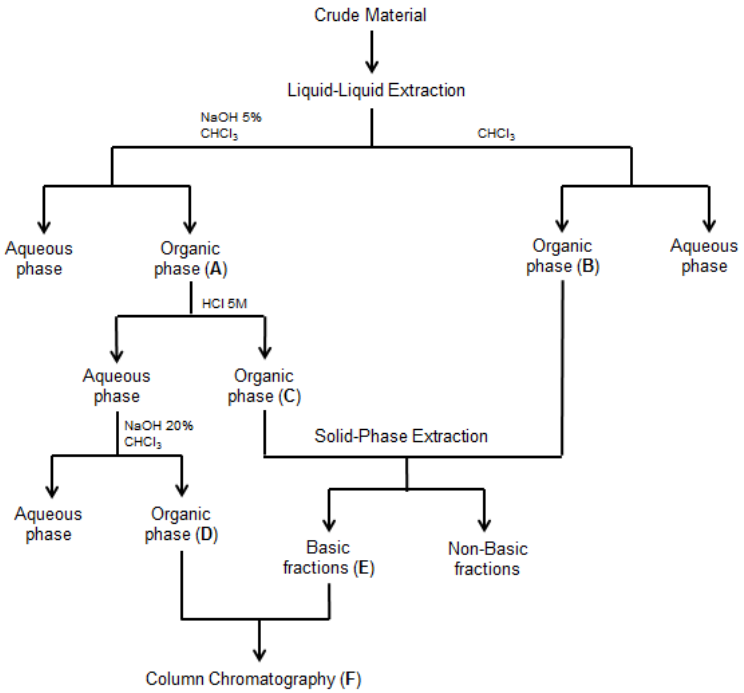

Scheme 10 – General reaction work-up of the new synthesized aminoxanthone derivatives **12-22**. (A) Amines **12, 13, 15, 19, 20, 21, 22**, (B) amines **14, 16, 17, 18**; (C) amines **19, 20, 21, 22**; (D) amines **12, 13, 15**; (E) amines **14, 17, 18, 19, 20, 21, 22**; (F) amines **12, 13, 14**.

3.2.1. Synthesis of alkylated linear aminoxanthone derivatives

With this procedure described in **Scheme 11**, three alkylated linear derivatives were obtained: 3,4-dimethoxy-1-(((2-morpholinoethyl)amino)methyl)-9*H*-xanthen-9-one (**12**), 1-(((3-(dimethylamino)propyl)(methyl)amino)methyl)-3,4-dimethoxy-9*H*-xanthen-9-one (**13**) and 1-(((2-(diethylamino)ethyl)amino)methyl)-3,4-dimethoxy-9*H*-xanthen-9-one (**14**), in 56%, 62%, and 40% yield respectively.

The alkylated linear aminoxanthone derivatives **12-14** were visualized by UV revelation at 254 and 365 nm. By chemical revelation with ninhydrin, only the secondary amines **12** and **14** were observed. Similar purification strategies were employed to purify the crude material containing each aminoxanthone derivative.

The amines **12** and **13** were purified by a liquid-liquid extraction under acidic and basic solutions. Initially, the crude material was basified in order to convert the amines to their non-ionized form and extracted with chloroform to remove the water-soluble reducing agent. An extraction with acid was performed to eliminate the non-basic impurities and the non-ionized amines were then recovered by basification and subsequent extraction with chloroform. In a different manner, the purification of **14** was carried out by a liquid-liquid extraction with water and chloroform. The resulting organic phase was then subjected to a solid-phase extraction (SPE) with a cation exchange cartridge to separate the basic

amines from the non-basic impurities, as the alcohol derivative **11**. According to this procedure, the amine **14** and its precursor were trapped on the cartridge due to their basicity and the non-basic impurities were eluted first. Then, the desired product was removed from the cartridge with extraction with basic solution. However, these two different purification approaches revealed to be insufficient for amines **12**, **13** and **14** because the amine precursors were not separated from respective products. In fact, a chromatography flash cartridge was performed in order to eliminate the amine precursors and obtain pure aminoxanthone derivatives.

The similarity of reaction yields between aminoxanthones **12** and **13** may reflect the same work-up procedures performed for these amines. A lower yield obtained for amine **14** may be justified by purification approach applied.

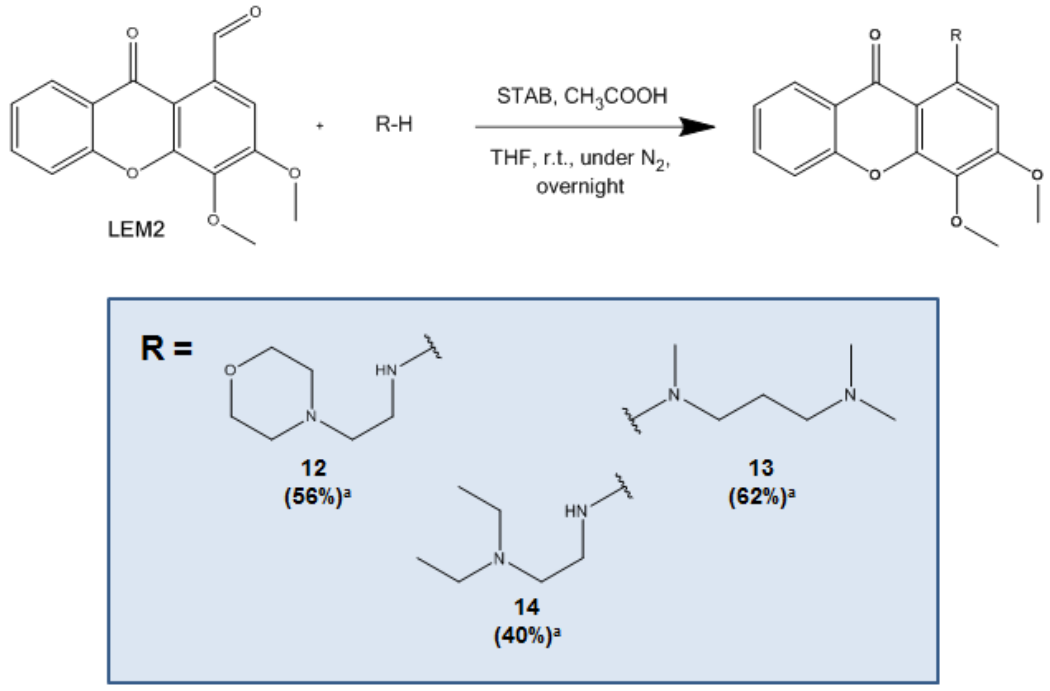

Scheme 11 – Synthesis of alkylated linear aminoxanthone derivatives from carbaldehydic xanthone **LEM2**. THF = tetrahydrofuran, r.t. = room temperature. [a] isolated yields.

3.2.2. Synthesis of heterocyclic aminoxanthone derivatives

Based on the reaction conditions described in **Scheme 12** and the experimental procedure, it was obtained four heterocyclic aminoxanthone derivatives: 1-((4-(2-hydroxyethyl)piperazin-1-yl)methyl)-3,4-dimethoxy-9*H*-xanthen-9-one (**15**), 4-((3,4-dimethoxy-9-oxo-9*H*-xanthen-1-yl)methyl)piperazin-2-one (**16**), 1-((5-amino-3,4-dihydroisoquinolin-2(1*H*)-yl)methyl)-3,4-dimethoxy-9*H*-xanthen-9-one (**17**) and 3,4-

dimethoxy-1-(piperidine-1-ylmethyl)-9*H*-xanthen-9-one (**18**) in 68%, 35%, 36%, and 58% respectively.

The tertiary heterocyclic aminoxanthone derivatives were only identifiable after UV revelation at 254 and 365 nm. Despite structural similarities of these heterocyclic aminoxanthones, different purification techniques were employed.

In case of amine **15**, a liquid-liquid extraction with acidic and basic solutions was carried out in an identical way of amines **12** and **13**. After this procedure, it was expectable the presence of the impurity corresponding to the amine precursor of **15**. Surprisingly, chemical revelation by ninhydrin did not identify the secondary amine precursor, which indicated that the liquid-liquid extraction was sufficient for a total purification of amine **15**. Probably, the water solubility of 1-(2-hydroxyethyl)piperazine, the amine precursor of **15**, allowed a prior elimination in the initial aqueous phase of liquid-liquid extraction.

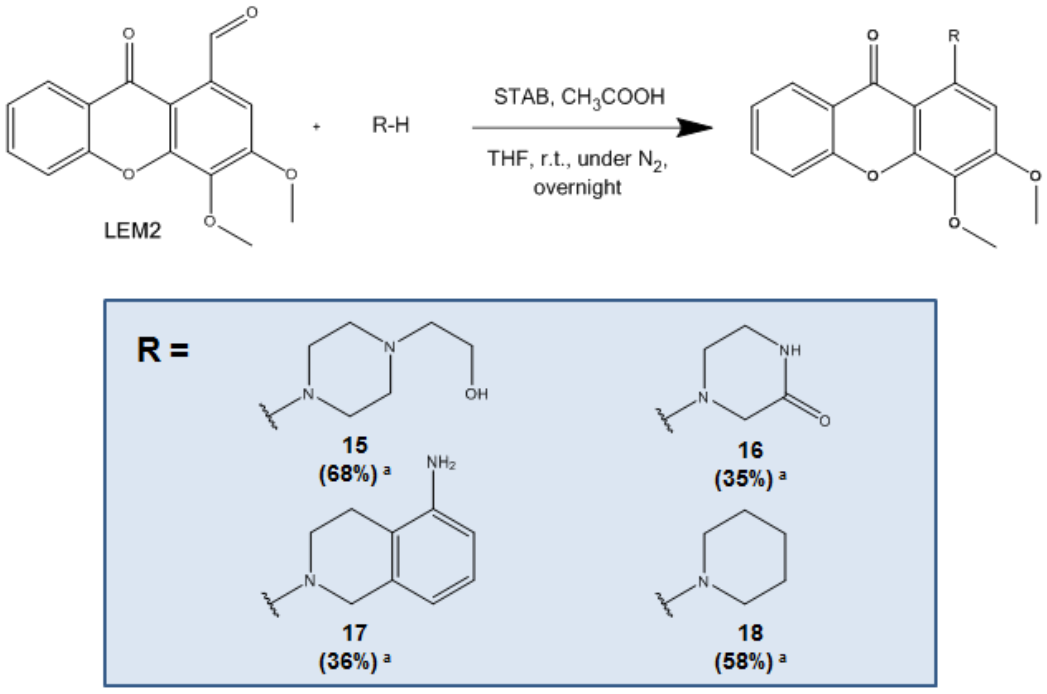

Scheme 12 – Synthesis of heterocyclic aminoxanthone derivatives from carbaldehydic xanthone **LEM2**. THF = tetrahydrofuran, r.t. = room temperature. [a] isolated yields.

The work-up of amines **17** and **18** consisted of a liquid-liquid extraction with water and chloroform to eliminate the water soluble sodium triacetoxyborohydride. In case of amine **16**, a liquid-liquid extraction with acidic and basic solution could destabilize the lactam ring of the aminoxanthone derivative. To avoid the hydrolysis of the lactam ring, the crude material was subjected to an identical work-up of **17** and **18**. The resulting organic phase containing each derivative was further purified by a SPE with a cation exchanger cartridge. Particularly, for amine **17**, the fractions eluted with basic solution

(NH_3 2% in methanol) were gathered and the compound was crystallized from the solvent mixture. The structure of **17** proposed in **Scheme 12** was confirmed by spectroscopic techniques. The preferential conjugation with the heterocyclic amine group was expectable since an aromatic amine group did not have its non-bonding electron pair available to proceed to nucleophilic addition to carbonyl group of **LEM2**. In case of amines **16** and **18**, the SPE allowed a total purification of these derivatives without any further procedures. These evidences were checked by the absence of the secondary amine precursors of **16** (2-oxopiperazine) and **18** (piperidine) after ninhydrin revelation. Probably, the water solubility of 2-oxopiperazine and piperidine allowed a prior removal from the aqueous phase on liquid-liquid extraction.

3.2.3. Synthesis of halogenated aromatic aminoxanthone derivatives

Based on the reaction conditions described in **Scheme 13** and the experimental procedure, four halogenated aromatic aminoxanthone derivatives were obtained: 1-(((4-fluorobenzyl)amino)methyl)-3,4-dimethoxy-9*H*-xanthen-9-one (**19**), 1-(((4-chlorobenzyl) amino)methyl)-3,4-dimethoxy-9*H*-xanthen-9-one (**20**), 1-(((1-(4-chlorophenyl)ethyl)amino) methyl)-3,4-dimethoxy-9*H*-xanthen-9-one (**21**) and 1-(((4-bromobenzyl)amino)methyl)-3,4-dimethoxy-9*H*-xanthen-9-one (**22**) in 40%, 57%, 63%, and 70% yield respectively.

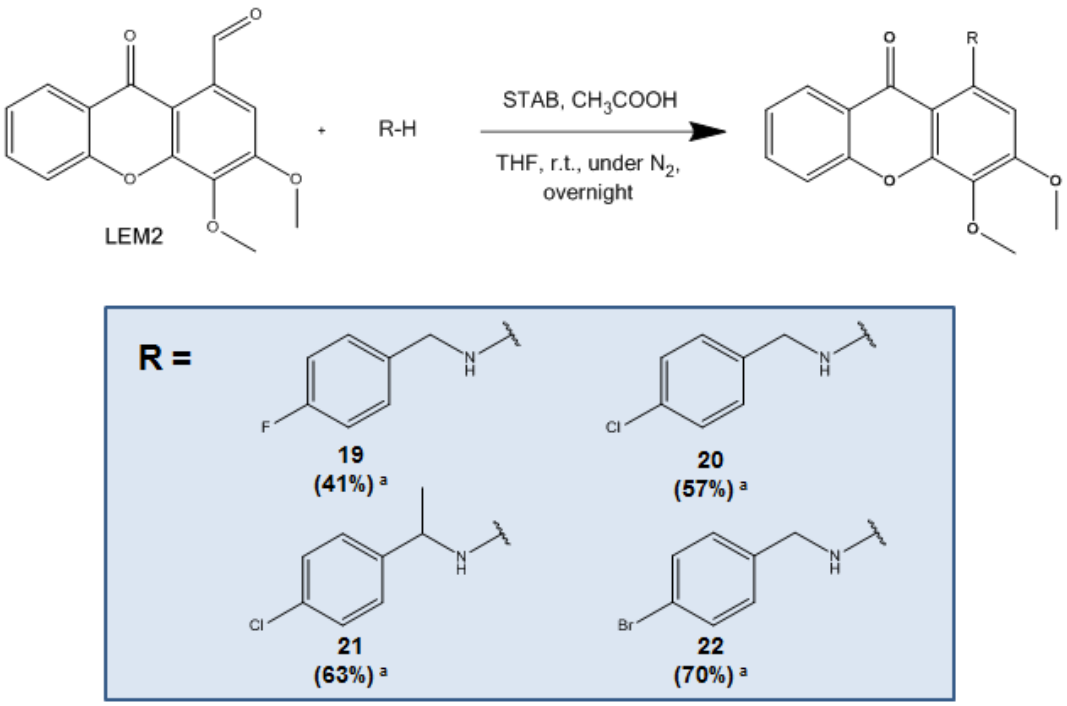

Scheme 13 – Synthesis of halogenated aromatic aminoxanthone derivatives from carbaldehydic xanthone **LEM2**. THF = tetrahydrofuran, r.t. = room temperature. [a] isolated yields.

The synthesis of this group of halogenated aromatic aminoxanthones was controlled by a chromatographic system (chloroform/acetone/TEA, 5:5:0.1) different from

the used for the other two groups (methanol/TEA, 100:0.1). The secondary halogenated aromatic aminoxanthone derivatives were easily identifiable after UV and chemical revelation with ninhydrin. In a similar manner of **12**, **13** and **15**, the purification strategy was based on a liquid-liquid extraction with acidic and basic solutions in order to remove the reducing agent and the non-basic impurities present in crude material. Surprisingly, it was evidenced that, upon extraction with acid solution, the halogenated aromatic aminoxanthones **19**, **20**, **21** and **22** remained exclusively in the chloroform phase, but their amine precursors were easily converted to their ionized-form. Probably, the halogenated aromatic aminoxanthones present a lower basicity than the respective amine precursors and this difference of basicity allowed an efficient separation of both aminoxanthones and amine precursors by using this procedure. However, additional purification techniques were employed to separate the non-basic impurities from the halogenated aromatic aminoxanthone derivatives contained the chloroform phase. To achieve this goal, a SPE with a cation exchange cartridge allowed an initial elimination of the non-basic impurities such as the alcohol derivative **11**. Then, the aminoxanthone derivatives were eluted with basic solution and the pure fractions were gathered.

According to the reaction yields, it was observed an increased yield with the decrease of electronegativity of the halogen atom. In fact, a higher yield was obtained for synthesis of amine **22** and, comparing the electronegativity of halogen atoms, the bromine is the least electronegative. The lower electronegativity of the *para* halogen atom may reflect in a lower electron-withdrawing inductive effect and, consequently, in a higher availability of the non-bonding electron pair of the amine group to undergo a nucleophilic addition to the carbonyl group of the carbaldehydic xanthone **LEM2.**

3.3. Strucuture elucidation

The structure characterization of new synthesized aminoxanthone derivatives as well as the alcohol derivative of **LEM2**, **11**, was established for the first time by melting points determination, IR, NMR and MS techniques. In this section, it will be presented IR, ^{1}H and ^{13}C NMR data for the carbaldehydic xanthone **LEM2** and their derivatives.

3.3.1. IR spectroscopy data

The IR data for carbaldehydic xanthone **LEM2** indicates the presence of, a band corresponding to the C=O at 1649 cm^{-1}, as well as, bands corresponding to the C=C at aromatic bond typical from the xanthone scaffold at 1580, 1464, 1320 and 1132 cm^{-1}. An additional band corresponding to the aldehydic C=O bond at 1684 cm^{-1} was observed in IR spectrum. For the alcohol derivative **11** and the aminoxanthone derivatives **12**-**22**, a similarity of IR spectrum profile was observed when compared to **LEM2** (**Table 3**).

Table 3 - IR data for **LEM2** and derivatives **11**-**22**.

Compounds	Group	ν (cm^{-1})
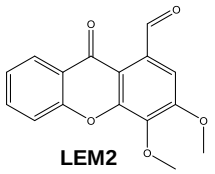 **LEM2**	C-H	2927
	Aldehydic C=O	1684
	C=O	1649
	C=C (Ar)	1580, 1464, 1320, 1132
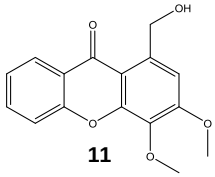 **11**	O-H	3460
	C-H	2938
	C=O	1618
	C-C (Ar)	1584, 1466, 1327, 1130
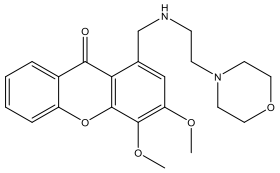 **12**	N-H	3303
	C-H	2925, 2853
	C=O	1615
	C-N	1257
	C-C (Ar)	1470, 1328, 1146
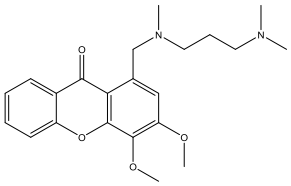 **13**	C-H	2938, 2785
	C=O	1615
	C-N	1259
	C-C (Ar)	1464, 1346, 1154
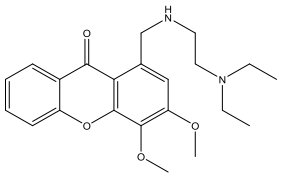 **14**	N-H	3316
	C-H	2940, 2841
	C=O	1615
	C-N	1258
	C-C (Ar)	1585, 1467, 1312, 1131
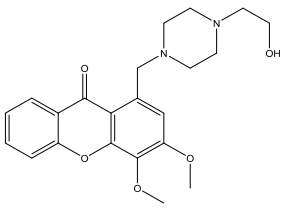 **15**	O-H	3423
	C-H	2932, 2804
	C=O	1617
	C-N	1256
	C-C (Ar)	1586, 1466, 1345, 1160
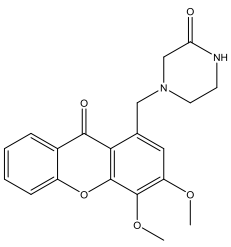 **16**	N-H (amide)	3280
	C-H	2923, 2852
	C=O (amide)	1675
	C=O	1617
	C-N	1259
	C-C (Ar)	1585, 1465, 1379, 1129

(continuing)

Compounds	Group	ν (cm^{-1})
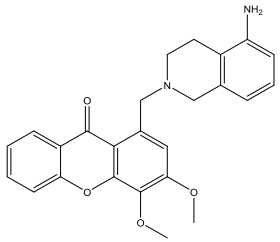 **17**	N-H (aromatic)	3387
	C-H	2927, 2866
	C=O	1617
	C-N	1257
	C-C (Ar)	1466, 1343, 1130
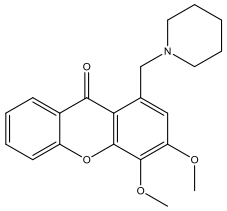 **18**	C-H	2929, 2853
	C=O	1618
	C-N	1257
	C-C (Ar)	1585, 1467, 1346, 1131
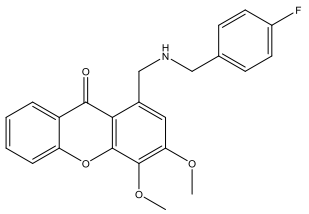 **19**	N-H	3322
	C-H	2921, 2853
	C=O	1614
	C-N	1260
	C-C (Ar)	1584, 1467, 1193, 1132
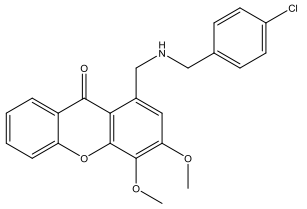 **20**	N-H	3315
	C-H	2919, 2847
	C=O	1615
	C-N	1258
	C-C (Ar)	1499, 1464, 1317, 1150
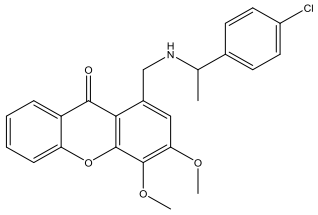 **21**	N-H	3310
	C-H	2936, 2730
	C=O	1616
	C-N	1260
	C-C (Ar)	1496, 1466, 1347, 1132
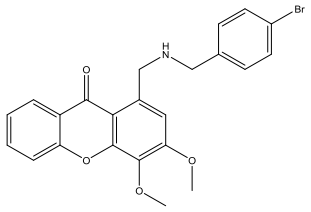 **22**	N-H	3317
	C-H	2919, 2850
	C=O	1613
	C-N	1256
	C-C (Ar)	1467, 1329, 1132

Comparing the IR spectrum of **11** with **LEM2**, the detection of a new band at 3460 cm^{-1} corresponding to a O-H bond in amine **11** spectrum and not the band corresponding to the aldehydic C=O of **LEM2** bond put in evidence the hypothesized transformation. In this case, the IR data confirmed that the formyl group of **LEM2** was reduced to a hydroxyl group. Since the different aminoxanthones were synthesized by conjugation of the amines with the formyl group of **LEM2**, it was expectable some differences on the IR spectrum profile as a consequence of the conversion of the carbonyl group of the carbaldehyde to an amine derivative. In fact, according to data provided by **Table 3**, the band characteristic of aldehydic C=O group is only present in **LEM2** spectrum and the detection of new bands characteristic of a C-N bond (and N-H bond for secondary aminoxanthone derivatives) evidenced for all aminoxanthones indicated that the reductive amination of the formyl group of **LEM2** was successfully accomplished.

3.3.2. Carbaldehydic xanthone LEM2 and alcohol derivative 11

3.3.2.1. ^{1}H NMR for LEM2 and alcohol derivative 11

The data corresponding to the ^{1}H NMR of **LEM2** and amine **11** is represented in **Table 4**.

Table 4 - ^{1}H NMR data* for **LEM2** and alcohol derivative **11.**

	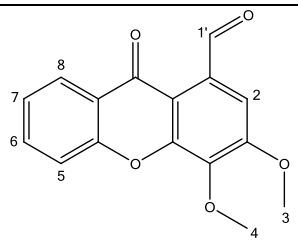 **LEM2**	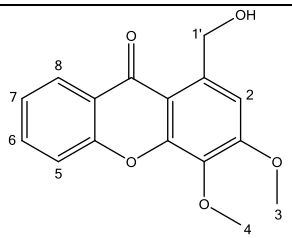 **11**
Protons	**δ_H**	**δ_H**
H-1’	11.21, 1H, s	4.95, 2H, s
H-8	8.31, 1H, dd, *J*=8.0 and 1.7	8.32, 1H, dd, *J*=8.0 and 1.7
H-6	7.77, 1H, ddd, *J*=8.5, 7.0 and 1.7	7.75, 1H, ddd, *J*=8.5, 7.0 and 1.7
H-5	7.60, 1H, dd, *J*=8.5 and 0.8	7.56, 1H, dd, *J*=8.5 and 0.9
H-2	7.56, 1H, s	6.98, 1H, s
H-7	7.43, 1H, ddd, *J*=8.0, 7.0 and 0.8	7.41, 1H, ddd, *J*=8.0, 7.0 and 0.9
H-4	4.11, 3H, s	4.04, 3H, s
H-3	4.07, 3H, s	4.02, 3H, s

*****Values in ppm (δ_H) relative to $(CH_3)_4Si$ as an internal reference. *J* values are in Hz.

The ^{1}H NMR spectrum of **LEM2** shows the presence of five signals corresponding to the five aromatic protons, namely H-2, H-5, H-6, H-7, and H-8 (δ_H 7.43-8.31 ppm). The aromatic protons most deshielded are the protons H-6 and H-8. The electron-withdrawing

effect of carbonyl group (C-9) for resonance contributes to an electronic deprotection of *orto* (H-8) and *para* (H-6) positions of the aromatic ring. The magnetic anisotropy of carbonyl group (C-9) deshields preferentially the proton H-8, which explains the higher chemical shift of proton H-8 in relation to H-6. The signal with the highest chemical shift value corresponds to the aldehydic proton H-1' (δ_H =11.21 ppm) due to magnetic anisotropy and electron-withdrawing effects of the carbonyl group of the carbaldehyde. The protons corresponding to the methoxyl groups (H-3 and H-4) are equivalent for each methoxyl group. In spite of their similarity, the protons H-4 present a slightly higher chemical shift than the protons H-3. This evidence was confirmed by heteronuclear single quantum correlation (HSQC) and heteronuclear multiple bond correlation (HMBC) techniques.

Analysing the ^{1}H NMR spectrum of **11**, the multiplicity and coupling constants of the four aromatic protons (H-5, H-6, H-7, and H-8) of the aromatic region of the xanthone scaffold (δ_H ranging from 7.41 to 8.32 ppm) as well as the six protons of the methoxyl group (δ_{H-3} 4.02 ppm; δ_{H-4} 4.04 ppm) were similar to **LEM2**. However, a decrease in chemical shift value for aromatic proton H-2 of **11** was observed. In the carbaldehydic xanthone **LEM2**, the aromatic proton H-2 is subjected to the deshielding effect of *orto* formyl group. The conversion of the carbonyl group to hydroxyl group contributes to the elimination of the deshielding effect at *orto* position. Also, the absence of signal corresponding to the carbonyl group of **LEM2** and the appearance of a singlet corresponding to the methylene group (-CH_2-) was evidenced on ^{1}H NMR spectrum (δ_H 4.95 ppm). This evidence confirmed the reduction of the carbaldehydic xanthone **LEM2**.

3.3.2.2. ^{13}C NMR for LEM2 and alcohol derivative 11

The data corresponding to the ^{13}C NMR of **LEM2** and amine **11** is represented in **Table 5**.

The ^{13}C NMR spectrum for **LEM2** revealed the presence of two signals with the highest chemical shifts corresponding to the carbons of carbonyl groups (δ_{C-9}=177.9 ppm; $\delta_{C-1'}$=192.8 ppm). It is also possible the visualization of signals corresponding to the carbons of the xanthone scaffold (values of δ_C between 108 and 156 ppm, corresponding to the remaining twelve carbons. The two carbons corresponding to the methoxyl groups present the lowest chemical shifts.

Table 5 – ^{13}C NMR data* for **LEM2** and alcohol derivative **11**

	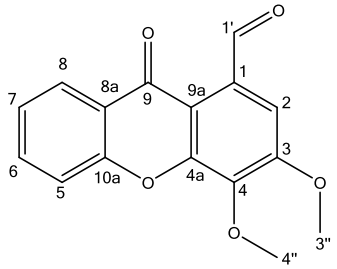 **LEM2**	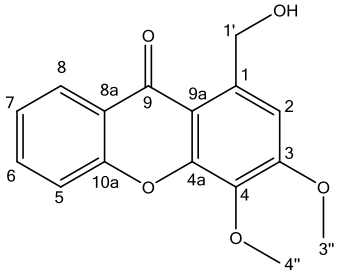 **11**
Carbons	**δ_C**	**δ_C**
C-1’	192.8	65.7
C-9	177.9	179.0
C-3	156.3	156.7
C-10a	155.5	155.4
C-4a	150.9	152.3
C-4	140.7	136.1
C-6	135.1	134.9
C-1	133.5	139.3
C-8	126.7	126.7
C-7	124.5	124.2
C-8a	121.9	121.9
C-5	117.8	117.7
C-9a	116.1	114.8
C-2	108.5	110.3
C-4’’	61.8	61.6
C-3’’	56.6	56.4

*****Values in ppm (δ_C) relative to $(CH_3)_4Si$ as an internal reference.

For **LEM2**, ^{13}C NMR assignments of the hydrogenated carbons were determined by HSQC and the carbon atoms not directly bonded to hydrogen atoms were deduced by HMBC experiments. The data provided by HMBC spectrum confirmed the structure of the carbaldehydic xanthone **LEM2** (**Figure 13**).

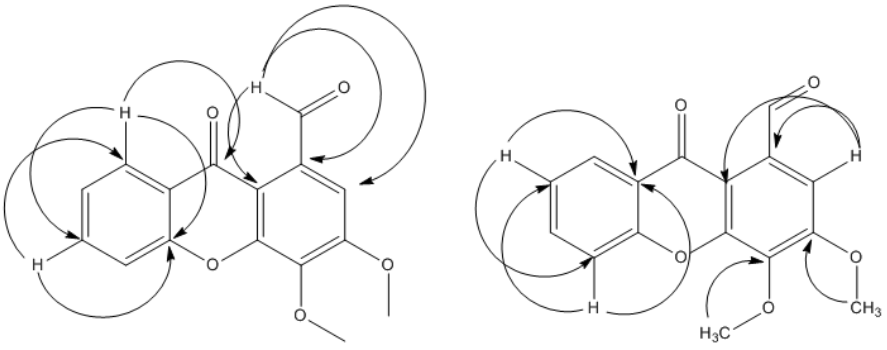

LEM2

Figure 13 – Correlations detected in HMBC spectrum for compound **LEM2**.

The ^{13}C NMR spectrum of **11** exhibited a similar profile of the respective precursor. In fact, the chemical shifts of the thirteen carbon atoms of the xanthone scaffold and the

two carbons of the methoxyl groups of **11** are almost equivalent. However, the carbon 1 in **11** presented a higher chemical shift value ($\delta_{C\text{-}1}$ 139.3 ppm) than in **LEM2** ($\delta_{C\text{-}1}$ 133.5 ppm)**.** Also, the appearance of a signal corresponding to the carbon of methylene group ($\delta_{C\text{-}1'}$ 65.7 ppm) evidenced that the conjugation between the starting material and the amine building block occurred.

3.3.3. Alkylated linear aminoxanthone derivatives: 12, 13, and 14

3.3.3.1. ^{1}H NMR for amines 12, 13, and 14

The ^{1}H NMR spectra of alkylated linear aminoxanthone derivatives (**Table 6**) displayed signals with similar chemical shifts of precursor **LEM2** corresponding to the aromatic protons H-5, H-6, H-7, and H-8 (δ_H values between 7.4 and 8.3 ppm) and to the six protons of the methoxyl groups H-3 and H-4 (δ_H values ranging from 4.0 to 4.1 ppm). For **12** and **14**, it was observed a decrease in chemical shift value for aromatic proton H-2 (**12**: $\delta_{H\text{-}2}$ 7.09 ppm; **14**: $\delta_{H\text{-}2}$ 7.14 ppm).

Table 6 - ^{1}H NMR data* for amines **12**, **13,** and **14**.

	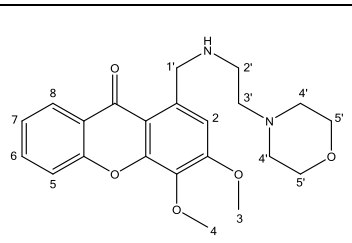 **12**	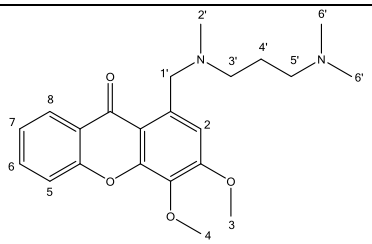 **13**	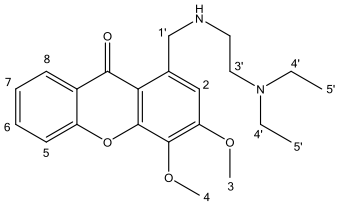 **14**
Protons	**δ_H**	**δ_H**	**δ_H**
H-8	8.25, 1H, dd, *J*=8.0 and 1.6	8.25, 1H, dd, *J*=8.0 and 1.6	8.27, 1H, dd, *J*=8.0 and 1.6
H-6	7.72, 1H, ddd, *J*=8.4, 7.0 and 1.6	7.69, 1H, ddd, *J*=8.5, 7.0 and 1.6	7.71, 1H, ddd, *J*=8.5, 7.0 and 1.6
H-5	7.57, 1H, dd, *J*=8.4, 0.9	7.54, 1H, dd, *J*=8.5 and 0.9	7.56, 1H, dd, *J*=8.5 and 0.9
H-7	7.38, 1H, ddd, *J*= 8.0, 7.0 and 0.9	7.35, 1H, ddd, *J*=8.0, 7.0 and 0.9	7.37, 1H, ddd, *J*=8.0, 7.0 and 0.9
H-2	7.09, 1H, s	7.53, 1H, s	7.14, 1H, s
H-1’	4.34, 2H, s	4.36, 2H, s	4.39, 2H, s
H-4	4.04, 3H, s	4.05, 3H, s	4.05, 3H. s
H-3	4.01, 3H, s	4.02, 3H, s	4.01, 3H, s
H-5’	3.66, 4H, t, *J*= 4.6	2.44, 2H, t, *J*=7.3	1.01, 6H, t, *J*=7.1
H-2’	2.90, 2H, t, *J*= 6.1	2.39, 3H, s	2.87, 2H, t, *J*=6.4
H-3’	2.60, 2H, t, *J*= 6.1	2.65, 2H, t, *J*=7.3	2.68, 2H, t, *J*=6.4
H-4’	2.47, 4H, t, *J*= 4.6	1.82, 2H, q, *J*=7.3	2.55, 4H, q, *J*=7.1
H-6’	-	2.28, 6H, s	-

*****Values in ppm (δ_H) relative to $(CH_3)_4Si$ as an internal reference. *J* values are in Hz.

Overall, the absence of the signal corresponding to an aldehydic proton and the presence of a singlet corresponding to the two protons H-1’ of methylene group (-CH_2-)

evidences the successful reductive amination of **LEM2** with the respective amine precursors.

The methylene groups appear at δ_H 4.34 (s, CH_2) ppm for **12**, δ_H 4.36 (s, CH_2) ppm for **13** and δ_H 4.39 (s, CH_2) ppm for **14**. The signal corresponding to the N-H group was not observed for the secondary amines **12** and **14**.

3.3.3.2. ^{13}C NMR for amines 12, 13, and 14

The ^{13}C NMR spectra for compounds **12**, **13,** and **14** (**Table 7**) displayed signals corresponding to the carbons atoms of the carbonyl group (C-9), the two aromatic rings (δ_C ranging from 110 to 157 ppm), the two methoxyl groups at position 3'' and 4'' and the carbon atoms of the aminated chain.

Table 7 – ^{13}C NMR data* for amines **12**, **13**, and **14.**

	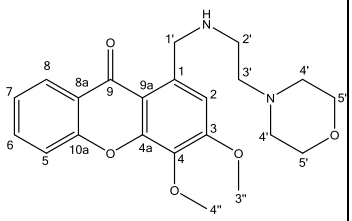 **12**	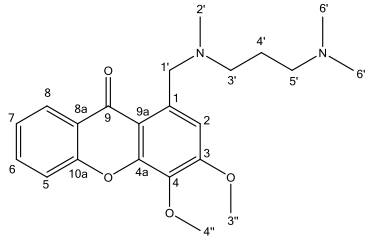 **13**	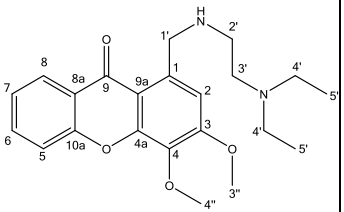 **14**
Carbons	**δ_C**	**δ_C**	**δ_C**
C-9	178.0	178.1	178.1
C-3	156.5	156.6	156.5
C-10a	155.3	155.2	155.3
C-4a	152.1	151.9	152.1
C-4	137.0	136.7	137.4
C-1	136.0	135.0	135.8
C-6	134.6	134.2	134.5
C-8	126.5	126.6	126.6
C-7	124.1	123.9	124.0
C-8a	122.1	122.4	122.2
C-5	117.7	117.6	117.7
C-9a	114.6	114.5	114.5
C-2	111.6	109.0	111.1
C-5'	67.0	57.8	11.6
C-4''	61.5	61.5	61.5
C-2'	57.4	42.5	46.8
C-3''	56.4	56.4	56.4
C-1'	53.7	60.1	52.4
C-4'	53.5	25.3	46.9
C-3'	45.3	56.1	53.4

*****Values in ppm (δ_C) relative to $(CH_3)_4Si$ as an internal reference.

The presence of a signal corresponding to the carbon atom of the methylene group (-CH_2-) that appear at δ_C 53.7 ppm for **12**, at δ_C 60.1 ppm for **13**, and at δ_C 52.4 ppm for

14 puts in evidence the successful coupling of the carbaldehydic xanthone **LEM2** with each amine precursor. The remaining signals corresponding to the carbons of the amine moiety presented lower chemical shifts when compared to the carbons of the xanthone scaffold (δ_C ranging from 45.3 to 67.0 ppm for **12**, δ_C ranging from 25.3 to 57.8 ppm for **13**, and δ_C ranging from 11.6 to 53.4 ppm for **14**).

3.3.4. Heterocyclic aminoxanthone derivatives: 15, 16, 17, and 18

3.3.4.1. ^{1}H NMR for amines 15, 16, 17, and 18

The data corresponding to the ^{1}H NMR of amines **15**, **16**, **17,** and **18** is represented in **Table 8** and **Table 9**.

Table 8 - ^{1}H NMR data* for amines **15** and **16**.

	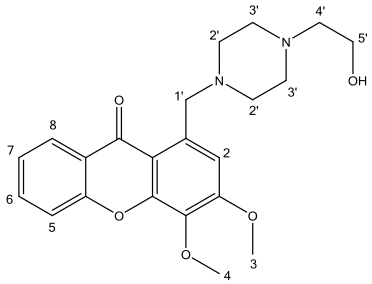 **15**	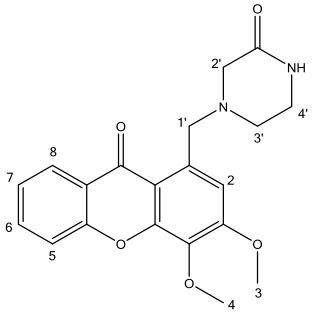 **16**
Protons	**δ_H**	**δ_H**
H-8	8.25, 1H, dd, *J*=8.0 and 1.6	8.13, 1H, dd, *J*=8.0 and 1.6
H-6	7.68, 1H, ddd, *J*=8.5, 7.0 and 1.6	7.82, 1H, ddd, *J*=8.5, 7.0 and 1.6
H-5	7.53, 1H, dd, *J*=8.5 and 0.9	7.65, 1H, dd, *J*=8.5 and 0.8
H-2	7.48, 1H, s	7.36, 1H, s
H-7	7.35, 1H, ddd, *J*=8.0, 7.0 and 0.9	7.45, 1H, ddd, *J*=8.0, 7.0 and 0.8
H-1’	4.32, 2H, s	4.24, 2H, s
H-4	4.03, 3H, s	3.98, 3H, s
H-3	4.01, 3H, s	3.90, 3H, s
H-5’	3.63, 2H, t, *J*=5.4	-
H-2’	2.68, 4H, m	3.13, 2H, s
H-3’	2.63, 4H, m	3.20, 2H, t, *J*=5.3
H-4’	2.58, 2H, t, *J*=5.4	2.66, 2H, t, *J*=5.3

*****Values in ppm (δ_H) relative to $(CH_3)_4Si$ as an internal reference. *J* values are in Hz.

The ^{1}H NMR spectra of heterocyclic aminoxanthone derivatives exhibited the presence of signals with identical chemical shifts of precursor **LEM2** which corresponded to the five aromatic protons H-2, H-5, H-6, H-7, and H-8 (δ_H values between 7.3 and 8.3) of the xanthone scaffold and to the six protons of the methoxyl groups H-3 and H-4 (δ_H values ranging from 3.9 to 4.1 ppm).

Table 9 - ^{1}H NMR data* for amines **17** and **18**.

	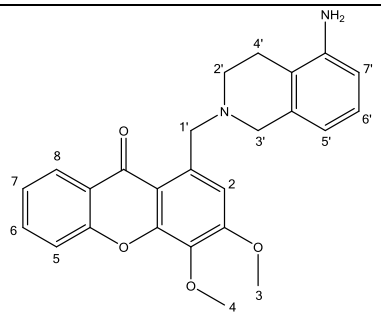 **17**	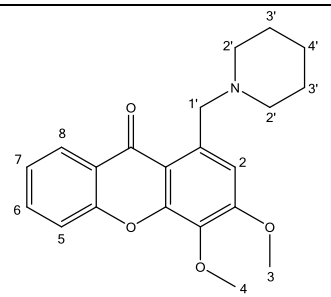 **18**
Protons	**δ_H**	**δ_H**
H-8	8.26, 1H, dd, *J*=8.0 and 1.5	8.25, 1H, dd, *J*=8.0 and 1.6
H-6	7.69, 1H, ddd, *J*=8.5, 7.0 and 1.5	7.66, 1H, ddd, *J*=8.5, 7.1 and 1.6
H-2	7.57, 1H, s	7.56, 1H, s
H-5	7.54, 1H, dd, *J*=8.5 and 0.9	7.57, 1H, dd, *J*=8.5 and 0.8
H-7	7.35, 1H, ddd, *J*=8.0, 7.0 and 0.9	7.33, 1H, ddd, *J*=8.0, 7.1 and 0.8
H-6'	6.99, 1H, t, *J*=7.7	-
H-7'	6.57, 1H, d, *J*=7.7	-
H-5'	6.53, 1H, d, *J*=7.7	-
H-1'	4.48, 2H, s	4.26, 2H, s
H-4	4.02, 3H, s	4.03, 3H, s
H-3	3.97, 3H, s	4.01, 3H, s
H-3'	3.81, 2H, s	1.65, 4H, q, *J*=5.3
H-2'	2.93, 2H, t, *J*=6.0	2.57, 4H, t, *J*=5.3
H-4'	2.66, 2H, t, *J*=6.0	1.50, 2H, q, *J*=5.3

*****Values in ppm (δ_H) relative to $(CH_3)_4Si$ as an internal reference. *J* values are in Hz.

As expectable, the absence of signal of an aldehydic proton and the presence of a singlet of the two protons H-1' of the methylene group (-CH_2) evidenced the success of the synthesis of these derivatives by reductive amination on formyl group of **LEM2**. The methylene group appears at δ_H 4.32 (s, CH_2) ppm for **15**, δ_H 4.24 (s, CH_2) ppm for **16**, δ_H 4.48 (s, CH_2) ppm for **17**, and δ_H 4.26 (s, CH_2) ppm for **18**. The remaining signals characteristic of the protons of the four aminated chains were observed at lower chemical shifts. The signals corresponding to aromatic amine group of **17** (-NH_2) and the N-H group of the lactam ring of **16** were not observed in the ^{1}H NMR spectra.

3.3.4.2. ^{13}C NMR for amines 15, 16, 17, and 18

The ^{13}C NMR spectra for compounds **15**, **16**, **17,** and **18** (**Table 10** and **Table 11**) revealed the presence of signals corresponding to the carbons atoms of the carbonyl group (C-9), the two aromatic rings (δ_C values ranging from 108 to 157 ppm) and the two methoxyl groups at position 3'' and 4'' (δ_C values between 56 and 62 ppm).

Table 10 - ^{13}C NMR data* for amines **15** and **16.**

	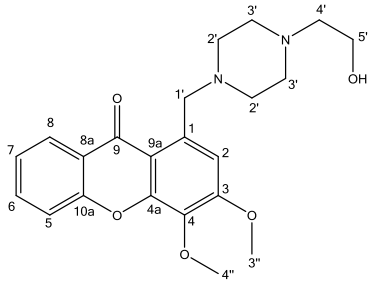 **15**	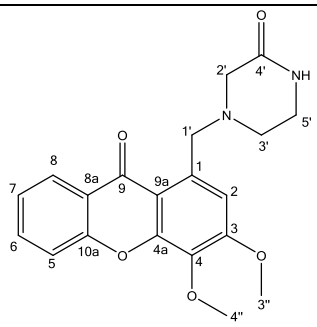 **16**
Carbons	**δ_C**	**δ_C**
C-9	178.1	176.7
C-3	156.5	156.2
C-10a	155.2	154.6
C-4a	152.0	151.8
C-4	138.8	136.9
C-1	134.8	135.0
C-6	134.2	134.7
C-8	126.6	126.1
C-7	123.9	124.3
C-8a	122.5	121.8
C-5	117.5	117.7
C-9a	114.6	113.7
C-2	108.2	109.2
C-4''	61.5	60.9
C-1'	60.2	58.5
C-5'	59.3	30.7
C-4'	57.7	168.0
C-3''	56.2	56.3
C-3'	53.5	48.7
C-2'	53.2	57.2

*****Values in ppm (δ_C) relative to $(CH_3)_4Si$ as an internal reference.

The signal appearing at δ_C 168.00 ppm corresponded to the downfield carbonyl group of the lactam ring of **16.** According to the ^{13}C NMR spectrum of **17**, the aromatic region displayed the presence of six additional signals characteristic of the six aromatic carbons of the tetrahydroisoquinolin ring. The carbon C-8' directly linked to the electronegative nitrogen atom of aromatic amine group exhibited the highest chemical shift value ($\delta_{C\text{-}8'}$ 144.1 ppm) followed by the carbons C-5' and C-9' ($\delta_{C\text{-}5'}$ 136.3 ppm; $\delta_{C\text{-}5'}$ 126.4 ppm) in *meta* position. In a similar manner of ^1H NMR spectra, the absence of the signal corresponded to the carbon of formyl group (-CHO) and the presence of a signal characteristic of the carbon atom of the methylene group ($-CH_2-$) confirmed the conjugation of the carbaldehydic xanthone **LEM2** with each amine precursor. The methylene groups appear at δ_C 60.2 ppm for **15**, at δ_C 58.5 ppm for **16**, at δ_C 60.1 ppm for **17** and at δ_C 54.3 ppm for **18**. The remaining upfield signals corresponded to non-aromatic carbons of the aminated chain (δ_C values ranging from 53.2 to 59.3 ppm for **15**, from 30.7 to 57.2 ppm for **16**, from 24.9 to 56.7 ppm for **17,** and from 23.8 to 55.7 ppm for **18**).

Table 11 - ^{13}C NMR data* for amines **17** and **18.**

	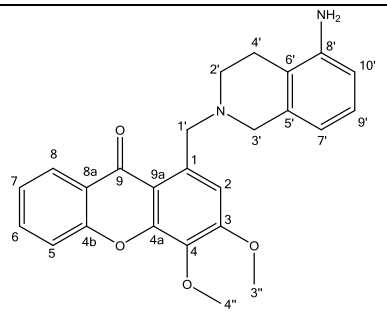 **17**	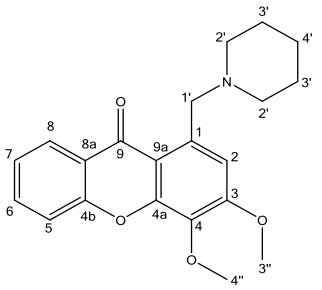 **18**
Carbons	**δ_C**	**δ_C**
C-9	178.2	177.5
C-3	156.7	156.1
C-10a	155.2	154.7
C-4a	151.9	151.3
C-8’	144.1	-
C-1	139.3	134.2
C-5’	136.3	-
C-4	134.8	138.9
C-6	134.2	133.8
C-8	126.6	126.0
C-9’	126.4	-
C-7	123.8	123.3
C-8a	122.5	121.9
C-6’	119.5	-
C-5	117.6	117.1
C-7’	117.1	-
C-9a	114.5	113.9
C-10’	112.7	-
C-2	108.0	107.8
C-4’’	61.5	60.8
C-1’	60.1	54.3
C-3’	56.7	25.7
C-3’’	56.3	56.1
C-2’	51.0	55.7
C-4’	24.9	

*****Values in ppm (δ_C) relative to $(CH_3)_4Si$ as an internal reference.

In case of aminoxanthone **17**, the respective amine precursor presents two potential sites for conjugation with **LEM2**: the heterocyclic and the aromatic amine group. The assignments of chemical shifts of carbon atoms by HSQC and HMBC confirmed the selective conjugation of LEM2 with the heterocyclic amine group of the amine precursor of **17** (**Figure 14**)**.**

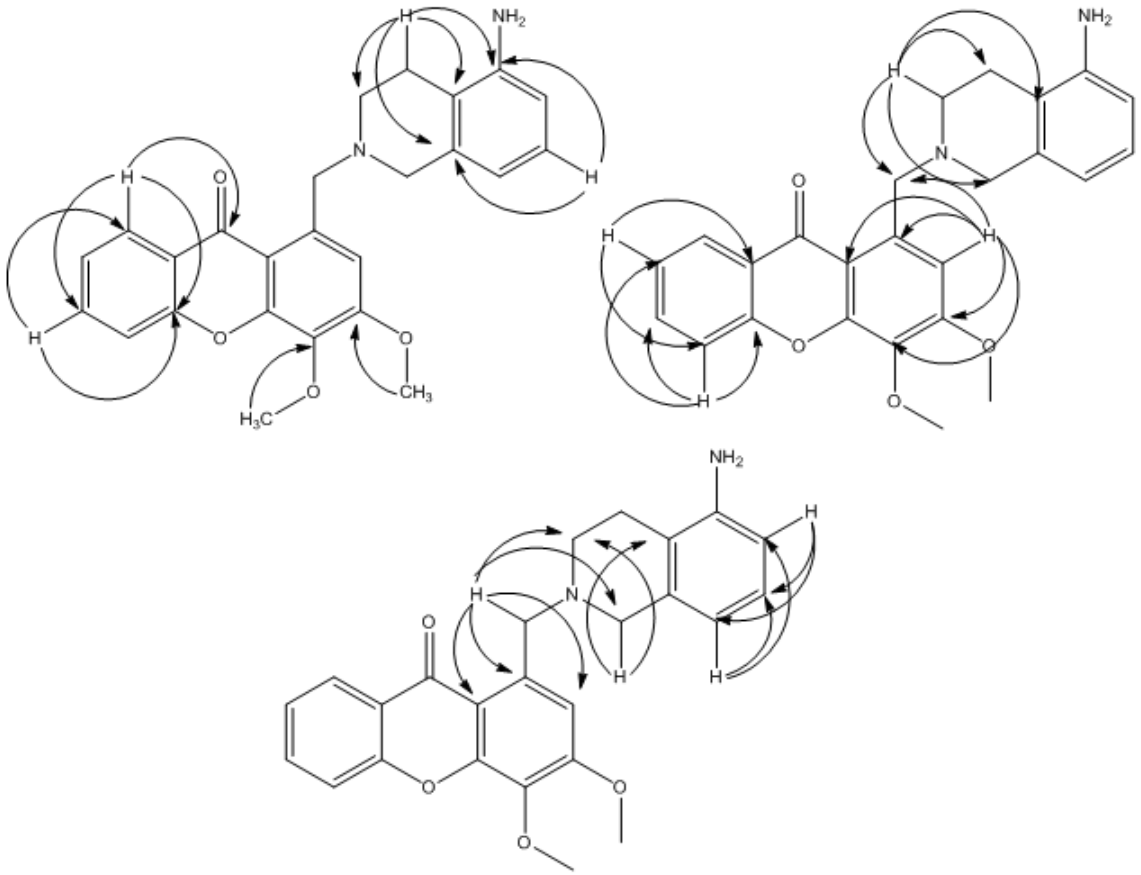

Figure 14 – Correlations between carbons and protons in HMBC spectrum of **17.**

3.3.5. Halogenated aromatic aminoxanthone derivatives: 19, 20, 21, and 22

3.3.5.1. ^{1}H NMR for amines 19, 20, 21, and 22

The data corresponding to the ^{1}H NMR of amines **19**, **20**, **21**, and **22** are represented in **Table 12** and **Table 13**.

The ^{1}H NMR spectra of halogenated aromatic aminoxanthone derivatives **19**, **20**, **21,** and **22** exhibited a similarity to the respective starting material, **LEM2**, particularly in the chemical shifts of the signals corresponded to the four aromatic protons H-5, H-6, H-7 and H-8 (δ_H values between 7.4 and 8.3 ppm) of the xanthone scaffold and to the six protons of the methoxyl groups H-3 and H-4 (δ_H values ranging from 4.0 to 4.1 ppm). The spectrum also revealed the presence of two additional signals that correspond to the four aromatic protons of the aminated chain. The occurrence of the reductive amination of LEM2 with each amine precursor was evidenced by the presence of a singlet characteristic of the two protons H-1' of the methylene group (-CH_2-) of aminoxanthones. In fact, the methylene group appears at δ_H 4.30 (s, CH_2) ppm for **19,** δ_H 4.33 (s, CH_2) ppm

for **20**, δ_H 4.27 (s, CH_2) ppm for **21,** and δ_H 4.31 (s, CH_2) ppm for **22**, The remaining upfield protons are characteristic of each of the four aminated chains. In the case of these secondary halogenated amines, the signal corresponding to the N-H was not observed in the spectra.

Table 12 - ^{1}H NMR data* for amines **19** and **20**.

	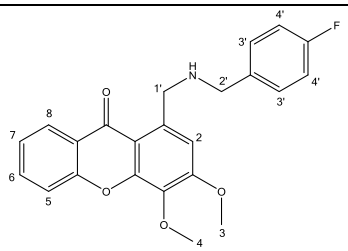 **19**	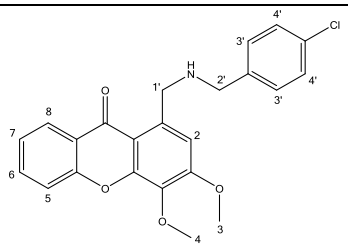 **20**
Protons	**δ_H**	**δ_H**
H-8	8.28, 1H, dd, *J*=8.0 and 1.6	8.25, 1H, dd, *J*=8.0 and 1.6
H-6	7.71, 1H, ddd, *J*=8.5, 7.0 and 1.6	7.79, 1H, ddd, *J*=8.6, 7.0 and 1.6
H-5	7.55, 1H, dd, *J*=8.5 and 0.8	7.60, 1H, dd, *J*=8.5 and 0.9
H-7	7.40, 1H, ddd, *J*=8.0, 7.0 and 0.8	7.43, 1H, ddd, *J*=8.0, 7.0 and 0.9
H-4’	7.36, 2H, m	7.66, 2H, m
H-3’	7.01, 2H, m	7.38, 2H, m
H-2	6.96, 1H, s	7.39, 1H, s
H-1’	4.30, 2H, s	4.33, 2H, s
H-4	4.01, 3H, s	4.07, 3H, s
H-3	4.01, 3H, s	4.01, 3H, s
H-2’	3.85, 2H, s	4.53, 2H, s

*****Values in ppm (δ_H) relative to $(CH_3)_4Si$ as an internal reference. *J* values are in Hz.

Table 13 - ^{1}H NMR data* for amines **21** and **22**.

	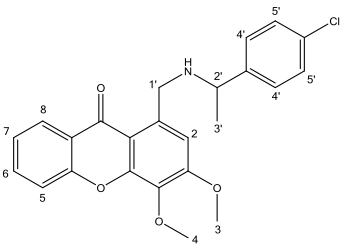 **21**	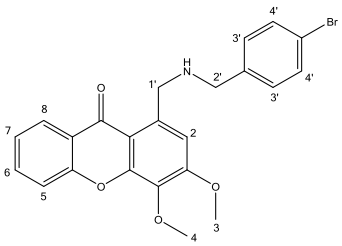 **22**
Protons	**δ_H**	**δ_H**
H-8	8.26, 1H, dd, *J*=8.0 and 1.6	8.27, 1H, dd, *J*=8.0 and 1.6
H-6	7.79, 1H, ddd, *J*=8.5, 7.0 and 1.6	7.73, 1H, ddd, *J*=8.5, 7.0 and 1.6
H-5’	7.70, 2H, m	-
H-5	7.59, 1H, dd, *J*=8.5 and 0.8	7.58, 1H, dd, *J*=8.5 and 0.8
H-7	7.43, 1H, ddd, *J*=8.0, 7.0 and 0.8	7.38, 1H, ddd, *J*=8.0, 7.1 and 0.8
H-4’	7.42, 2H, m	7.48, 2H, m
H-2	7.25, 1H, s	7.08, 1H, s
H-2’	4.54, 1H, q, *J*=6.8	3.88, 2H, s
H-1’	4.27, 2H, s	4.31, 2H, s
H-4	4.04, 3H, s	4.01, 3H, s
H-3	4.01, 3H, s	4.01, 3H, s
H-3’	1.83, 3H, d, *J*=6.8	-

*****Values in ppm (δ_H) relative to $(CH_3)_4Si$ as an internal reference. *J* values are in Hz.

3.3.5.2. ^{13}C NMR for amines 19, 20, 21, and 22

The ^{13}C NMR spectra for compounds **19**, **20**, **21**, and **22** revealed the presence of signals corresponding to the carbons atoms of the carbonyl group (C-9), the two aromatic rings (δ_C values ranging from 111 to 157 ppm) and the two methoxyl groups at position 3'' and 4'' (δ_C values between 56 and 62 ppm) (**Table 14** and **Table 15**).

Table 14 - ^{13}C NMR data* for amines **19** and **20.**

	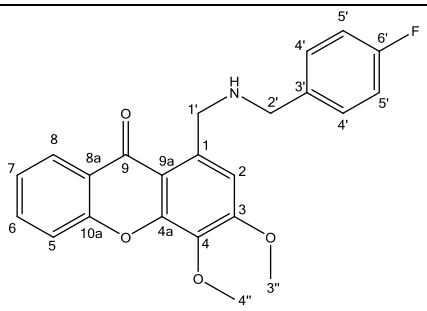 **19**	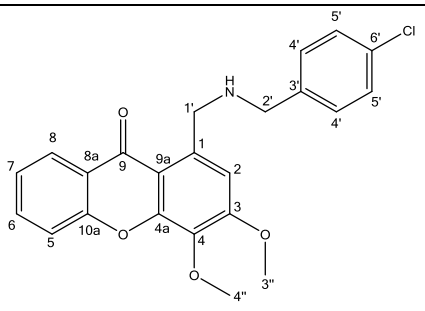 **20**
Carbons	**δ_C**	**δ_C**
C-9	178.1	179.6
C-6'	160.3	127.3
C-3	156.3	157.0
C-10a	155.3	155.5
C-4a	152.2	152.0
C-4	138.6	137.7
C-3'	135.9	129.4
C-1	135.7	135.8
C-6	134.5	135.6
C-5'	129.8	131.7
C-8	126.7	126.6
C-7	124.0	124.6
C-8a	122.2	121.3
C-5	117.7	117.9
C-4'	115.3	129.5
C-9a	114.7	114.8
C-2	110.9	115.5
C-4''	61.5	61.6
C-3''	56.3	57.1
C-1'	53.3	51.3
C-2'	52.5	50.7

*****Values in ppm (δ_C) relative to Me_4Si as an internal reference.

In the aromatic region of these four aminoxanthone derivatives, it was evidenced the presence of four additional signals corresponding to the six aromatic carbons of the halogenated aromatic amine precursor. The carbons positioned *orto* are subjected a higher deshielding effect in relation to *meta* carbons due to the inductive electron-withdrawing effect of the halogen atom. Also, NMR data of these derivatives revealed an

increase of the chemical shift value of the carbon directly linked to halogen atom with the increase of the electronegativity of the halogen.

In a similar manner of ^{1}H NMR spectra, a signal corresponding to the carbon of formyl group (-CHO) was not detected and the presence of a signal characteristic of the carbon atom of the methylene group (-CH_2-) confirmed the success of the reductive amination. The methylene groups appear at δ_C 53.3 ppm for **19**, at δ_C 51.3 ppm for **20**, at δ_C 50.2 ppm for **21,** and at δ_C 52.7 ppm for **22**. The remaining signals corresponded to non-aromatic carbons of the aminated chain.

Table 15 - ^{13}C NMR data* for amines **21** and **22.**

	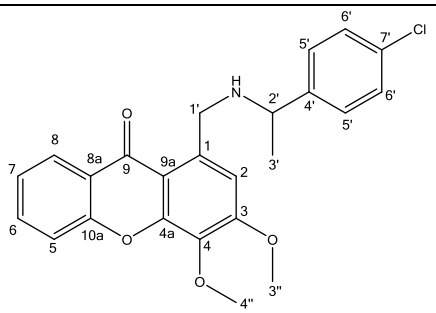 **21**	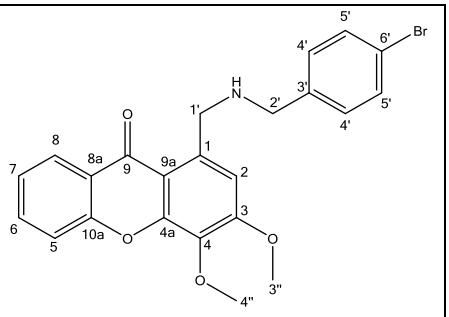 **22**
Carbons	**δ_C**	**δ_C**
C-9	179.6	178.6
C-3	156.8	156.5
C-10a	155.4	155.3
C-4a	151.9	152.2
C-4	137.6	136.4
C-6	135.5	134.9
C-1	134.5	136.2
C-7’	131.8	-
C-6’	129.8	121.8
C-5’	129.5	131.8
C-4’	127.3	130.7
C-8	126.6	126.6
C-7	124.6	124.2
C-8a	121.3	121.9
C-5	117.9	117.7
C-2	115.6	112.5
C-9a	114.9	114.7
C-4’’	61.6	61.6
C-2’	58.9	52.0
C-3’’	57.0	56.7
C-1’	50.2	52.7
C-3’	20.2	128.4

*****Values in ppm (δ_C) relative to $(CH_3)_4Si$ as an internal reference.

The derivative **22** was structurally elucidated by HQSC to identify the chemical shifts of hydrogenated carbons and by HMBC to deduce to chemical shifts of carbon

atoms not directly bonded to hydrogen atoms. The proposed structure corresponding to the derivative **22** (**Figure 15**) was confirmed by HMBC spectrum.

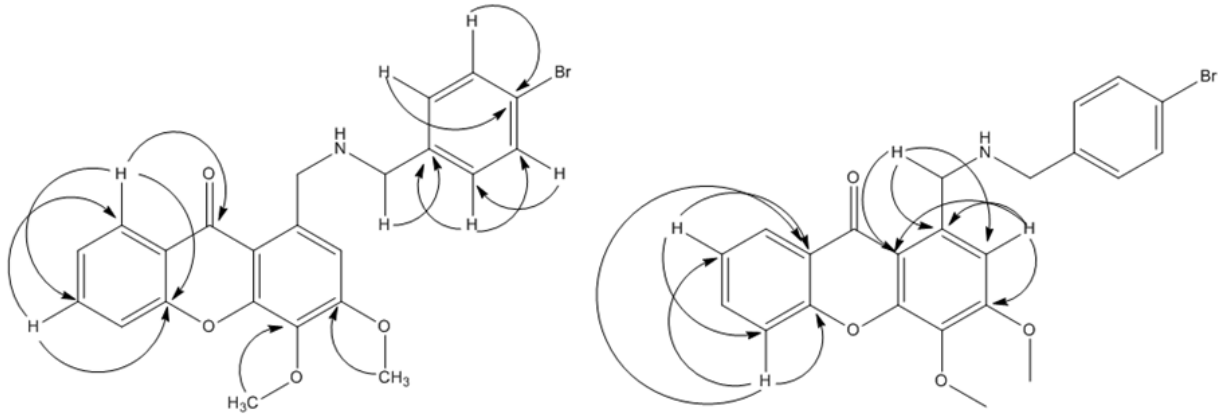

22

Figure 15 – Correlations between carbons and protons in HMBC spectrum of **22**.

Summarized NMR data of the xanthone scaffold representing of aminated derivatives **12**-**22** is represented in **Figure 16**. According to the data provided by ^{1}H NMR and ^{13}C NMR spectra, the chemical shifts of the protons and carbons of the xanthone scaffold of the aminoxanthones were not significantly different.

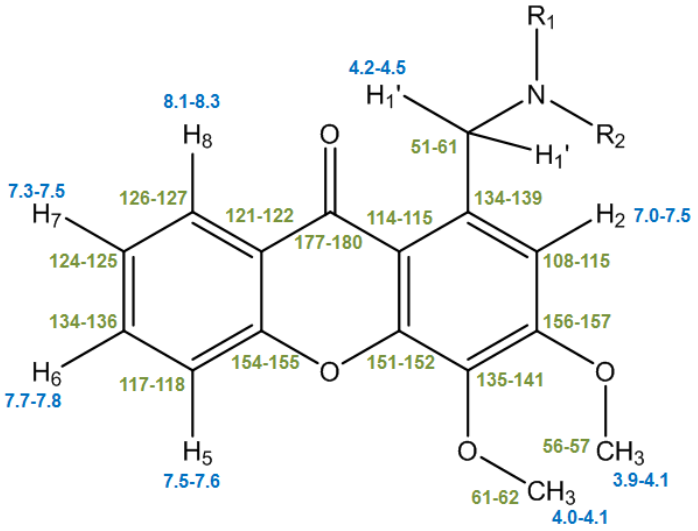

Figure 16 – General structure elucidation of the xanthone scaffold of the aminoxanthone derivatives by **proton** and **carbon** NMR chemical shifts (ppm)

3.4. Docking simulation studies

The need for a rapid search for small molecules that may interact to targets of biological interest is crucial in the drug discovery process[37]. Computational methods such as virtual screening constitute a promising approach for identification of hit compounds,

playing an important role in drug discovery research[97]. Virtual screening, also called *in silico* screening, is a detailed compound database searching approach that allows the discovery of new promising scaffolds and small-molecules with a required biological activity[98]. This method involves the rapid computational screening of large libraries of chemical structures in order to identify those structures which are most likely to bind to a therapeutic target[99]. Therefore, virtual screening represents a fast and effective tool to search for novel lead compounds.

Depending on the information obtained about the three-dimensional structure of therapeutic target, virtual screening can be divided into two approaches: ligand based virtual screening, when information about biological target is not available, and structure based virtual screening, if the three dimensional structure of target is known. If the structure of the biological target is not available, but there are known active ligands, they can be used to build a pharmacophore or a three dimensional quantitative structure-activity relationship (QSAR) study[59]. Another approach consists in the application of techniques of protein structure prediction (homology modeling) to build a structurally homologous model of the biological target. When the three-dimensional structure of the biological target is known by experimental techniques such as X-ray crystallography, a library of virtual ligands is docked against a biological target in order to predict their binding affinity[100].

The virtual screening of large libraries of compounds against a target in search of novel promising scaffolds is useful approach for Medicinal Chemistry.

In case of the biological interaction between p53 and MDM2, a structure based virtual screening was performed since the three-dimensional structure of the p53:MDM2 interface is known.

To predict the inhibitory activity of newly synthesized aminoxanthone derivatives against MDM2 protein, docking simulation studies were performed using MDM2 protein (PDB code 1YCR).

The virtual screening of a library of new aminoxanthone derivatives described in this dissertation and other obtained *in-house* compounds derived from three distinct building blocks (**LEM2**, **LEM3**, and **PEX**) (**Figure 17**) resulted in a list of potential MDM2 ligands, ranked according to their binding affinity to the target. Docking simulation studies carried out in PyRx/AutoDock Vina produced nine conformations for each ligand. From the total number of 27 compounds screened, four small-molecule inhibitors of p53:MDM2 interaction (nutlin-3a, α-mangostin, gambogic acid, and pyranoxanthone **LEM1**) were used in the docking studies as positive controls.

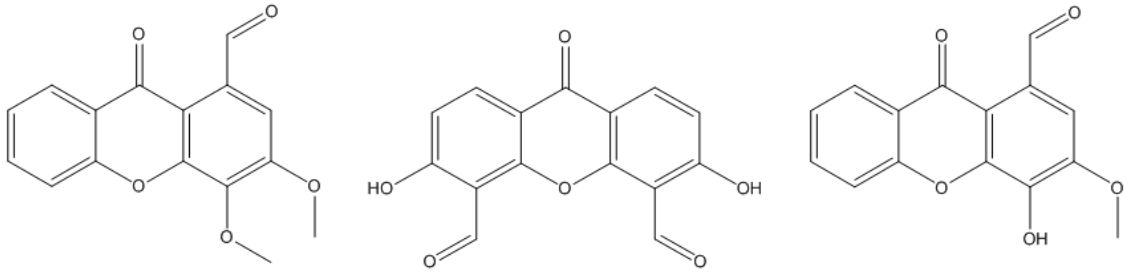

Figure 17 – Distinct xanthonic building blocks of the library of aminoxanthone derivatives used in the docking studies.

MDM2 residues Gly58, Asp68, Val75 and Cys77 are described as being critical for interaction with p53[101]. Therefore, docking calculations were restricted to the MDM2 binding site that contains those residues by building grid box centered on that binding site (**Figure 18**).

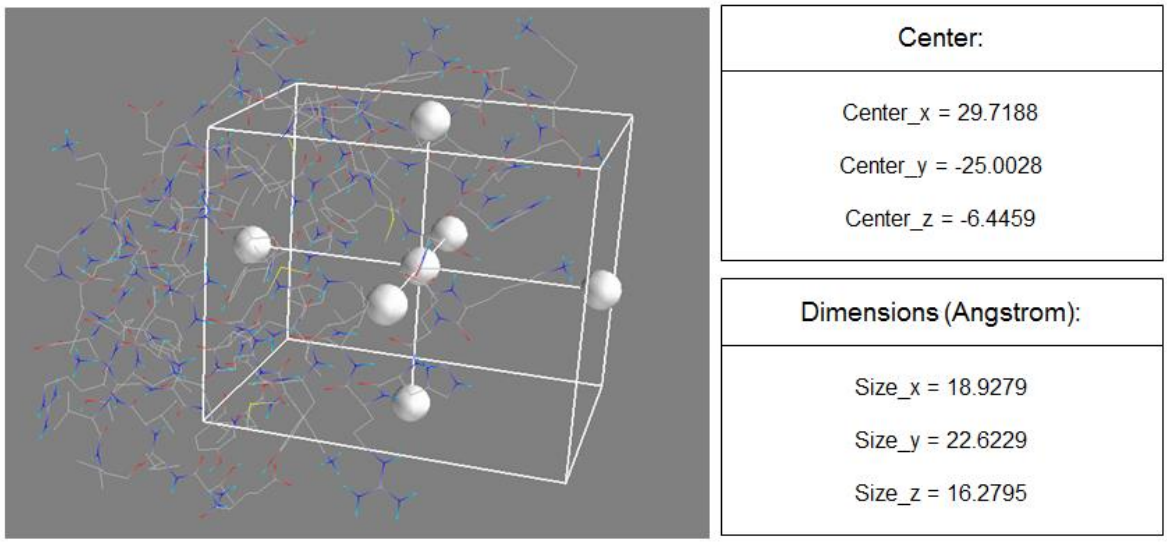

Figure 18 – Vina search space (grid box) dimensions and positions in MDM2 (PDB code: 1YCR) in PyRx/AutoDock Vina.

The binding free energies for the best scoring conformations are summarized in **Table 16**. The binding energy values found for known inhibitors of p53:MDM2 interaction, which are known to interact with MDM2, were -7.8 kcal.mol^{-1} for nutlin-3a, -7.7 kcal.mol^{-1} for **LEM1** and gambogic acid**,** -6.6 kcal.mol^{-1} for α-mangostin, and -5.6 kcal.mol^{-1} for the inhibitor of p73:MDM2 interaction, **LEM2**. The remaining 22 xanthone derivatives exhibited binding energy values in this range with the molecule **PPX4** displaying the highest binding affinity, and therefore, the lowest binding free energy (-7.9 kcal.mol^{-1})

Table 16 – Results of docking simulations for MDM2 (with grid box) performed in PyRx/AutoDock Vina.

Ligand	Binding Energy (kcal mol^{-1})	Ligand	Binding Energy (kcal mol^{-1})
PPX4	-7.9	**12**	-6.7
Nutlin-3a	-7.8	**PPX3**	-6.7
Gambogic acid	-7.7	**α-Mangostin**	-6.6
LEM1	-7.7	**14**	-6.5
17	-7.6	**15**	-6.5
19	-7.6	**PEX1**	-6.3
20	-7.6	**PEX3**	-6.3
22	-7.3	**13**	-6.0
21	-7.2	**PEX**	-6.0
PPX2	-7.1	**11**	-5.9
18	-7.0	**LEM2**	-5.9
16	-6.9	**LEM3**	-5.7
PEX2	-6.9	**PPX1**	-5.2
PEX4	-6.8		

Analysing the docking score values, it was observed that the aminoxanthone derivatives presented a higher binding affinity (higher absolute binding energy value) than the respective xanthonic building blocks. This observation was expectable since the conversion of a formyl group to a bulky amine substituent may contribute to the establishment of additional interactions in the binding site of MDM2, resulting in an increased binding affinity.

Nevertheless, concerning the aminoxanthones obtained, all of these derivatives showed lower binding affinities (lower absolute binding energy value) than the described p53:MDM2 inhibitors **LEM1**, gambogic acid and nutlin-3a.

Subsequently, a visual inspection of the **LEM2** derivatives and the best ligand **PPX4** docked onto MDM2 binding site was performed. As shown on **Figures 19**, **20** and **21** the best fitting molecule **PPX4** and the **LEM2** derivatives **11**-**22** adopted a pose within the p53-binding site which filled the space occupied by p53 helix.

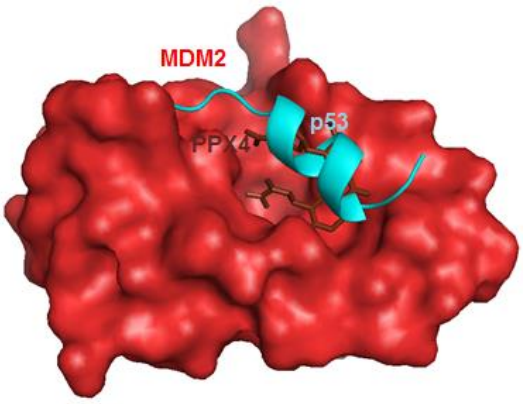

Figure 19 – **PPX4** in the binding site of MDM2.

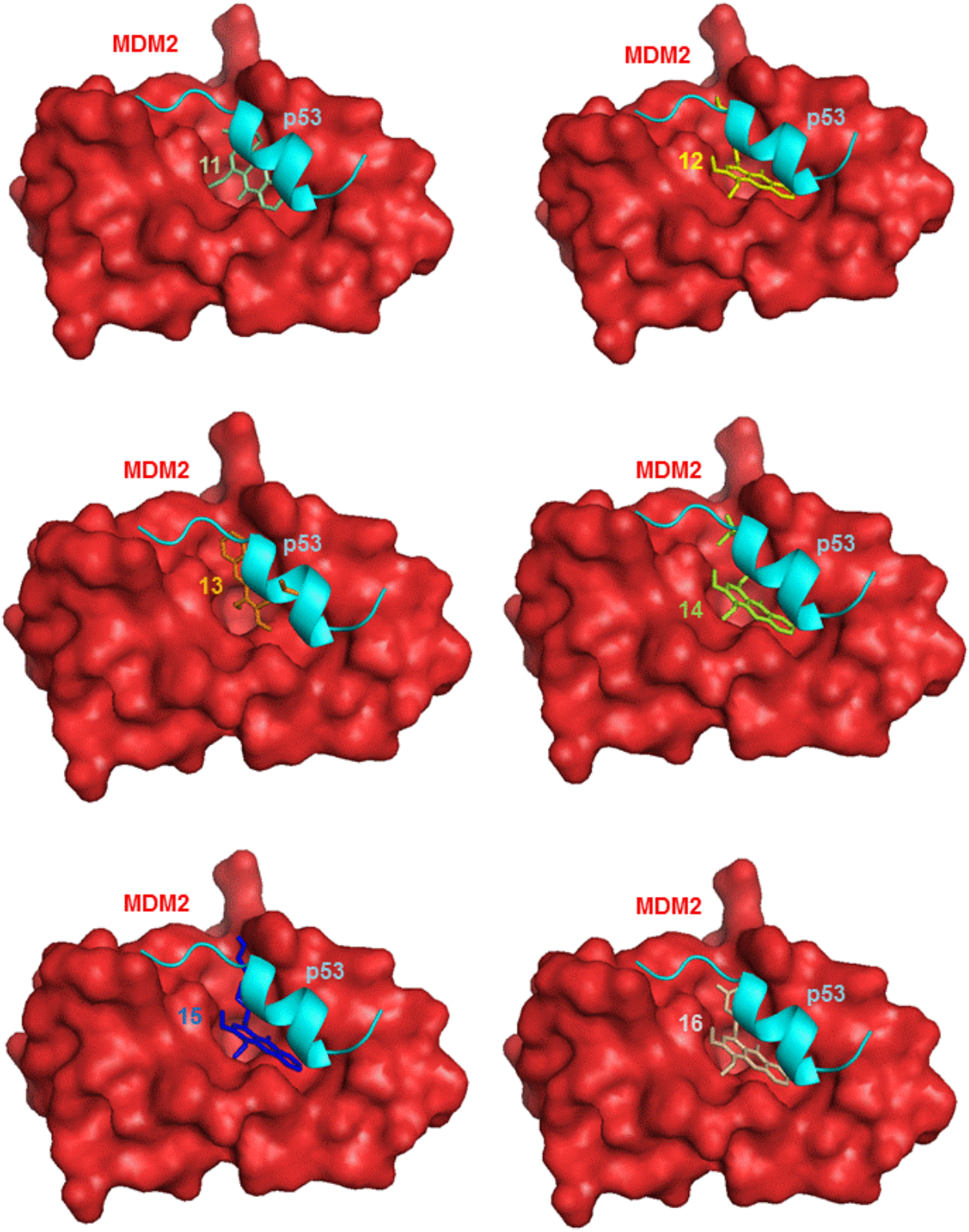

Figure 20 – Derivatives **11**-**16** in the binding site of MDM2.

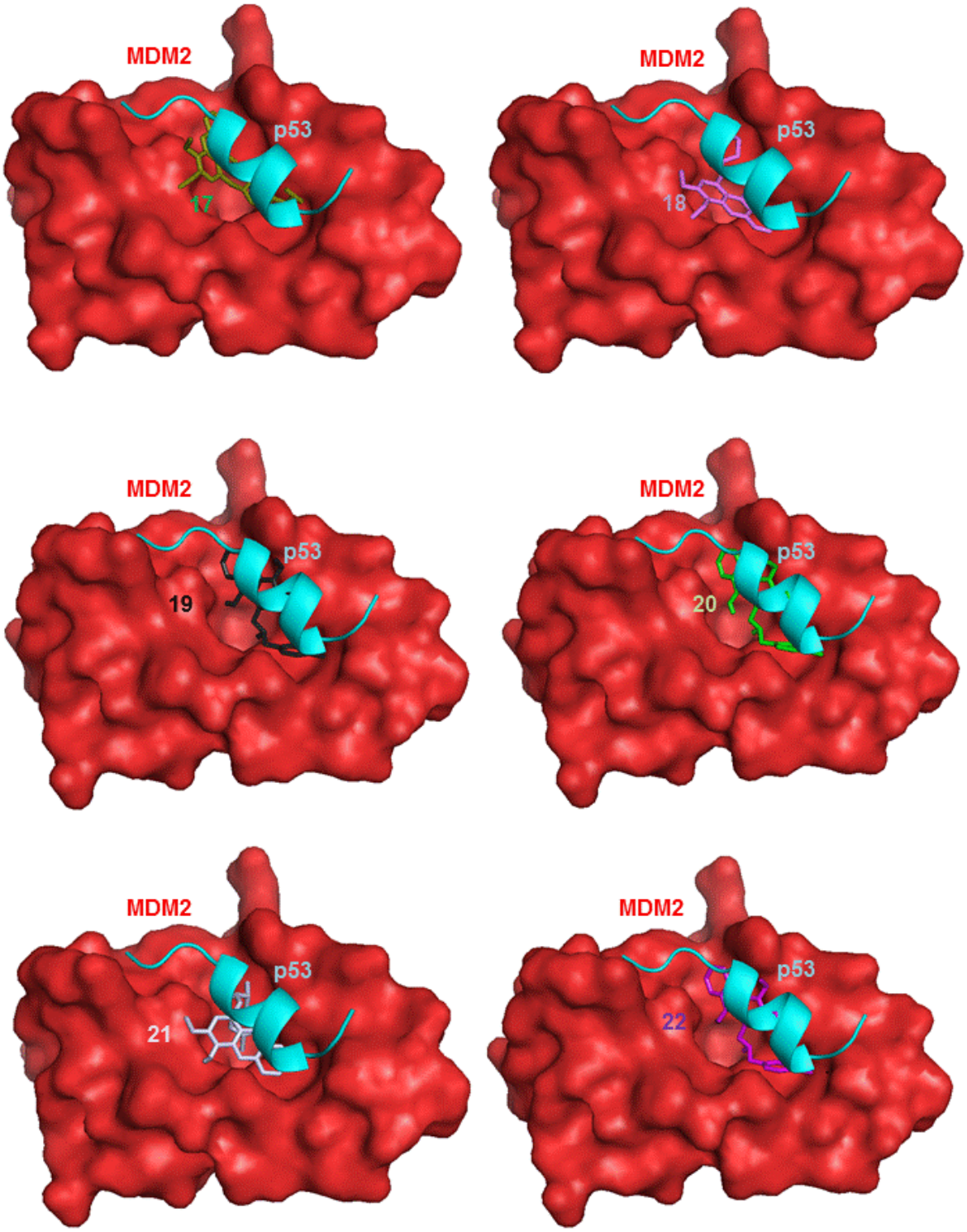

Figure 21 – Derivatives **17**-**22** in the binding site of MDM2.

3.5. Evaluation of the inhibitory activity on p53:MDM2 interaction using yeast screening assays

The inhibitory activity of the library of aminoxanthone derivatives was investigated using yeast-phenotypic assays developed for an initial screening of inhibitors of p53:MDM2 interaction[75]. This study was performed with the assistance of Master Ana Sara Gomes and with the supervision of Prof. Lucília Saraiva at UCIBIO, Laboratory of Microbiology, FFUP. The effectiveness of these yeast-screening assays for the identification of small-molecule inhibitors of p53:MDM2 interaction was displayed not only by testing nutlin-3a, a known small-molecule inhibitor of p53:MDM2 interaction, but also by the identification of pyranoxanthone **LEM1** as a promising inhibitor of the p53:MDM2 interaction, for which the molecular mechanism of action was confirmed using human tumor cell lines[75]. In this context, using the yeast-growth inhibition assay, the effect of aminoxanthone derivatives **12**, **13**, **15**, **16**, **19**, **20**, and **22** on the growth of the yeast expressing human p53 and MDM2 proteins was evaluated at concentrations of 1 μM and 10 μM. Based on the results represented in **Figure 22**, a significant difference between the percentages of growth of the yeast cells treated with DMSO and the yeast treated with the compounds was not observed at 1 μM and 10 μM.

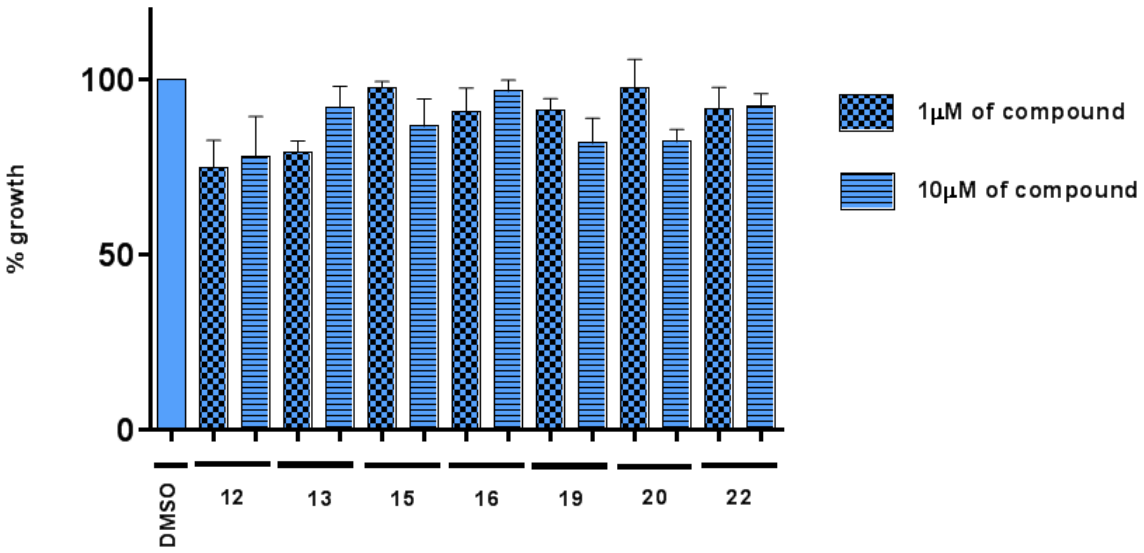

Figure 22 - Effect of **12**, **13**, **15**, **16**, **19**, **20** and **22** at concentrations of 1μM and 10μM on the growth of yeast co-expressing p53 and MDM2; results were plotted setting as 100% growth the number of CFUs with yeast co-expressing p53 and MDM2 incubated with DMSO only; data are mean ± SEM of four independent experiments; significantly different values are indicated (*P < 0.05). CFU = colony-forming unit; DMSO = dimethylsulfoxide; SEM = standard error of the mean.

These results suggested that these seven aminoxanthone derivatives did not show an inhibitory activity on p53:MDM2 interaction.

Further studies will pursuit with the investigation of the effect of aminoxanthones on p73:MDM2 interaction and in tumor cell growth inhibition.

CHAPTER 4

CONCLUSIONS

CHAPTER 4 - CONCLUSIONS

The p53:MDM2 constitutes a valuable target for identification of activators of the p53-dependent pathway. The identification of small-molecule inhibitors of p53:MDM2/MDMX interaction may restore the antiproliferative activity of p53 constituting an appealing approach for cancer therapy. Several new small-molecules inhibitors of p53:MDM2/MDMX interaction have been described. In last years, dual inhibitors have emerged due to their ability of fully activating p53-dependent pathway by simultaneous inhibition of MDM2 and MDMX.

Among the strategies and techniques used to identify small-molecule inhibitors of p53:MDM2 interaction, the structure-based design and yeast-screening assays were used in this dissertation.

The reaction conditions used for the reductive amination of the carbaldehydic xanthone **LEM2** allowed a successful synthesis of a library of aminoxanthone derivatives. Reductive amination of **LEM2** was quite sensitive to reagent and solvent conditions and the STAB/THF system was successful in providing the desirable aminoxanthones. The spectroscopic techniques IR and NMR put in evidence the desirable transformations.

With the objective of predicting the binding affinity of these derivatives and the respective xanthonic building blocks towards MDM2, docking simulation studies were performed. These studies have shown that the aminoxanthone derivatives presented a higher binding affinity than the respective building blocks. However, the inhibitory activity of these derivatives against the p53:MDM2 interaction using yeast-screening assays was not concordant with the promising docking results. The results of biological activity allowed to conclude that the molecular hybridization strategy of coupling an amine moiety of known inhibitors of p53:MDM2 interaction at position C-1 was not successful in providing inhibitors of this interaction. Nevertheless, the presence of an amine group at position C-1 seems to be essential for the identification of small-molecules with antitumor activity and similar scaffolds. In fact, the thioxanthones lucanthone and hycanthone[102], and the antraquinone mitoxantrone are antitumor agents that present an aliphatic amine group at position C-1 of the tricyclic scaffold. Since **LEM2** is an inhibitor of p73:MDM2 interaction with a weak effect on p53:MDM2 interaction (unpublished data), the investigation of the effect of **LEM2** derivatives on p73:MDM2 interaction should be performed in future work.

Overall, these results may contribute to the study of the most favorable structural requirements in order to obtain novel and potent p53/p73 activators with an antitumor effectiveness.

CHAPTER 5

MATERIAL AND METHODS

CHAPTER 5 - MATERIAL AND METHODS

5.1. General Methods

All reagents and solvents were purchased from Sigma Aldrich, and had no further purification process. Solvents were evaporated using rotary evaporator under reduced pressure, Buchi Waterchath B-480. All reactions were monitored by TLC carried out on precoated plates with 0.2 mm of thickness using Merck silica gel 60 (GF254). The UV light at 254 and 365 nm and a solution of ninhydrin in ethanol 3 mg/ml (activated by heat) were used for visualization of chromatograms. Microwave (MW) reactions were performed in glassware open vessel reactors in a MicroSYNTH 1600 Microwave Labstation from Millestone (ThermoUnicam, Portugal). The internal reaction temperature was controlled by a fiber-optic probe sensor. Purification of the synthesized compounds was performed by chromatography flash column using Merck silica gel 60 (0.040-0.063 mm), chromatography flash cartridge (GraceResolv®, Grace Company, Deerfield, IL, USA), Discovery® DSC-SCX SPE cationic exchange cartridge. Melting points (mp) were measured in a Köfler microscope and are uncorrected. Infrared (IR) spectra were obtained in KBr microplates in a Fourier transform infrared spectroscopy spectrometer Nicolet iS10 from Thermo Scientific with Smart OMNI-Transmisson accessory (Software OMNIC 8.3) (cm^{-1}). NMR spectra were performed in University of Aveiro, Department of Chemistry, and were taken in $CDCl_3$ (Deutero GmbH) at room temperature on Bruker Avance 300 spectrometer (300.13 MHz for ^{1}H and 75.47 MHz for ^{13}C).

Qualitative GC-MS analyses were performed by Dr. Sara Cravo, Department of Chemistry, Laboratory of Organic and Pharmaceutical Chemistry, Faculty of Pharmacy, University of Porto. The analyses were performed on a Trace GC 2000 Series ThermoQuest gas chromatography equipped with ion-trap GCQ Plus ThermoQuest Finnigan mass detector. Chromatographic separation was achieved using a capillary columm (30m × 0.25 mm × 0.25 µm, cross-linked 5% diphenyl and 95% dimethyl polysiloxane) from Thermo Scientific™ and high-purity helium C-60 as carrier gas. An initial temperature of 80ºC was maintained for 1 min, increased to 310ºC at 10ºC/min, and held for 5 min giving a total run time of 33 min. The flow of the carrier gas was maintained at 1.5 ml/min. The injector port was set at 280ºC. Analyses were performed with splitless injection in the full-scan mode in the scan range of m/z 50-700. For derivatized samples 30 µL of MSTFA were added and samples heated at 80ºC for 30 min. to accomplish silylation. An aliquot of 1 µl of the derivatized extract was injected into the GC-MS system.

5.2. Synthesis of the carbaldehydic xanthone LEM2

5.2.1. Synthesis of benzophenone intermediate 3, (2-hydroxy-3,4-dimethoxy-6-methylphenyl) methoxyphenyl) methanone

$AlCl_3$ anhydrous (18.3 g, 137.2 mmol) was added to a dry ether solution (200 ml) of 2-methoxybenzoyl chloride (11.2 g, 65.85 mmol) and trimethoxytoluene (10 g, 54.88 mmol). The resulting deep red mixture was stirred at room temperature for 5 h. The reaction was monitored using *n*-hexane/ethyl acetate in a proportion of 7:3. After completing the reaction, the suspension was acidified with HCl 5M and extracted with chloroform. The evaporation of the dried organic layer gave a brown oil[103].

5.2.2. Synthesis of 3,4-diethyl-1-methyl-9*H*-xanthen-9-one (4): cyclization of benzophenone intermediate 3

To a solution of NaOH (48 g, 1.2 mol) in MeOH (240 ml) and water (160 ml), the crude material containing 2-hydroxy-3,4-dimethoxy-6-methylphenyl) methoxyphenyl) methanone (**3**) was added. The mixture was submitted to 6 h of microwave (MW) irradiation at 300 W of potency. The evolution of reaction was made using *n*-hexane/ethyl acetate in a proportion of 7:3. After completing the reaction and cooling at room temperature, the white solid formed was filtered, washed with methanol and dried. The solid of 3,4-diethyl-1-methyl-9*H*-xanthen-9-one (**4**, 2.52 g) was crystallized from ethyl acetate/*n*-hexane (procedure adapted from [87]).

5.2.3. Synthesis of 1-(dibromomethyl)-3,4-dimethoxy-9*H*-xanthen-9-one (5)

A mixture of 3,4-diethyl-1-methyl-9*H*-xanthen-9-one (2.52 g, 9.32 mmol), *N*-bromosuccinimide (3.32 g, 2.0 eq.) and benzoyl peroxide (0.68g, 0.3 eq.) in carbon tetrachloride (25 ml) was refluxed for 2 h. The chromatographic system n-hexane/ethyl acetate in a proportion of 8:2, was used to control the progression of the reaction. Once completed the reaction, the suspension was cooled at 0°C and stirred 1-2 h. The precipitate was filtered and washed with cold carbon tetrachloride. The mother liquor was evaporated and then purified by a flash column chromatography (silica gel, *n*-hexane/ethyl acetate in gradient) using several proportions to obtain a white solid of 1-(dibromomethyl)-3,4-dimethoxy-9*H*-xanthen-9-one (**5**, 3.14 g, 80%). The experimental procedure was adapted from [89].

5.2.4. Synthesis of 3,4-dimethoxy-9-oxo-9*H*-xanthene-1-carbaldehyde (LEM2)

A mixture of the dibromoxanthone derivative **5** (3.14 g, 7.34 mmol) and ionic liquid, 1-butyl-3-methylimidazolium tetrafluoroborate mixed with water (6 ml, 5:1) was heated at 100°C with stirring for 2.5 h. The mobile phase *n*-hexane/ethyl acetate 7:3 was used to control the progression of reaction. The reaction was allowed to cool, diluted in water, and extracted with ethyl acetate (3 x 200 ml). The organic layer was dried with anhydrous sodium sulphate, concentrated under reduced pressure and the crude material was purified by flash column chromatography (silica gel, *n*-hexane/ethyl acetate in gradient). A light yellow solid corresponding to 3,4-dimethoxy-9-oxo-9*H*-xanthene-1-carbaldehyde was obtained (**LEM2**, 1.33 g, 64%). The experimental procedure described here was adapted from [90].

3,4-Dimethoxy-9-oxo-9*H*-xanthene-1-carbaldehyde (**LEM2**); mp > 330°C (ethyl acetate); IR (KBr): ν_{max}= 3433, 2927, 1684, 1649, 1580, 1464, 1320, 1132, 758; ^{1}H NMR ($CDCl_3$, 300.13 MHz): δ = 11.21 (1H, s, H-1'), 8.31 (1H, dd, *J* = 8.0 and 1.7 Hz, H-8), 7.77 (1H, ddd, *J* = 8.5, 7.0, and 1.7 Hz, H-6), 7.60 (1H, dd, *J* = 8.5 and 0.8 Hz, H-5), 7.56 (1H, s, H-2), 7.43 (1H, ddd, *J* = 8.0, 7.0 and 0.8 Hz, H-7), 4.11 (3H, s, H-4), 4.07 (3H, s, H-3); ^{13}C-NMR ($CDCl_3$, 75.47 MHz): *δ* = 192.8 (C-1'), 177.9 (C-9), 156.3 (C-3), 155.5 (C-10a), 150.9 (C-4a), 140.7 (C-4), 135.1 (C-6), 133.5 (C-1), 126.7 (C-8), 124.5 (C-7), 121.9 (C-8a), 117.8 (C-5), 116.1 (C-9a), 108.5 (C-2), 61.8 (C-4''), 56.6 (C-3''). HRMS-ESI m/z calc for $C_{16}H_{12}O_5$ $[M+H]^+$ 284.06847, found: 285.07627.

5.3. Synthesis of aminoxanthone derivatives of carbaldehydic xanthone LEM2

5.3.1. General procedure for reductive amination

5.3.1.1. Synthesis of 1-(hydroxymethyl)-3,4-dimethoxy-9*H*-xanthen-9-one (11)

The 3,4-dimethoxy-9-oxo-9*H*-xanthene-1-carbaldehyde (**LEM2**, 20 mg, 0.071 mmol) and the amine precursors (0.099 mmol) were dissolved/suspended in methanol (5ml) and the MP-BH_4 (112.7 mg, 0.281 mmol, loading 2.5 mmol/g) was added to the reaction mixture. The reaction mixture was stirred at room temperature and monitored using the mobile phase *n*-hexane/ ethyl acetate, 7:3. A solid phase extraction with a cation exchange cartridge Discovery® DSC-SCX was performed in work-up of the crude

material, following the steps: activation of the cartridge with methanol (50 ml); loading the cartridge with the sample; elution with NH_3 2% in methanol. The non-basic and basic fractions were controlled by TLC using the mobile phase *n*-hexane/ ethyl acetate, 7:3. The non-basic fractions were gathered and concentrated under reduced pressure. The solid thus obtained was purified by a chromatography flash cartridge (Grace Resolv®) with *n*-hexane/ethyl acetate in gradient. The fractions containing the derivative **11** were gathered and concentrated under reduced pressure to furnish a white solid of 1-(hydroxymethyl)-3,4-dimethoxy-9H-xanthen-9-one (**11**). This procedure was adapted from ******.

1-(Hydroxymethyl)-3,4-dimethoxy-9H-xanthen-9-one (**11**); mp 187-189°C (ethyl acetate); IR (KBr): ν_{max} (cm^{-1}) = 3496, 3460, 2938, 1638, 1618, 1601, 1584, 1510, 1466, 1405, 1327, 1132, 1093, 1053, 993, 765, 755; ^{1}H NMR ($CDCl_3$, 300.13 MHz): δ (ppm) = 8.32 (1H, dd, *J* = 8.0 and 1.7 Hz, H-8), 7.75 (1H, ddd, *J* = 8.5, 7.0, and 1.7 Hz, H-6), 7.59 (1H, dd, *J* = 8.4 and 0.9 Hz, H-5), 7.41 (1H, ddd, *J* = 8.0, 7.1 and 0.9 Hz, H-7), 6.98 (1H, s, H-2), 4.95 (2H, s, H-1'); 4.03 (3H, s, H-4), 4.01 (3H, s, H-3); ^{13}C-NMR ($CDCl_3$, 75.47 MHz): δ (ppm) = 179.0 (C-9), 156.7 (C-3), 155.4 (C-10a), 152.3 (C-4a), 139.3 (C-1), 136.1 (C-1), 134.9 (C-6), 126.7 (C-8), 124.2 (C-7), 121.9 (C-8a), 117.7 (C-5), 114.8 (C-9a), 110.3 (C-2), 65.7 (C-1'), 61.6 (C-4''), 56.4 (C-3''). EI-MS (70 eV) m/z (rel. intensity, %): 286.1 (M^+, 56), 257.1 (100), 242.1 (55), 213.1 (86), 211.0 (39), 115.1 (43), 92.1 (16), 77.1 (62), 51.0 (72).

5.3.1.2. General synthesis of the aminoxanthone derivatives of LEM2

The 3,4-dimethoxy-9-oxo-9*H*-xanthene-1-carbaldehyde (**LEM2**, 40 mg, 0.141 mmol) and the amine precursors (0.197mmol) (**Table 15**) were dissolved/suspended in THF (3 ml) and added to the reaction mixture the sodium triacetoxyborohydride (119.3 mg, 0.563 mmol). After adding the acetic acid (24 µl, 0.423 mmol), the mixture was stirred at r.t. overnight, under N_2. For monitoring the synthesis of aminoxanthone derivatives by TLC, two chromatographic systems were used: *n*-hexane/ ethyl acetate, 7:3; methanol/TEA 100:0.1 for amines **12-18** and chloroform/acetone/TEA 5:5:0.1 for amines **19-22**.

The crude product obtained from the reductive amination of each amine precursor was subjected to different work-up strategies. The experimental procedure was adapted from [94].

** Biotage. (2006). Synthesis and Purification CATALOG 58-113.

5.3.2. Synthesis and structure elucidation

5.3.2.1. Synthesis of 3,4-dimethoxy-1-(((2-morpholinoethyl)amino)methyl)-9*H*-xanthen-9-one (12) and 1-(((3-(dimethylamino)propyl)methyl)amino) methyl)-3,4-dimethoxy-9*H*-xanthen-9-one (13)

Compounds **12** and **13** were synthesized based on the protocol described on section 3.1.2. After the completion of reaction, a liquid-liquid extraction under acidic and basic solutions was performed. Initially, the crude material was basified with NaOH 5% and extracted with chloroform (3 x 10 ml). The crude product contained in the resulting organic layer was then extracted with HCl 5M (3 x 30 ml). The resulting aqueous layer was basified with NaOH 20% and extracted with chloroform (3 x 100 ml). The dried organic layer was concentrated under reduced pressure and the crude product was purified by a column chromatography (chloroform/acetone/NH_3 in gradient) yielding a light green solid of 3,4-dimethoxy-1-(((2-morpholinoethyl)amino)methyl)-9*H*-xanthen-9-one (**12**, 31.6 mg, 56%) and a white solid of 1-(((3-(dimethylamino)propyl)methyl)amino)methyl)-3,4-dimethoxy-9*H*-xanthen-9-one (**13**, 33.3 mg, 62%).

3,4-Dimethoxy-1-(((2-morpholinoethyl)amino)methyl)-9*H*-xanthen-9-one (**12**); mp 125-126 °C (chloroform); IR (KBr): ν_{max} (cm^{-1}) = 3432, 3303, 2961, 2853, 2816, 1643, 1615, 1584, 1470, 1412, 1328, 1313, 1296, 1276, 1257, 1232, 1146, 1132, 1117, 1076, 1031, 921, 809, 769, 755, 669; ^{1}H NMR ($CDCl_3$, 300.13 MHz): δ (ppm) = 8.25 (1H, dd, *J* = 8.0 and 1.6 Hz, H-8), 7.72 (1H, ddd, *J* = 8.1, 7.0, and 1.6 Hz, H-6), 7.57 (1H, dd, *J* = 8.4 and 0.8 Hz, H-5), 7.38 (1H, ddd, *J* = 8.0, 7.1 and 0.9 Hz, H-7), 7.09 (1H, s, H-2), 4.34 (2H, s, H-1'); 4.04 (3H, s, H-4), 4.01 (3H, s, H-3), 3.66 (4H, t, *J* = 4.6 Hz, H-5'), 2.90 (2H, t, *J* = 6.1 Hz, H-2'), 2.60 (2H, t, *J* = 6.1 Hz, H-3'), 2.47 (4H, t, *J* = 4.3 Hz, H-4'); ^{13}C-NMR ($CDCl_3$, 75.47 MHz): δ (ppm) = 178.0 (C-9), 156.5 (C-3), 155.3 (C-10a), 152.1 (C-4a), 137.0 (C-1), 136.0 (C-4), 134.6 (C-6), 126.5 (C-8), 124.1 (C-7), 122.1 (C-8a), 117.7 (C-5), 114.6 (C-9a), 111.6 (C-2), 67.0 (C-5'), 61.5 (C-4''), 57.4 (C-2'), 56.4 (C-3''), 53.7 (C-1'), 53.5 (C-4'), 45.3 (C-3').

1-(((3-(Dimethylamino)propyl)methyl)amino)methyl)-3,4-dimethoxy-9*H*-xanthen-9-one (**13**); mp 84-85 °C (chloroform); IR (KBr): ν_{max} (cm^{-1}) = 3436, 2938, 2857, 2817, 1650, 1615, 1599, 1584, 1464, 1428, 1414, 1346, 1314, 1274, 1259, 1233, 1154, 1129, 1084, 1039, 997, 925, 913, 893, 765, 674; ^{1}H NMR ($CDCl_3$, 300.13 MHz): δ (ppm) = 8.25 (1H, dd, *J* = 8.0 and 1.6 Hz, H-8), 7.69 (1H, ddd, *J* = 8.5, 7.0, and 1.6 Hz, H-6), 7.54 (1H, dd, *J*

= 7.4 and 0.7, H-5), 7.53 (1H, s, H-2), 7.35 (1H, ddd, *J* = 8.0, 7.1 and 1.0 Hz, H-7), 4.36 (2H, s, H-1'); 4.05 (3H, s, H-4), 4.02 (3H, s, H-3), 2.65 (2H, t, *J* = 7.2 Hz, H-3'), 2.44 (2H, t, *J* = 7.5 Hz, H-5'), 2.39 (3H, s, H-2'), 2.28 (6H, s, H-6'), 1.82 (2H, m, *J* = 7.3 Hz, H-4'); ^{13}C-NMR ($CDCl_3$, 75.47 MHz): δ (ppm) = 178.1 (C-9), 156.6 (C-3), 155.2 (C-10a), 151.9 (C-4a), 135.2 (C-1), 135.0 (C-4), 134.2 (C-6), 126.6 (C-8), 123.9 (C-7), 122.4 (C-8a), 117.6 (C-5), 114.5 (C-9a), 109.0 (C-2), 61.5 (C-4''), 60.1 (C-1'), 57.8 (C-5'), 56.4 (C-3''), 56.1 (C-3'), 45.3 (C-6'), 42.5 (C-2'), 25.3 (C-4').

5.3.2.2. Synthesis of 1-(((2-(diethylamino)ethyl)amino)methyl)-3,4-dimethoxy-9*H*-xanthen-9-one (14)

Compound **14** was synthesized based on the procedure described in 3.1.2. After the completion of reaction, a liquid-liquid extraction of the crude material was performed only with chloroform (3 x 10 ml). The organic layers were gathered, washed with water (10 ml), dried over anhydrous sodium sulphate and was concentrated under reduced pressure. The solid obtained was purified by solid phase extraction with a cation exchange cartridge Discovery® DSC-SCX, following an identical procedure of section 3.1.1. for derivative **11**. The non-basic and basic fractions were controlled by TLC using methanol/TEA 100:0.1 as mobile phase. The basic fractions were gathered and evaporated under reduced pressure. Then, the crude material was purified by a chromatography flash cartridge (chloroform/acetone/TEA in gradient), resulting in a pure green solid of 1-(((2-(diethylamino)ethyl)amino)methyl)-3,4-dimethoxy-9*H*-xanthen-9-one (**14**, 21.3 mg, 40%).

1-(((2-(Diethylamino)ethyl)amino)methyl)-3,4-dimethoxy-9*H*-xanthen-9-one (**14**); mp 68-69 °C (chloroform); IR (KBr): ν_{max} (cm^{-1}) = 3444, 3316, 2968, 2940, 2841, 1645, 1615, 1600, 1585, 1567, 1467, 1435, 1409, 1313, 1258, 1232, 1198, 1131, 1075, 1031, 983, 937, 767, 752, 685; ^{1}H NMR ($CDCl_3$, 300.13 MHz): δ (ppm) = 8.27 (1H, dd, *J* = 8.0 and 1.4 Hz, H-8), 7.71 (1H, ddd, *J* = 8.5, 7.0, and 1.6 Hz, H-6), 7.56 (1H, dd, *J* = 8.4 and 0.7 Hz, H-5), 7.37 (1H, ddd, *J* = 8.0, 7.1 and 1.0 Hz, H-7), 7.14 (1H, s, H-2), 4.39 (2H, s, H-1'); 4.05 (3H, s, H-4), 4.01 (3H, s, H-3), 2.87 (2H, t, *J* = 6.4 Hz, H-2'), 2.68 (2H, t, *J* = 6.4 Hz, H-3'), 2.55 (4H, m, *J* = 7.1 Hz, H-4'), 1.01 (6H, t, *J* = 7.1 Hz, H-5'); ^{13}C-NMR ($CDCl_3$, 75.47 MHz): δ (ppm) = 178.1 (C-9), 156.5 (C-3), 155.3 (C-10a), 152.1 (C-4a), 137.4 (C-1), 135.8 (C-4), 134.5 (C-6), 126.6 (C-8), 124.0 (C-7), 122.2 (C-8a), 117.7 (C-5), 114.5 (C-9a), 111.1 (C-2), 61.5 (C-4''), 56.4 (C-3''), 53.4 (C-3'), 52.4 (C-1'), 46.9 (C-4'), 46.8 (C-2'), 11.6 (C-5'). EI-MS (70 eV) m/z (rel. intensity, %): 383.8 (M^+, 2), 368.4 (8), 355.0 (9), 326.4 (3), 301.1

(9), 300.1 (21), 298.1 (40), 269.2 (45), 250.3 (6), 225.1 (27), 208.4 (10), 155.2 (6), 115.1 (22), 86.2 (100), 58.1 (45).

5.3.2.3. Synthesis of 1-((4-(2-hydroxyethyl)piperazin-1-yl)methyl)-3,4-dimethoxy-9*H*-xanthen-9-one (15)

Compound **15** was synthesized based on the procedure described in 3.1.2. After the completion of reaction, the crude material was subjected to a similar liquid-liquid extraction procedure described in section 3.2.1. The organic layer resulting from the liquid-liquid extraction was dried and concentrated under reduced pressure furnishing a yellow solid corresponding to 1-((4-(2-hydroxyethyl)piperazin-1-yl)methyl)-3,4-dimethoxy-9*H*-xanthen-9-one (**15**, 38 mg, 68%).

1-((4-(2-Hydroxyethyl)piperazin-1-yl)methyl)-3,4-dimethoxy-9*H*-xanthen-9-one (**15**); mp 129-130 °C (chloroform); IR (KBr): ν_{max} (cm^{-1}) = 3423, 2932, 2804, 2759, 1652, 1617, 1601, 1586, 1569, 1505, 1466, 1448, 1405, 1345, 1315, 1268, 1256, 1234, 1160, 1129. 1065, 1033, 996, 918, 896, 765, 754; ^{1}H NMR ($CDCl_3$, 300.13 MHz): δ (ppm) = 8.25 (1H, dd, *J* = 8.0 and 1.6 Hz, H-8), 7.68 (1H, ddd, *J* = 8.5, 7.0, and 1.6 Hz, H-6), 7.53 (1H, dd, *J* = 8.4 and 0.7 Hz, H-5), 7.48 (1H, s, H-2), 7.35 (1H, ddd, *J* = 8.0, 7.1 and 1.0 Hz, H-7), 4.32 (2H, s, H-1'), 4.03 (3H, s, H-4), 4.01 (3H, s, H-3), 3,63 (2H, t, *J* = 5.4 Hz), 2.58 (2H, t, *J* = 5.4 Hz); ^{13}C-NMR ($CDCl_3$, 75.47 MHz): δ (ppm) = 178.1 (C-9), 156.5 (C-3), 155.2 (C-10a), 152.0 (C-4a), 138.8 (C-1), 134.8 (C-4), 134.2 (C-6), 126.6 (C-8), 123.9 (C-7), 122.5 (C-8a), 117.5 (C-5), 114.6 (C-9a), 108.2 (C-2), 61.5 (C-4''), 60.2 (C-1'), 59.3 (C-5'), 57.7 (C-4'), 56.2 (C-3''), 53.5 (C-3'), 53.2 (C-2'). EI-MS (70 eV) m/z (rel. intensity, %): 399.0 (M^+, 8), 312.0 (49), 311.1 (17), 310.1 (11), 270.1 (35), 269.1 (54), 255.1 (31), 225.2 (28), 176.1 (24), 139.1 (6), 130.1 (17), 111.1 (38), 98.1 (100), 73.1 (70), 56.1 (33).

5.3.2.4. Synthesis of 4-((3,4-dimethoxy-9-oxo-9*H*-xanthen-1-yl)methyl) piperazin-2-one (16), 1-((5-amino-3,4-dihydroisoquinolin-2(1*H*)-yl)methyl)-3,4-dimethoxy-9*H*-xanthen-9-one (17), and 3,4-dimethoxy-1-(piperidin-1-ylmethyl)-9*H*-xanthen-9-one (18)

Compounds **16**, **17,** and **18** were synthesized based on the procedure described in 3.1.2. After the completion of reaction, a liquid-liquid extraction of the crude material was performed only with chloroform. The resulting organic layer was dried and concentrated under reduced pressure. The solid thus obtained was subjected to a solid phase

extraction with cation exchange cartridge Discovery® DSC-SCX, following an identical procedure described in section 3.1.1. The non-basic and basic fractions were controlled by TLC using methanol/TEA 100:0.1 as mobile phase. The basic fractions containing a single spot of **16** and **18** were gathered and concentrated under reduced pressure, furnishing a pure orange solid of 4-((3,4-dimethoxy-9-oxo-9*H*-xanthen-1-yl)methyl)piperazin-2-one (**16**, 18.2 mg, 35%) and a pure yellow solid of 3,4-dimethoxy-1-(piperidin-1-ylmethyl)-9*H*-xanthen-9-one (**18**, 28.8 mg, 58%). The crystallization from the fraction with NH_3 2% in methanol resulted in a pure white solid of 1-((5-amino-3,4-dihydroisoquinolin-2(1*H*)-yl)methyl)-3,4-dimethoxy-9*H*-xanthen-9-one (**17**, 21 mg, 36%).

4-((3,4-Dimethoxy-9-oxo-9*H*-xanthen-1-yl)methyl)piperazin-2-one (**16**); mp 245-247 °C (methanol); IR (KBr): ν_{max} (cm^{-1}) = 3547, 3421, 3280, 2958, 2923, 2852, 1675, 1646, 1617, 1599, 1585, 1569, 1505, 1465, 1430, 1380, 1350, 1320, 1259, 1232, 1129, 1108, 1060, 1000, 978, 927, 765; ^{1}H NMR (DMSO, 300.13 MHz): δ (ppm) = 8.13 (1H, dd, *J* = 8.0 and 1.5 Hz, H-8), 7.82 (1H, ddd, *J* = 8.5, 7.0, and 1.6 Hz, H-6), 7.65 (1H, dd, *J* = 8.4 and 0.6, H-5), 7.45 (1H, ddd, *J* = 8.0, 7.1 and 1.0 Hz, H-7), 7.36 (1H, s, H-2), 4.24 (2H, s, H-1'); 3.98 (3H, s, H-4), 3.90 (3H, s, H-3), 3.20 (2H, t, *J* = 5.3 Hz, H-3'), 3.13 (2H, s, H-2'), 2.66 (2H, t, *J* = 5.3 Hz, H-4'); ^{13}C-NMR (DMSO, 75.47 MHz): δ (ppm) = 176.7 (C-9), 168.0 (C-4'), 156.2 (C-3), 154.6 (C-10a), 151.8 (C-4a), 136.9 (C-1), 135.0 (C-4), 134.7 (C-6), 126.1 (C-8), 124.3 (C-7), 121.8 (C-8a), 117.7 (C-5), 113.7 (C-9a), 109.2 (C-2), 60.9 (C-4''), 58.5 (C-1'), 57.2 (C-3'), 56.3 (C-3''), 48.7 (C-2'), 30.7 (C-5').

1-((5-Amino-3,4-dihydroisoquinolin-2(1*H*)-yl)methyl)-3,4-dimethoxy-9*H*-xanthen-9-one (**17**); mp 171-172 °C (methanol); IR (KBr): ν_{max} (cm^{-1}) = 3463, 3387, 2927, 2866, 1654, 1617, 1600, 1585, 1567, 1504, 1466, 1416, 1362, 1343, 1315, 1257, 1232, 1187, 1130, 1062, 1017, 998, 927, 765; ^{1}H NMR ($CDCl_3$, 300.13 MHz): δ (ppm) = 8.26 (1H, dd, *J* = 8.0 and 1.4 Hz, H-8), 7.69 (1H, ddd, *J* = 8.5, 7.0, and 1.6 Hz, H-6), 7.57 (1H, s, H-2), 7.54 (1H, dd, *J* = 8.4 and 0.7 Hz, H-5), 7.35 (1H, ddd, *J* = 8.0, 7.1 and 1.0 Hz, H-7), 6.99 (1H, t, *J* = 7.7 Hz, H-6'), 6.57 (1H, d, *J* = 7.8 Hz, H-7'), 6.53 (1H, d, *J* = 7.6 Hz, H-7'), 4.48 (2H, s, H-1'); 4.02 (3H, s, H-4), 3.97 (3H, s, H-3), 3.81 (2H, s, H-3'), 2.93 (2H, t, *J* = 5.9 Hz, H-2'), 2.66 (2H, t, *J* = 5.9 Hz, H-4'); ^{13}C-NMR ($CDCl_3$, 75.47 MHz): δ (ppm) = 178.2 (C-9), 156.7 (C-3), 155.2 (C-10a), 151.9 (C-4a), 144.1 (C-8'), 139.3 (C-1), 136.3 (C-5'), 134.8 (C-4), 134.2 (C-6), 126.6 (C-8), 126.4 (C-9'), 123.8 (C-7), 122.5 (C-8a), 119.5 (C-6'), 117.6 (C-5), 117.1 (C-7'), 114.5 (C-9a), 112.7 (C-10'), 108.0 (C-2), 61.5 (C-4''), 60.1 (C-1'), 56.7 (C-3'), 56.3 (C-3''), 51.0 (C-2'), 24.9 (C-4').

3,4-Dimethoxy-1-(piperidin-1-ylmethyl)-9*H*-xanthen-9-one (**18**); mp 108-109 °C (chloroform); IR (KBr): ν_{max} (cm^{-1}) = 3432, 2929, 2853, 1653, 1617, 1600, 1568, 1502, 1465, 1447, 1405, 1344, 1315, 1257, 1233, 1188, 1130, 1063, 999, 895, 765; ^{1}H NMR ($CDCl_3$, 300.13 MHz): δ (ppm) = 8.25 (1H, dd, *J* = 8.0 and 1.6 Hz, H-8), 7.66 (1H, ddd, *J* = 8.5, 8.0, and 1.6 Hz, H-6), 7.56 (1H, s, H-2), 7.52 (1H, dd, *J* = 8.3 and 0.7 Hz, H-5), 7.33 (1H, ddd, *J* = 7.9, 7.1 and 0.9 Hz, H-7), 4.26 (2H, s, H-1'); 4.03 (3H, s, H-4), 4.01 (3H, s, H-3), 2.57 (4H, t, *J* = 4.6 Hz, H-2'), 1.65 (4H, m, *J* = 5.5 Hz, H-3'), 1,50 (2H, m, *J* = 5.5 Hz, H-4'); ^{13}C-NMR ($CDCl_3$, 75.47 MHz): δ (ppm) = 177.5 (C-9), 156.1 (C-3), 154.7 (C-10a), 151.3 (C-4a), 138.9 (C-4), 134.2 (C-1), 133.8 (C-6), 126.0 (C-8), 123.3 (C-7), 121.9 (C-8a), 117.1 (C-5), 113.9 (C-9a), 107.8 (C-2), 60.8 (C-4''), 56.1 (C-3''), 55.7 (C-2'), 54.3 (C-1'), 25.7 (C-3'), 23.8 (C-4'). EI-MS (70 eV) m/z (rel. intensity, %): 352.9 (M^+, 6), 309.9 (8), 280.2 (9), 268.0 (27), 255.0 (23), 253.1 (15), 225.0 (13), 184.0 (9), 127.1 (14), 126.0 (6), 84.0 (100), 56.0 (14).

5.3.2.5. Synthesis of 1-(((4-fluorobenzyl)amino)methyl)-3,4-dimethoxy-9*H*-xanthen-9-one (19), 1-(((4-chlorobenzyl)amino)methyl)-3,4-dimethoxy-9*H*-xanthen-9-one (20), 1-(((1-(4-chlorophenyl)ethyl)amino)methyl)-3,4-dimethoxy-9*H*-xanthen-9-one (21), and 1-(((4-bromobenzyl)amino)methyl)-3,4-dimethoxy-9*H*-xanthen-9-one (22)

Compounds **19**, **20**, **21,** and **22** were synthesized based on the procedure described in 3.1.2. After the completion of reaction, the crude material was subjected to a similar liquid-liquid extraction procedure described in section 3.2.1. for amines **12** and **13**. The organic layer resulting from the extraction with HCl 5M, containing the halogenated aromatic derivatives, was dried and concentrated under reduced pressure. Afterwards, a solid phase extraction with cation exchange cartridge Discovery® DSC-SCX was carried out, following an identical procedure described in section 3.1.1. The non-basic and basic fractions were controlled by TLC using chloroform/acetone/TEA 5:5:0.1 as mobile phase. The basic fractions containing only a single spot corresponding to these aminoxanthone derivatives were gathered and concentrated under reduced pressure. It was obtained a pure light yellow solid of 1-(((4-chlorobenzyl)amino)methyl)-3,4-dimethoxy-9*H*-xanthen-9-one (**20**, 33 mg, 57%) and a pure white solid of 1-(((4-fluorobenzyl)amino)methyl)-3,4-dimethoxy-9*H*-xanthen-9-one (**19**, 22.5 mg, 41%), 1-(((1-(4-chlorophenyl)ethyl)amino) methyl)-3,4-dimethoxy-9*H*-xanthen-9-one (**21**, 37.5 mg, 63%) and 1-(((4-bromobenzyl) amino)methyl)-3,4-dimethoxy-9*H*-xanthen-9-one (**22,** 44.5 mg, 70%).

1-(((4-Fluorobenzyl)amino)methyl)-3,4-dimethoxy-9*H*-xanthen-9-one (**19**); mp 163-165 °C (methanol); IR (KBr): ν_{max} (cm^{-1}) = 3426, 3322, 2921, 2853, 1645, 1614, 1600, 1584, 1563, 1507, 1467, 1429, 1405, 1329, 1312, 1260, 1233, 1217, 1193, 1132, 1089, 1073, 1010, 974, 933, 815, 765, 685; ^{1}H NMR ($CDCl_3$, 300.13 MHz): δ = 8.28 (1H, dd, *J* = 8.0 and 1.6 Hz, H-8), 7.71 (1H, ddd, *J* = 8.5, 7.0, and 1.6 Hz, H-6), 7.55 (1H, dd, *J* = 8.5 and 0.8 Hz, H-5), 7.40 (1H, ddd, *J* = 8.0, 7.0 and 0.8 Hz, H-7), 7.36 (2H, m, H-4'), 7.01 (2H, m, H-3'), 6.96 (1H, s, H-2), 4.30 (2H, s, H-1'), 4.01 (3H, s, H-4), 4.01 (3H, s, H-3), 3.85 (2H, s, H-2'); ^{13}C-NMR ($CDCl_3$, 75.47 MHz): *δ* = 178.1 (C-9), 160.3 (C-6'), 156.3 (C-3), 155.3 (C-10a), 152.2 (C-4a), 138.6 (C-4), 135.9 (C-3'), 135.7 (C-1), 134.5 (C-6), 129.8 (C-5'), 126.7 (C-8), 124.0 (C-7), 122.2 (C-8a), 117.7 (C-5), 115.3 (C-4'), 114.7 (C-9a), 110.9 (C-2), 61.5 (C-4''), 56.3 (C-3''), 53.3 (C-1'), 52.5 (C-2'). EI-MS (70 eV) m/z (rel. intensity, %): 395.1 (M+1, 3), 394.0 (M^+, 6), 357.1 (12), 356.0 (47), 340.1 (11), 268.1 (10), 266.1 (24), 252.1 (12), 222.2 (8), 139.2 (4), 110.1 (9), 109.1 (100), 83.1 (31), 73.0 (94).

1-(((4-Chlorobenzyl)amino)methyl)-3,4-dimethoxy-9*H*-xanthen-9-one (**20**); mp 162-163°C; IR (KBr) (methanol): ν_{max} (cm^{-1}) = 3443, 3315, 2919, 2847, 2779, 1655, 1615, 1595, 1569, 1499, 1464, 1437, 1408, 1317, 1258, 1229, 1150, 1134, 1085, 1055, 1018, 972, 895, 806, 762, 688; ^{1}H NMR ($CDCl_3$, 300.13 MHz): δ (ppm) = 8.25 (1H, dd, *J* = 8.0 and 1.6 Hz, H-8), 7.79 (1H, ddd, *J* = 8.5, 7.0, and 1.6 Hz, H-6), 7.66 (2H, m, H-4'), 7.60 (1H, dd, *J* = 8.5 and 0.9 Hz, H-5), 7.43 (1H, ddd, *J* = 8.0, 7.0 and 0.9 Hz, H-7), 7.39 (1H, s, H-2), 7.38 (2H, m, H-3'), 4.53 (2H, s, H-2'); 4.33 (2H, s, H-1'), 4.07 (3H, s, H-4), 4.01 (3H, s, H-3); ^{13}C-NMR ($CDCl_3$, 75.47 MHz): δ (ppm) = 179.6 (C-9), 157.0 (C-3), 155.5 (C-10a), 152.0 (C-4a), 137.7 (C-4), 135.8 (C-1), 135.6 (C-6), 131.7 (C-5'), 129.5 (C-4'), 129.4 (C-3'), 127.3 (C-6'), 126.6 (C-8), 124.6 (C-7), 121.3 (C-8a), 117.9 (C-5), 115.5 (C-2), 114.8 (C-9a), 61.6 (C-4''), 57.1 (C-3''), 51.3 (C-1'), 50.7 (C-2'). EI-MS (70 eV) m/z (rel. intensity, %): 410.8 (M+1, 5), 409.8 (M^+, 4), 406.9 (9), 357.8 (10), 355.2 (18), 319.0 (4), 306.0 (20), 268.0 (100), 253.0 (25), 221.1 (14), 209.3 (28), 190.2 (18), 168.1 (10), 139.1 (24), 125.1 (18), 89.0 (26), 77.1 (24).

1-(((1-(4-Chlorophenyl)ethyl)amino)methyl)-3,4-dimethoxy-9*H*-xanthen-9-one (**21**); mp 163-164 °C; IR (KBr) (methanol): ν_{max} (cm^{-1}) = 3425, 3310, 2936, 2847, 2730, 2665, 1655, 1616, 1600, 1567, 1515, 1496, 1465, 1410, 1348, 1321, 1260, 1232, 1205, 1132, 1076, 1018, 980, 922, 844, 766, 755, 670; ^{1}H NMR ($CDCl_3$, 300.13 MHz): δ (ppm) = 8.26 (1H, dd, *J* = 8.0 and 1.6 Hz, H-8), 7.79 (1H, ddd, *J* = 8.5, 7.0, and 1.6 Hz, H-6), 7.70 (2H, m, H-5'), 7.59 (1H, dd, *J* = 8.5 and 0.8 Hz, H-5), 7.43 (1H, ddd, *J* = 8.0, 7.0 and 0.8 Hz, H-7), 7.42 (2H, m, H-4'), 7.25 (1H, s, H-2), 4.54 (2H, s, H-1'); 4.27 (1H, q, *J* = 6.8 Hz, H-1'),

4.04 (3H, s, H-4), 4.01 (3H, s, H-3), 1.83 (3H, d, *J* = 6.8 Hz, H-3'); ^{13}C-NMR ($CDCl_3$, 75.47 MHz): δ (ppm) = 179.6 (C-9), 156.8 (C-3), 155.4 (C-10a), 151.9 (C-4a), 137.6 (C-4), 135.5 (C-6), 134.5 (C-1), 131.8 (C-7'), 129.8 (C-6'), 129.5 (C-5'), 127.3 (C-4'), 126.6 (C-8), 124.6 (C-7), 121.3 (C-8a), 117.9 (C-5), 115.6 (C-2), 114.9 (C-9a), 61.6 (C-4''), 58.9 (C-2'), 57.0 (C-3''), 50.2 (C-1'), 20.2 (C-3'). EI-MS (70 eV) m/z (rel. intensity, %): 423.8 (M^+, 2), 407.6 (4), 319.6 (3), 285.1 (27), 284.1 (100), 268.1 (24), 223.1 (19), 213.1 (27), 196.2 (19), 155.0 (10), 139.0 (25), 103.0 (41), 77.0 (24).

1-(((4-Bromobenzyl)amino)methyl)-3,4-dimethoxy-9*H*-xanthen-9-one (**22**); mp 161-162 °C (methanol); IR (KBr): ν_{max} (cm^{-1}) = 3424, 3317, 2920, 2851, 1645, 1613, 1600, 1585, 1562, 1467, 1430, 1405, 1328, 1314, 1256, 1235, 1151, 1132, 1090, 1073, 1029, 1010, 971, 908, 798, 769, 687; ^{1}H NMR ($CDCl_3$, 300.13 MHz): δ (ppm) = 8.27 (1H, dd, *J* = 8.0 and 1.6 Hz, H-8), 7.73 (1H, ddd, *J* = 8.5, 7.0, and 1.6 Hz, H-6), 7.58 (1H, dd, *J* = 8.5 and 0.8 Hz, H-5), 7.48 (2H, m, H-4'), 7.39 (2H, m, H-3'), 7.38 (1H, ddd, *J* = 8.0, 7.0 and 0.8 Hz, H-7), 7.08 (1H, s, H-2), 4.31 (2H, s, H-1'); 4.01 (3H, s, H-4), 4.01 (3H, s, H-3), 3.88 (2H, s, H-2'); ^{13}C-NMR ($CDCl_3$, 75.47 MHz): δ (ppm) = 178.6 (C-9), 156.5 (C-3), 155.3 (C-10a), 152.2 (C-4a), 136.4 (C-4), 136.2 (C-1), 134.9 (C-6), 131.8 (C-5'), 130.7 (C-4'), 128.4 (C-3'), 126.6 (C-8), 124.2 (C-7), 121.9 (C-8a), 121.8 (C-6'), 117.7 (C-5), 114.7 (C-9a), 112.5 (C-2), 61.6 (C-4''), 56.7 (C-3''), 52.7 (C-1'), 52.0 (C-2'). EI-MS (70 eV) m/z (rel. intensity, %): 454.0 (M^+, 5), 358.2 (2), 357.1 (20), 356.1 (56), 326.1 (9), 295.1 (6), 269.2 (14), 266.1 (23), 255.2 (11), 225.2 (7), 171.0 (22), 169.0 (30), 91.1 (11), 90.1 (40), 73.1 (100).

5.4. Computational chemistry

5.4.1. Preparation of a library of virtual xanthones and known inhibitors of p53:MDM2 interaction

Twenty-two xanthone derivatives, four known inhibitors of p53:MDM2 interaction and one known inhibitor of p73:MDM2 interaction were drawn in ChemSketch (ACD/Labs 2007) and subjected to energy minimization (using ArgusLab version 4.0.1 for Windows) by molecular mechanics using the force field method[104].

5.4.2. Docking studies

Docking simulations in MDM2 (PDB code 1YCR) were undertaken in AutoDock embedded in PyRx – Virtual Screening Tool Software[105]. AutoDock Vina considered the

target conformation as a rigid unit while the ligands were allowed to be flexible and adaptable to the target. The software Vina searched for the lowest binding energy conformations and returned nine different conformations for each ligand.

The following parameters were used in AutoDock Vina:

- Exhaustiveness: 8
- Vina search space (grid box) dimensions and positions in the MDM2:

Center:	Dimensions (Angstrom):
Center_x = 29.7188	Size_x = 18.9279
Center_y = -25.0028	Size_y = 22.6229
Center_z = -6.4459	Size_z = 16.2795

The grid box was defined in PyRx by clicking and dragging the center and edges of the grid box in order to position it as shown in **Figure 18.**

The input files of the virtually designed xanthones were in *mol* format and *pdb* was chosen as the output file format. PyMOL version 0.99[106] was used for visual inspection of results.

5.5. Evaluation of the inhibitory activity on p53:MDM2 interaction using yeast-screening assays

5.5.1. Yeast p53:MDM2 screening assay

For the yeast growth-inhibition assay, the previously[75] obtained *Saccharomyces cerevisiae* CG379 cells expressing p53 and/or MDM2 were used. Yeast cells were routinely grown in a minimal selective medium with 2% (w/w) glucose, 0.7% (w/w) yeast nitrogen base without amino acids from Difco (Quilaban, Sintra, Portugal) and all the amino acids required for yeast growth (50 µg ml^{-1}) except leucine and tryptophan, to approximately 1 optical density at 600 nm (OD_{600}). To induce expression of wt p53 and MDM2 proteins, yeast cells were diluted to 0.05 OD_{600} into selective induction medium with 2% (w/w) galactose and 2% (w/w) raffinose (instead of glucose), and incubated at 30°C under continuous orbital shaking (200 rpm) for approximately 42 h. Yeast cell growth was analyzed by counting the number of CFU per mL (CFU mL^{-1}) after 2 days incubation at 30°C on Sabouraud Dextrose Agar plates from Liofilchem (Frilabo, Porto, Portugal).

To evaluate the effect of tested compounds on cell growth, yeast cells were incubated in selective induction medium in the presence of 1 μm and 10 μm of compounds **12**, **13**, **15**, **16**, **19**, **20** and **22**, or 0.1% DMSO only for approximately 42 h (for analysis of p53:MDM2 interaction), at 30°C, under continuous shaking. Results were estimated considering 100% growth the number of CFU obtained with yeast co-expressing p53 and MDM2 incubated with DMSO only.

CHAPTER 6

REFERENCES

CHAPTER 6 - REFERENCES

1. Suzuki, K.; Matsubara, H., Recent advances in p53 research and cancer treatment. *Journal of biomedicine & biotechnology* **2011,** *2011*, 978312.

2. May, P.; May, E., Twenty years of p53 research: structural and functional aspects of the p53 protein. *Oncogene* **1999,** *18* (53), 7621-36.

3. Isobe, M.; Emanuel, B. S.; Givol, D.; Oren, M.; Croce, C. M., Localization of gene for human p53 tumour antigen to band 17p13. *Nature* **1986,** *320* (6057), 84-5.

4. Joerger, A. C.; Fersht, A. R., The tumor suppressor p53: from structures to drug discovery. *Cold Spring Harbor perspectives in biology* **2010,** *2* (6), a000919.

5. Chene, P., Inhibition of the p53-MDM2 interaction: targeting a protein-protein interface. *Molecular cancer research : MCR* **2004,** *2* (1), 20-8.

6. Coutts, A. S.; Adams, C. J.; La Thangue, N. B., p53 ubiquitination by Mdm2: a never ending tail? *DNA repair* **2009,** *8* (4), 483-90.

7. Zhao, Y.; Aguilar, A.; Bernard, D.; Wang, S., Small-Molecule Inhibitors of the MDM2-p53 Protein-Protein Interaction (MDM2 Inhibitors) in Clinical Trials for Cancer Treatment. *Journal of medicinal chemistry* **2015,** *58* (3), 1038-52.

8. Khoury, K.; Popowicz, G. M.; Holak, T. A.; Domling, A., The p53-MDM2/MDMX axis - A chemotype perspective. *Medchemcomm* **2011,** *2*, 246-260.

9. Popowicz, G. M.; Dömling, A.; Holak, T. A., The Structure-Based Design of Mdm2/Mdmx–p53 Inhibitors Gets Serious. *Angewandte Chemie International Edition* **2011,** *50* (12), 2680-2688.

10. Wang, W.; Hu, Y., Small molecule agents targeting the p53-MDM2 pathway for cancer therapy. *Medicinal research reviews* **2012,** *32* (6), 1159-96.

11. Wade, M.; Wang, Y. V.; Wahl, G. M., The p53 orchestra: Mdm2 and Mdmx set the tone. *Trends in cell biology* **2010,** *20* (5), 299-309.

12. Toledo, F.; Wahl, G. M., MDM2 and MDM4: p53 regulators as targets in anticancer therapy. *The international journal of biochemistry & cell biology* **2007,** *39* (7-8), 1476-82.

13. Moll, U. M.; Petrenko, O., The MDM2-p53 interaction. *Molecular cancer research : MCR* **2003,** *1* (14), 1001-8.

14. Jones, S. N.; Roe, A. E.; Donehower, L. A.; Bradley, A., Rescue of embryonic lethality in Mdm2-deficient mice by absence of p53. *Nature* **1995,** *378* (6553), 206-8.

15. Freedman, D. A.; Wu, L.; Levine, A. J., Functions of the MDM2 oncoprotein. *Cellular and molecular life sciences : CMLS* **1999,** *55* (1), 96-107.

16. Dickens, M. P.; Fitzgerald, R.; Fischer, P. M., Small-molecule inhibitors of MDM2 as new anticancer therapeutics. *Seminars in cancer biology* **2010,** *20* (1), 10-8.

17. Hu, C. Q.; Hu, Y. Z., Small molecule inhibitors of the p53-MDM2. *Current medicinal chemistry* **2008,** *15* (17), 1720-30.

18. (a) Lam, S.; Lodder, K.; Teunisse, A. F.; Rabelink, M. J.; Schutte, M.; Jochemsen, A. G., Role of Mdm4 in drug sensitivity of breast cancer cells. *Oncogene* **2010,** *29* (16), 2415-26; (b) Shvarts, A.; Steegenga, W. T.; Riteco, N.; van Laar, T.; Dekker, P.; Bazuine, M.; van Ham, R. C.; van der Houven van Oordt, W.; Hateboer, G.; van der Eb, A. J.; Jochemsen, A. G., MDMX: a novel p53-binding protein with some functional properties of MDM2. *The EMBO journal* **1996,** *15* (19), 5349-57.

19. Lane, D. P.; Cheok, C. F.; Lain, S., p53-based cancer therapy. *Cold Spring Harbor perspectives in biology* **2010,** *2* (9), a001222.

20. Joseph, T. L.; Madhumalar, A.; Brown, C. J.; Lane, D. P.; Verma, C. S., Differential binding of p53 and nutlin to MDM2 and MDMX: computational studies. *Cell cycle* **2010,** *9* (6), 1167-81.

21. Madden, M. M.; Muppidi, A.; Li, Z.; Li, X.; Chen, J.; Lin, Q., Synthesis of cell-permeable stapled peptide dual inhibitors of the p53-Mdm2/Mdmx interactions via photoinduced cycloaddition. *Bioorganic & medicinal chemistry letters* **2011,** *21* (5), 1472-5.

22. (a) Kaghad, M.; Bonnet, H.; Yang, A.; Creancier, L.; Biscan, J. C.; Valent, A.; Minty, A.; Chalon, P.; Lelias, J. M.; Dumont, X.; Ferrara, P.; McKeon, F.; Caput, D., Monoallelically expressed gene related to p53 at 1p36, a region frequently deleted in neuroblastoma and other human cancers. *Cell* **1997,** *90* (4), 809-19; (b) Yang, A.; Kaghad, M.; Wang, Y.; Gillett, E.; Fleming, M. D.; Dotsch, V.; Andrews, N. C.; Caput, D.; McKeon, F., p63, a p53 homolog at 3q27-29, encodes multiple products with transactivating, death-inducing, and dominant-negative activities. *Mol Cell* **1998,** *2* (3), 305-16.

23. Murray-Zmijewski, F.; Lane, D. P.; Bourdon, J. C., p53//p63//p73 isoforms: an orchestra of isoforms to harmonise cell differentiation and response to stress. *Cell Death Differ* **2006,** *13* (6), 962-972.

24. Khoury, M. P.; Bourdon, J. C., The isoforms of the p53 protein. *Cold Spring Harbor perspectives in biology* **2010,** *2* (3), a000927.

25. Khoury, M. P.; Bourdon, J.-C., p53 Isoforms An Intracellular Microprocessor? *Genes & cancer* **2011,** *2* (4), 453-465.

26. Bourdon, J.-C.; Fernandes, K.; Murray-Zmijewski, F.; Liu, G.; Diot, A.; Xirodimas, D. P.; Saville, M. K.; Lane, D. P., p53 isoforms can regulate p53 transcriptional activity. *Genes & development* **2005,** *19* (18), 2122-2137.

27. Ongkeko, W. M.; Wang, X. Q.; Siu, W. Y.; Lau, A. W.; Yamashita, K.; Harris, A. L.; Cox, L. S.; Poon, R. Y., MDM2 and MDMX bind and stabilize the p53-related protein p73. *Current biology* **1999,** *9* (15), 829-832.

28. Zeng, X.; Chen, L.; Jost, C. A.; Maya, R.; Keller, D.; Wang, X.; Kaelin, W. G.; Oren, M.; Chen, J.; Lu, H., MDM2 suppresses p73 function without promoting p73 degradation. *Molecular and cellular biology* **1999,** *19* (5), 3257-3266.

29. (a) Wang, X.; Arooz, T.; Siu, W. Y.; Chiu, C. H.; Lau, A.; Yamashita, K.; Poon, R. Y., MDM2 and MDMX can interact differently with ARF and members of the p53 family. *FEBS letters* **2001,** *490* (3), 202-208; (b) Collavin, L.; Lunardi, A.; Del Sal, G., p53-family proteins and their regulators: hubs and spokes in tumor suppression. *Cell Death Differ* **2010,** *17* (6), 901-11.

30. Khoury, K.; Popowicz, G. M.; Holak, T. A.; Domling, A., The p53-MDM2/MDMX axis - A chemotype perspective. *MedChemComm* **2011,** *2* (4), 246-260.

31. Kussie, P. H.; Gorina, S.; Marechal, V.; Elenbaas, B.; Moreau, J.; Levine, A. J.; Pavletich, N. P., Structure of the MDM2 oncoprotein bound to the p53 tumor suppressor transactivation domain. *Science (New York, N.Y.)* **1996,** *274* (5289), 948-53.

32. Popowicz, G. M.; Czarna, A.; Holak, T. A., Structure of the human Mdmx protein bound to the p53 tumor suppressor transactivation domain. *Cell cycle* **2008,** *7* (15), 2441-3.

33. Zhao, Y.; Bernard, D.; Wang, S., Small molecule inhibitors of MDM2-p53 and MDMX-p53 interactions as new cancer therapeutics. *BioDiscovery* **2013,** *8*.

34. Koblish, H. K.; Zhao, S.; Franks, C. F.; Donatelli, R. R.; Tominovich, R. M.; LaFrance, L. V.; Leonard, K. A.; Gushue, J. M.; Parks, D. J.; Calvo, R. R.; Milkiewicz, K. L.; Marugan, J. J.; Raboisson, P.; Cummings, M. D.; Grasberger, B. L.; Johnson, D. L.; Lu, T.; Molloy, C. J.; Maroney, A. C., Benzodiazepinedione inhibitors of the Hdm2:p53 complex suppress human tumor cell proliferation in vitro and sensitize tumors to doxorubicin in vivo. *Molecular cancer therapeutics* **2006,** *5* (1), 160-9.

35. Yuan, Y.; Liao, Y. M.; Hsueh, C. T.; Mirshahidi, H. R., Novel targeted therapeutics: inhibitors of MDM2, ALK and PARP. *Journal of hematology & oncology* **2011,** *4*, 16.

36. Essmann, F.; Schulze-Osthoff, K., Translational approaches targeting the p53 pathway for anti-cancer therapy. *British journal of pharmacology* **2012,** *165* (2), 328-44.

37. Beck, H. P.; DeGraffenreid, M.; Fox, B.; Allen, J. G.; Rew, Y.; Schneider, S.; Saiki, A. Y.; Yu, D.; Oliner, J. D.; Salyers, K.; Ye, Q.; Olson, S., Improvement of the synthesis and pharmacokinetic properties of chromenotriazolopyrimidine MDM2-p53 protein-protein inhibitors. *Bioorganic & medicinal chemistry letters* **2011,** *21* (9), 2752-5.

38. Secchiero, P.; Bosco, R.; Celeghini, C.; Zauli, G., Recent advances in the therapeutic perspectives of Nutlin-3. *Current pharmaceutical design* **2011,** *17* (6), 569-77.

39. Kunkele, A.; De Preter, K.; Heukamp, L.; Thor, T.; Pajtler, K. W.; Hartmann, W.; Mittelbronn, M.; Grotzer, M. A.; Deubzer, H. E.; Speleman, F.; Schramm, A.; Eggert, A.; Schulte, J. H., Pharmacological activation of the p53 pathway by nutlin-3 exerts anti-tumoral effects in medulloblastomas. *Neuro-oncology* **2012,** *14* (7), 859-69.

40. Tovar, C.; Graves, B.; Packman, K.; Filipovic, Z.; Higgins, B.; Xia, M.; Tardell, C.; Garrido, R.; Lee, E.; Kolinsky, K.; To, K. H.; Linn, M.; Podlaski, F.; Wovkulich, P.; Vu, B.; Vassilev, L. T., MDM2 small-molecule antagonist RG7112 activates p53 signaling and regresses human tumors in preclinical cancer models. *Cancer research* **2013,** *73* (8), 2587-97.

41. Voltan, R.; Secchiero, P.; Corallini, F.; Zauli, G., Selective induction of TP53I3/p53-inducible gene 3 (PIG3) in myeloid leukemic cells, but not in normal cells, by Nutlin-3. *Molecular carcinogenesis* **2014,** *53* (6), 498-504.

42. Patil, S. P.; Pacitti, M. F.; Gilroy, K. S.; Ruggiero, J. C.; Griffin, J. D.; Butera, J. J.; Notarfrancesco, J. M.; Tran, S.; Stoddart, J. W., Identification of antipsychotic drug fluspirilene as a potential p53-MDM2 inhibitor: a combined computational and experimental study. *Journal of computer-aided molecular design* **2015,** *29* (2), 155-63.

43. Hardcastle, I. R.; Liu, J.; Valeur, E.; Watson, A.; Ahmed, S. U.; Blackburn, T. J.; Bennaceur, K.; Clegg, W.; Drummond, C.; Endicott, J. A.; Golding, B. T.; Griffin, R. J.; Gruber, J.; Haggerty, K.; Harrington, R. W.; Hutton, C.; Kemp, S.; Lu, X.; McDonnell, J. M.; Newell, D. R.; Noble, M. E.; Payne, S. L.; Revill, C. H.; Riedinger, C.; Xu, Q.; Lunec, J., Isoindolinone inhibitors of the murine double minute 2 (MDM2)-p53 protein-protein interaction: structure-activity studies leading to improved potency. *Journal of medicinal chemistry* **2011,** *54* (5), 1233-43.

44. Carry, J. C.; Garcia-Echeverria, C., Inhibitors of the p53/hdm2 protein-protein interaction-path to the clinic. *Bioorganic & medicinal chemistry letters* **2013,** *23* (9), 2480-5.

45. Rothweiler, U.; Czarna, A.; Krajewski, M.; Ciombor, J.; Kalinski, C.; Khazak, V.; Ross, G.; Skobeleva, N.; Weber, L.; Holak, T. A., Isoquinolin-1-one inhibitors of the MDM2-p53 interaction. *ChemMedChem* **2008,** *3* (7), 1118-28.

46. Gonzalez, A. Z.; Li, Z.; Beck, H. P.; Canon, J.; Chen, A.; Chow, D.; Duquette, J.; Eksterowicz, J.; Fox, B. M.; Fu, J.; Huang, X.; Houze, J.; Jin, L.; Li, Y.; Ling, Y.; Lo, M. C.; Long, A. M.; McGee, L. R.; McIntosh, J.; Oliner, J. D.; Osgood, T.; Rew, Y.; Saiki, A. Y.; Shaffer, P.; Wortman, S.; Yakowec, P.; Yan, X.; Ye, Q.; Yu, D.; Zhao, X.; Zhou, J.; Olson, S. H.; Sun, D.; Medina, J. C., Novel inhibitors of the MDM2-p53 interaction featuring hydrogen bond acceptors as carboxylic acid isosteres. *Journal of medicinal chemistry* **2014,** *57* (7), 2963-88.

47. Bernard, D.; Zhao, Y.; Wang, S., AM-8553: a novel MDM2 inhibitor with a promising outlook for potential clinical development. *Journal of medicinal chemistry* **2012,** *55* (11), 4934-5.

48. Rew, Y.; Sun, D.; Yan, X.; Beck, H. P.; Canon, J.; Chen, A.; Duquette, J.; Eksterowicz, J.; Fox, B. M.; Fu, J.; Gonzalez, A. Z.; Houze, J.; Huang, X.; Jiang, M.; Jin, L.; Li, Y.; Li, Z.; Ling, Y.; Lo, M. C.; Long, A. M.; McGee, L. R.; McIntosh, J.; Oliner, J. D.; Osgood, T.; Saiki, A. Y.; Shaffer, P.; Wang, Y. C.; Wortman, S.; Yakowec, P.; Ye, Q.; Yu, D.; Zhao, X.; Zhou, J.; Medina, J. C.; Olson, S. H., Discovery of AM-7209, a potent and selective 4-amidobenzoic acid inhibitor of the MDM2-p53 interaction. *Journal of medicinal chemistry* **2014,** *57* (24), 10499-511.

49. Zhuang, C.; Miao, Z.; Zhu, L.; Dong, G.; Guo, Z.; Wang, S.; Zhang, Y.; Wu, Y.; Yao, J.; Sheng, C.; Zhang, W., Discovery, synthesis, and biological evaluation of orally

active pyrrolidone derivatives as novel inhibitors of p53-MDM2 protein-protein interaction. *Journal of medicinal chemistry* **2012,** *55* (22), 9630-42.

50. Rew, Y.; Sun, D.; Gonzalez-Lopez De Turiso, F.; Bartberger, M. D.; Beck, H. P.; Canon, J.; Chen, A.; Chow, D.; Deignan, J.; Fox, B. M.; Gustin, D.; Huang, X.; Jiang, M.; Jiao, X.; Jin, L.; Kayser, F.; Kopecky, D. J.; Li, Y.; Lo, M. C.; Long, A. M.; Michelsen, K.; Oliner, J. D.; Osgood, T.; Ragains, M.; Saiki, A. Y.; Schneider, S.; Toteva, M.; Yakowec, P.; Yan, X.; Ye, Q.; Yu, D.; Zhao, X.; Zhou, J.; Medina, J. C.; Olson, S. H., Structure-based design of novel inhibitors of the MDM2-p53 interaction. *Journal of medicinal chemistry* **2012,** *55* (11), 4936-54.

51. Sun, D.; Li, Z.; Rew, Y.; Gribble, M.; Bartberger, M. D.; Beck, H. P.; Canon, J.; Chen, A.; Chen, X.; Chow, D.; Deignan, J.; Duquette, J.; Eksterowicz, J.; Fisher, B.; Fox, B. M.; Fu, J.; Gonzalez, A. Z.; Gonzalez-Lopez De Turiso, F.; Houze, J. B.; Huang, X.; Jiang, M.; Jin, L.; Kayser, F.; Liu, J. J.; Lo, M. C.; Long, A. M.; Lucas, B.; McGee, L. R.; McIntosh, J.; Mihalic, J.; Oliner, J. D.; Osgood, T.; Peterson, M. L.; Roveto, P.; Saiki, A. Y.; Shaffer, P.; Toteva, M.; Wang, Y.; Wang, Y. C.; Wortman, S.; Yakowec, P.; Yan, X.; Ye, Q.; Yu, D.; Yu, M.; Zhao, X.; Zhou, J.; Zhu, J.; Olson, S. H.; Medina, J. C., Discovery of AMG 232, a potent, selective, and orally bioavailable MDM2-p53 inhibitor in clinical development. *Journal of medicinal chemistry* **2014,** *57* (4), 1454-72.

52. Ding, Q.; Zhang, Z.; Liu, J. J.; Jiang, N.; Zhang, J.; Ross, T. M.; Chu, X. J.; Bartkovitz, D.; Podlaski, F.; Janson, C.; Tovar, C.; Filipovic, Z. M.; Higgins, B.; Glenn, K.; Packman, K.; Vassilev, L. T.; Graves, B., Discovery of RG7388, a potent and selective p53-MDM2 inhibitor in clinical development. *Journal of medicinal chemistry* **2013,** *56* (14), 5979-83.

53. Cheok, C. F.; Verma, C. S.; Baselga, J.; Lane, D. P., Translating p53 into the clinic. *Nature reviews. Clinical oncology* **2011,** *8* (1), 25-37.

54. Conradt, L.; Henrich, A.; Wirth, M.; Reichert, M.; Lesina, M.; Algul, H.; Schmid, R. M.; Kramer, O. H.; Saur, D.; Schneider, G., Mdm2 inhibitors synergize with topoisomerase II inhibitors to induce p53-independent pancreatic cancer cell death. *International journal of cancer. Journal international du cancer* **2013,** *132* (10), 2248-57.

55. Schilling, D.; Duwel, M.; Molls, M.; Multhoff, G., Radiosensitization of wildtype p53 cancer cells by the MDM2-inhibitor PXN727 is associated with altered heat shock protein 70 (Hsp70) levels. *Cell stress & chaperones* **2013,** *18* (2), 183-91.

56. Lu, Y.; Nikolovska-Coleska, Z.; Fang, X.; Gao, W.; Shangary, S.; Qiu, S.; Qin, D.; Wang, S., Discovery of a nanomolar inhibitor of the human murine double minute 2 (MDM2)-p53 interaction through an integrated, virtual database screening strategy. *Journal of medicinal chemistry* **2006,** *49* (13), 3759-62.

57. Ding, K.; Lu, Y.; Nikolovska-Coleska, Z.; Qiu, S.; Ding, Y.; Gao, W.; Stuckey, J.; Krajewski, K.; Roller, P. P.; Tomita, Y.; Parrish, D. A.; Deschamps, J. R.; Wang, S., Structure-based design of potent non-peptide MDM2 inhibitors. *Journal of the American Chemical Society* **2005,** *127* (29), 10130-1.

58. Ding, K.; Lu, Y.; Nikolovska-Coleska, Z.; Wang, G.; Qiu, S.; Shangary, S.; Gao, W.; Qin, D.; Stuckey, J.; Krajewski, K.; Roller, P. P.; Wang, S., Structure-based design of spiro-oxindoles as potent, specific small-molecule inhibitors of the MDM2-p53 interaction. *Journal of medicinal chemistry* **2006,** *49* (12), 3432-5.

59. Jahn, A.; Hinselmann, G.; Fechner, N.; Zell, A., Optimal assignment methods for ligand-based virtual screening. *Journal of Cheminformatics* **2009,** *1*, 14-14.

60. Shangary, S.; Qin, D.; McEachern, D.; Liu, M.; Miller, R. S.; Qiu, S.; Nikolovska-Coleska, Z.; Ding, K.; Wang, G.; Chen, J.; Bernard, D.; Zhang, J.; Lu, Y.; Gu, Q.; Shah, R. B.; Pienta, K. J.; Ling, X.; Kang, S.; Guo, M.; Sun, Y.; Yang, D.; Wang, S., Temporal activation of p53 by a specific MDM2 inhibitor is selectively toxic to tumors and leads to complete tumor growth inhibition. *Proceedings of the National Academy of Sciences of the United States of America* **2008,** *105* (10), 3933-8.

61. Mohammad, R. M.; Wu, J.; Azmi, A. S.; Aboukameel, A.; Sosin, A.; Wu, S.; Yang, D.; Wang, S.; Al-Katib, A. M., An MDM2 antagonist (MI-319) restores p53 functions and increases the life span of orally treated follicular lymphoma bearing animals. *Molecular cancer* **2009,** *8*, 115.

62. Shangary, S.; Wang, S., Small-molecule inhibitors of the MDM2-p53 protein-protein interaction to reactivate p53 function: a novel approach for cancer therapy. *Annual review of pharmacology and toxicology* **2009,** *49*, 223-41.

63. Azmi, A. S.; Aboukameel, A.; Banerjee, S.; Wang, Z.; Mohammad, M.; Wu, J.; Wang, S.; Yang, D.; Philip, P. A.; Sarkar, F. H.; Mohammad, R. M., MDM2 inhibitor MI-319 in combination with cisplatin is an effective treatment for pancreatic cancer independent of p53 function. *European journal of cancer (Oxford, England : 1990)* **2010,** *46* (6), 1122-31.

64. Azmi, A. S.; Philip, P. A.; Aboukameel, A.; Wang, Z.; Banerjee, S.; Zafar, S. F.; Goustin, A. S.; Almhanna, K.; Yang, D.; Sarkar, F. H.; Mohammad, R. M., Reactivation of p53 by novel MDM2 inhibitors: implications for pancreatic cancer therapy. *Current cancer drug targets* **2010,** *10* (3), 319-31.

65. Wagner, A. J.; Zhang, Y.; Sicinska, E.; Czaplinski, J.; Remillard, S.; Demetri, G.; Weng, S.; Debussche, L., L08. 03POTENT INHIBITION OF HUMAN LIPOSARCOMA GROWTH AND SURVIVAL BY NOVEL MODULATORS OF THE MDM2-P53 INTERACTION. *Annals of Oncology* **2013,** *24* (suppl 1), i14-i14.

66. Zhao, Y.; Yu, S.; Sun, W.; Liu, L.; Lu, J.; McEachern, D.; Shargary, S.; Bernard, D.; Li, X.; Zhao, T., A potent small-molecule inhibitor of the MDM2–p53 interaction (MI-888) achieved complete and durable tumor regression in mice. *Journal of medicinal chemistry* **2013,** *56* (13), 5553-5561.

67. Aguilar, A.; Sun, W.; Liu, L.; Lu, J.; McEachern, D.; Bernard, D.; Deschamps, J. R.; Wang, S., Design of chemically stable, potent, and efficacious MDM2 inhibitors that exploit the retro-mannich ring-opening-cyclization reaction mechanism in spiro-oxindoles. *Journal of medicinal chemistry* **2014,** *57* (24), 10486-98.

68. Gomez-Monterrey, I.; Bertamino, A.; Porta, A.; Carotenuto, A.; Musella, S.; Aquino, C.; Granata, I.; Sala, M.; Brancaccio, D.; Picone, D., Identification of the spiro (oxindole-3, 3′-thiazolidine)-based derivatives as potential p53 activity modulators. *J. Med. Chem* **2010,** *53* (23), 8319-8329.

69. Bertamino, A.; Soprano, M.; Musella, S.; Rusciano, M. R.; Sala, M.; Vernieri, E.; Di Sarno, V.; Limatola, A.; Carotenuto, A.; Cosconati, S.; Grieco, P.; Novellino, E.; Illario, M.; Campiglia, P.; Gomez-Monterrey, I., Synthesis, in Vitro, and in Cell Studies of a New Series of [Indoline-3,2′-thiazolidine]-Based p53 Modulators. *Journal of medicinal chemistry* **2013,** *56* (13), 5407-5421.

70. Sorriento, D.; Del Giudice, C.; Bertamino, A.; Ciccarelli, M.; Gomez-Monterrey, I.; Campiglia, P.; Novellino, E.; Illario, M.; Trimarco, B.; De Luca, N.; Iaccarino, G., New small molecules, ISA27 and SM13, inhibit tumour growth inducing mitochondrial effects of p53. *Br J Cancer* **2015,** *112* (1), 77-85.

71. Galatin, P. S.; Abraham, D. J., A nonpeptidic sulfonamide inhibits the p53-mdm2 interaction and activates p53-dependent transcription in mdm2-overexpressing cells. *Journal of medicinal chemistry* **2004,** *47* (17), 4163-4165.

72. Chen, L.; Yin, H.; Farooqi, B.; Sebti, S.; Hamilton, A. D.; Chen, J., p53 α-Helix mimetics antagonize p53/MDM2 interaction and activate p53. *Molecular cancer therapeutics* **2005,** *4* (6), 1019-1025.

73. Yin, H.; Lee, G. i.; Park, H. S.; Payne, G. A.; Rodriguez, J. M.; Sebti, S. M.; Hamilton, A. D., Terphenyl-Based Helical Mimetics That Disrupt the p53/HDM2 Interaction. *Angewandte Chemie* **2005,** *117* (18), 2764-2767.

74. Leão, M.; Gomes, S.; Pedraza-Chaverri, J.; Machado, N.; Sousa, E.; Pinto, M.; Inga, A.; Pereira, C.; Saraiva, L., α-Mangostin and Gambogic Acid as Potential Inhibitors of the p53–MDM2 Interaction Revealed by a Yeast Approach. *Journal of Natural Products* **2013,** *76* (4), 774-778.

75. Leao, M.; Pereira, C.; Bisio, A.; Ciribilli, Y.; Paiva, A. M.; Machado, N.; Palmeira, A.; Fernandes, M. X.; Sousa, E.; Pinto, M.; Inga, A.; Saraiva, L., Discovery of a new small-molecule inhibitor of p53-MDM2 interaction using a yeast-based approach. *Biochemical pharmacology* **2013,** *85* (9), 1234-45.

76. Paiva, A. M.; Pinto, R. A.; Teixeira, M.; Barbosa, C. M.; Lima, R. T.; Vasconcelos, M. H.; Sousa, E.; Pinto, M., Development of noncytotoxic PLGA nanoparticles to improve the effect of a new inhibitor of p53-MDM2 interaction. *International journal of pharmaceutics* **2013,** *454* (1), 394-402.

77. Wang, H.; Ma, X.; Ren, S.; Buolamwini, J. K.; Yan, C., A small-molecule inhibitor of MDMX activates p53 and induces apoptosis. *Molecular cancer therapeutics* **2011,** *10* (1), 69-79.

78. Wang, H.; Yan, C., A small-molecule p53 activator induces apoptosis through inhibiting MDMX expression in breast cancer cells. *Neoplasia* **2011,** *13* (7), 611-IN6.

79. Reed, D.; Shen, Y.; Shelat, A. A.; Arnold, L. A.; Ferreira, A. M.; Zhu, F.; Mills, N.; Smithson, D. C.; Regni, C. A.; Bashford, D., Identification and characterization of the first small molecule inhibitor of MDMX. *Journal of Biological Chemistry* **2010,** *285* (14), 10786-10796.

80. Blackburn, T. J.; Ahmed, S.; Coxon, C. R.; Liu, J.; Lu, X.; Golding, B. T.; Griffin, R. J.; Hutton, C.; Newell, D. R.; Ojo, S., Diaryl-and triaryl-pyrrole derivatives: inhibitors of the MDM2–p53 and MDMX–p53 protein–protein interactions. *MedChemComm* **2013,** *4* (9), 1297-1304.

81. (a) Sousa, M. E.; Pinto, M. M., Synthesis of xanthones: an overview. *Current medicinal chemistry* **2005,** *12* (21), 2447-79; (b) Pinto, M. M.; Sousa, M. E.; Nascimento, M. S., Xanthone derivatives: new insights in biological activities. *Current medicinal chemistry* **2005,** *12* (21), 2517-38; (c) Vieira, L. M.; Kijjoa, A., Naturally-occurring xanthones: recent developments. *Current medicinal chemistry* **2005,** *12* (21), 2413-46.

82. Fotie, J.; Bohle, D. S., Pharmacological and biological activities of xanthones. *Anti-Infective Agents in Medicinal Chemistry (Formerly Current Medicinal Chemistry-Anti-Infective Agents)* **2006,** *5* (1), 15-31.

83. Pouli, N.; Marakos, P., Fused xanthone derivatives as antiproliferative agents. *Anti-cancer agents in medicinal chemistry* **2009,** *9* (1), 77-98.

84. Jun, K.-Y.; Lee, E.-Y.; Jung, M.-J.; Lee, O.-H.; Lee, E.-S.; Choo, H.-Y. P.; Na, Y.; Kwon, Y., Synthesis, biological evaluation, and molecular docking study of 3-(3′-heteroatom substituted-2′-hydroxy-1′-propyloxy) xanthone analogues as novel topoisomerase IIα catalytic inhibitor. *European journal of medicinal chemistry* **2011,** *46* (6), 1964-1971.

85. (a) Gu, H.; Rao, S.; Zhao, J.; Wang, J.; Mu, R.; Rong, J.; Tao, L.; Qi, Q.; You, Q.; Guo, Q., Gambogic acid reduced bcl-2 expression via p53 in human breast MCF-7 cancer cells. *Journal of cancer research and clinical oncology* **2009,** *135* (12), 1777-82; (b) Han, A. R.; Kim, J. A.; Lantvit, D. D.; Kardono, L. B.; Riswan, S.; Chai, H.; Carcache de Blanco, E. J.; Farnsworth, N. R.; Swanson, S. M.; Kinghorn, A. D., Cytotoxic xanthone constituents of the stem bark of Garcinia mangostana (mangosteen). *J Nat Prod* **2009,** *72* (11), 2028-31.

86. (a) Gu, H.; Wang, X.; Rao, S.; Wang, J.; Zhao, J.; Ren, F. L.; Mu, R.; Yang, Y.; Qi, Q.; Liu, W., Gambogic acid mediates apoptosis as a p53 inducer through down-regulation of mdm2 in wild-type p53-expressing cancer cells. *Molecular cancer therapeutics* **2008,** *7* (10), 3298-3305; (b) Rong, J.-J.; Hu, R.; Qi, Q.; Gu, H.-Y.; Zhao, Q.; Wang, J.; Mu, R.; You, Q.-D.; Guo, Q.-L., Gambogic acid down-regulates MDM2 oncogene and induces p21 Waf1/CIP1 expression independent of p53. *Cancer letters* **2009,** *284* (1), 102-112; (c) Aisha, A. F.; Abu-Salah, K. M.; Ismail, Z.; Majid, A. M. S. A., In vitro and in vivo anti-colon cancer effects of Garcinia mangostana xanthones extract. *BMC complementary and alternative medicine* **2012,** *12* (1), 104.

87. Fernandes, C.; Masawang, K.; Tiritan, M. E.; Sousa, E.; de Lima, V.; Afonso, C.; Bousbaa, H.; Sudprasert, W.; Pedro, M.; Pinto, M. M., New chiral derivatives of

xanthones: synthesis and investigation of enantioselectivity as inhibitors of growth of human tumor cell lines. *Bioorganic & medicinal chemistry* **2014,** *22* (3), 1049-62.

88. Djerassi, C., Brominations with N-Bromosuccinimide and Related Compounds. The Wohl-Ziegler Reaction. *Chemical reviews* **1948,** *43* (2), 271-317.

89. Varache-Lembège, M.; Moreau, S.; Larrouture, S.; Montaudon, D.; Robert, J.; Nuhrich, A., Synthesis and antiproliferative activity of aryl- and heteroaryl-hydrazones derived from xanthone carbaldehydes. *European Journal of Medicinal Chemistry* **2008,** *43* (6), 1336-1343.

90. Ranu, B. C.; Chattopadhyay, K.; Jana, R., Ionic liquid promoted selective debromination of α-bromoketones under microwave irradiation. *Tetrahedron* **2007,** *63* (1), 155-159.

91. Ghandi, K., A review of ionic liquids, their limits and applications. *Green and Sustainable Chemistry* **2014,** *2014*.

92. Ma, D.; Cai, Q., N,N-Dimethyl Glycine-Promoted Ullmann Coupling Reaction of Phenols and Aryl Halides. *Organic Letters* **2003,** *5* (21), 3799-3802.

93. Roughley, S. D.; Jordan, A. M., The Medicinal Chemist's Toolbox: An Analysis of Reactions Used in the Pursuit of Drug Candidates. *Journal of medicinal chemistry* **2011,** *54* (10), 3451-3479.

94. Abdel-Magid, A. F.; Carson, K. G.; Harris, B. D.; Maryanoff, C. A.; Shah, R. D., Reductive Amination of Aldehydes and Ketones with Sodium Triacetoxyborohydride. Studies on Direct and Indirect Reductive Amination Procedures1. *The Journal of organic chemistry* **1996,** *61* (11), 3849-3862.

95. Tripathi, R. P.; Verma, S. S.; Pandey, J.; Tiwari, V. K., Recent development on catalytic reductive amination and applications. *Current Organic Chemistry* **2008,** *12* (13), 1093-1115.

96. Clinton, F., Sodium cyanoborohydride—a highly selective reducing agent for organic functional groups. *Synthesis* **1975,** *3*, 135-146.

97. Lavecchia, A.; Di Giovanni, C., Virtual screening strategies in drug discovery: a critical review. *Current medicinal chemistry* **2013,** *20* (23), 2839-60.

98. Schneider, G.; Bohm, H. J., Virtual screening and fast automated docking methods. *Drug discovery today* **2002,** *7* (1), 64-70.

99. Schneider, G., Virtual screening: an endless staircase? *Nat Rev Drug Discov* **2010,** *9* (4), 273-276.

100. Huang, S. Y.; Grinter, S. Z.; Zou, X., Scoring functions and their evaluation methods for protein-ligand docking: recent advances and future directions. *Physical chemistry chemical physics : PCCP* **2010,** *12* (40), 12899-908.

101. Freedman, D. A.; Epstein, C. B.; Roth, J. C.; Levine, A. J., A genetic approach to mapping the p53 binding site in the MDM2 protein. *Molecular Medicine* **1997,** *3* (4), 248.

102. Naidu, M. D.; Agarwal, R.; Pena, L. A.; Cunha, L.; Mezei, M.; Shen, M.; Wilson, D. M., 3rd; Liu, Y.; Sanchez, Z.; Chaudhary, P.; Wilson, S. H.; Waring, M. J., Lucanthone and its derivative hycanthone inhibit apurinic endonuclease-1 (APE1) by direct protein binding. *PloS one* **2011,** *6* (9), e23679.

103. Quillinan, A. J.; Scheinmann, F., Studies in the xanthone series. Part XII. A general synthesis of polyoxygenated xanthones from benzophenone precursors. *Journal of the Chemical Society, Perkin Transactions 1* **1973,** (0), 1329-1337.

104. Kini, R. M.; Evans, H. J., Molecular modeling of proteins: a strategy for energy minimization by molecular mechanics in the AMBER force field. *Journal of biomolecular structure and dynamics* **1991,** *9* (3), 475-488.

105. Trott, O.; Olson, A. J., AutoDock Vina: Improving the speed and accuracy of docking with a new scoring function, efficient optimization, and multithreading. *Journal of Computational Chemistry* **2010,** *31* (2), 455-461.

106. Seeliger, D.; de Groot, B. L., Ligand docking and binding site analysis with PyMOL and Autodock/Vina. *Journal of computer-aided molecular design* **2010,** *24* (5), 417-22.